Chapter 7
Polyhedral Oligomeric Silsesquioxanes in Electronics and Energy Applications

Claire Hartmann-Thompson

Introduction

This chapter is of broad scope and and covers the use of hybrid polyhedral oligomeric silsesquioxane (POS) materials to enhance performance in various electronics, optical and energy-related applications. It reviews the liquid crystal phase behavior of Si_8O_{12} compounds and their use in LC devices, their use as electroluminescent (EL) materials in light-emitting devices (with a particular focus upon the problematic area of blue emission), their use as lithographic resists in the fabrication of electronic and optical devices, their use in diverse sensor systems, and their use in fuel cell membranes, battery electrolytes and lubricants. Si_8O_{12} materials have also been successfully employed as coatings and adhesives in space photovoltaic solar cells, and this topic is reviewed in Chapter 8, along with various other space material-related applications.

7.1 Polyhedral Oligomeric Silsesquioxanes in Liquid Crystal Systems

Liquid crystalline (LC) phases [1] are phases intermediate between the disordered liquid state and the highly ordered crystalline solid state, and are an important

Claire Hartmann-Thompson
Michigan Molecular Institute, Midland, MI USA

C. Hartmann-Thompson (ed.), *Applications of Polyhedral Oligomeric Silsesquioxanes*, Advances in Silicon Science 3, DOI 10.1007/978-90-481-3787-9_7,

example of the phenomenon of self-assembly. LC phases may be either nematic (N), chiral nematic (N*, also termed cholesteric) or smectic (S_m), Fig. 7.1. Nematic phases have long-range orientational order and short-range positional order. Chiral nematic phases are periodically twisted about an axis perpendicular to the direction of molecular orientation (termed the director), and are associated with mesogens containing chiral centers. Smectic phases have layered structures, and possess long-range orientational order and a degree of long-range positional order. In the smectic A phase (S_mA), the director is perpendicular to the layers, and in the smectic C phase (S_mC), the director is inclined at an angle to the perpendicular (Fig. 7.1). Chiral groups (denoted by *) cause nematic and tilted smectic phases to form twisted helical structures. Nematic or chiral tilted smectic phases in materials containing rod-like mesogens can display ferroelectric effects. The nematic phase is of the greatest interest for commercial display technologies. The crystalline phase is denoted as C and the isotropic phase is denoted as I.

Polarized optical microscopy (POM) is used to identify textures and phase transition temperatures associated with the various mesophases. Different mesophases have distinctive textures, e.g., a Schlieren (threaded marble-type) texture is characteristic of nematic phases, a streaky oily texture is characteristic of cholesteric phases, a focal-conic fan texture is characteristic of smectic A phases, and a granulated texture is characteristic of smectic C phases. Differential scanning calorimetry (DSC) may also be used to determine transition temperatures, and X-ray diffraction may be used to characterize liquid crystalline phases. At the isotropization temperature (also referred to as the clearing temperature) the final transition from a mesophase to a normal liquid phase with no positional or orientational order occurs.

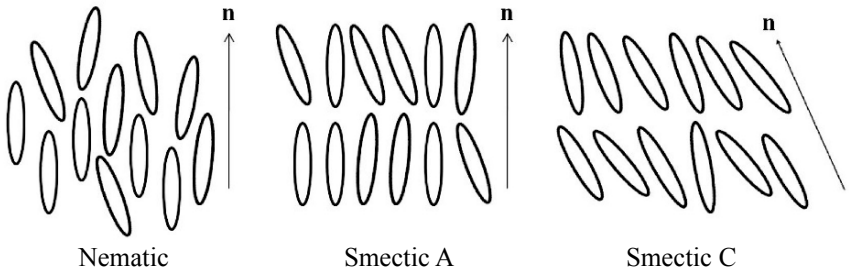

Fig. 7.1 Illustration of various liquid crystalline phases, where n denotes the direction of molecular orientation (i.e., the director)

Main chain LC polymers have rigid aromatic groups in their backbones, and form LC phases in solution or in the melt. Examples include aromatic polyamide fibers such as Dupont Kevlar® (the first commercial LC polymer, developed in the 1960s), and aromatic polyesters such as Ticona Vectra®, Dupont Zenite® and Solvay Xydar®. Side chain LC polymers are comprised of rigid rod mesogenic side-chains attached to polymer backbones. The first liquid crystal displays (LCDs), based on cyanobiphenyl materials, were developed in the early 1970s, and in order to obtain processible materials for commercial LCD applications, side-chain LC polymers

were developed. It was found that a spacer between the backbone and the mesogen was necessary in order to decouple the mesogen from the backbone, and to enable the mesogens to align to form mesophases. The majority of electroluminescent (EL) polymers are also liquid crystalline (see Section 7.2), and LC POS materials and EL POS materials have been reviewed together [2]. Any rigid anisotropically-shaped molecule (e.g., rods or discs) has the potential to form mesophases. Discotic liquid crystals form either nematic phases (denoted N_D) or columnar phases (denoted D, the discotic analog of the smectic phase). In non-emissive thermotropic LC displays (attractive for large area display technologies), scattering occurs either from nematic liquid crystals in a continuous polymer phase, or from solid particles in a continuous nematic LC phase.

In this section, various categories of LC Si_8O_{12} materials are reviewed. Si_8O_{12} cores partially or fully functionalized with a range of mesogens (standard cyanobiphenyl, metallomesogen, end-on, side-on lateral, chiral or bent-core) constitute the largest body of work, but Si_8O_{12}-mesogen dyads, main chain LC polymers end-capped with Si_8O_{12}, Si_8O_{12} cores functionalized with side-chain jacketed LC polymers, and linear polymers carrying both pendant Si_8O_{12} and pendant mesogens are also reviewed. In addition, the use of Si_8O_{12} compounds at interfaces in LC devices in order to induce spontaneous vertical alignment and to improve device performance is discussed.

In the 1990s, hydrosilylation of polymethylhydridosiloxanes, $(SiMeHO)_n$, by vinyl-functionalized mesogens was the method of choice for creating a vast range of side-chain liquid crystalline polysiloxanes [3], although it is interesting to note that some polysiloxanes are able to form LC phases without carrying mesogens (e.g., di-*n*-alkylpolysiloxanes). The flexibility of the siloxane backbone was an advantage in enabling the mesogens to align. The structure-property relationships of these compounds were studied intensively; structure variables included calamitic versus discotic mesogens, the length and composition of the spacer, the fraction of siloxane repeat units carrying a mesogen and the distribution of the mesogen along the backbone, and property variables included the category of mesophase and the transition temperature. This approach was then extended beyond linear siloxanes [4,5,6] to include cyclic siloxanes, polysilsesquioxanes [7,8] and polyhedral oligomeric silsesquioxanes [9] as variables, where some or all of the silicon atoms in the Si_8O_{12} cage were substituted with mesogenic LC moieties. The attachment of a mesogen to an Si_8O_{12} core is also of interest because the mesogen is immobilized on a substrate, but is still free to align in an externally applied field [10]. Because most liquid crystalline side-chain polysiloxanes were synthesized by hydrosilylation, this also became the synthetic route of choice for silsesquioxane analogues [11] (although metal-containing mesogens [12] can create difficulties in conventional metal-catalyzed hydrosilylation chemistry). $Si_8O_{12}(H)_8$ and $Si_8O_{12}(OSiMe_2H)_8$ undergo clean α-hydrosilylation with most alkenes, while oxyallyl compounds give some β-silylated side-products. Since platinum catalyst residues can affect LC transition temperatures [13], deactivation of the catalyst (e.g., by using a phosphorus compound) and removal of the catalyst (e.g., by use of a silica column) is important [9].

The first study of LC Si_8O_{12} compounds was carried out in 1991 by Kreuzer and co-workers at Wacker-Chemie GmbH in Germany [9]. Si_8O_{12} $(OSiMe_2H)_8$ was reacted with an alkene-functionalized mesogen in a dicyclopentadienyl platinum dichloride-catalyzed hydrosilylation, and platinum residues were removed using a short silica gel column. All of the products displayed smectic phases (Table 7.1) with the associated focal conic textures. When a mesogen was linked laterally (side-on) to a T_8 core (Fig. 7.2), a nematic texture was observed at 23 °C. The lateral attachment of mesogens had previously been demonstrated for side-chain LC polysiloxanes [14].

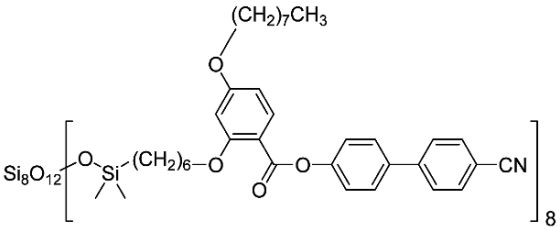

Fig 7.2 Cyanobiphenyl mesogen laterally attached to an Si_8O_{12} core [9]

Table 7.1 Phase transitions for various mesogen-functionalized polyhedral oligomeric silsesquioxanes where C denotes crystalline, G denotes glassy, I denotes isotropic, S_mA denotes smectic A and Chol denotes cholesteryl [9]

Core	Substituent	Phase transitions (°C)
T_8	$[(CH_2)_{10}COO\text{-}Chol]_8$	C 128 (G 46) S_mA 157 I
T_6	$[OSiMe_2(CH_2)_{10}COO\text{-}Chol]_6$	G 30 S_X 37 S_mA 142 I
T_8	$[OSiMe_2(CH_2)_{10}COO\text{-}Chol]_8$	C 108 S_mA 160 I
T_8	$[OSiMe_2(CH_2)_3O\text{-}Ph\text{-}COO\text{-}Ph\text{-}CN]_8$	C 119 S_mA 146 I
T_8	$[OSiMe_2(CH_2)_3O\text{-}Ph\text{-}COO\text{-}Ph\text{-}Ph\text{-}CN]_8$	G 102 S_X 127 S_mA >300 I
T_{10}	$[OSiMe_2(CH_2)_{10}COO\text{-}Chol]_{10}$	C 122 (G 51) S_mA 164 I
T_{10}	$[OSiMe_2(CH_2)_3O\text{-}Ph\text{-}COO\text{-}Chol]_{10}$	C 115 (G 87) S_mA 262 I
T_8	$[OSiMe_2(CH_2)_{10}COO\text{-}Chol]_4[Me]_4$	G 35 S_X 63 S_mA 148 I
T_8	$[OSiMe_2(CH_2)_{10}COO\text{-}Chol]_4[OSiMe_2(CH_2)_{10}\text{-}COO\text{-}Ph\text{-}Ph]_4$	G 17 S_X 60 S_mA 107 I
T_8	$[OSiMe_2(CH_2)_3O\text{-}Ph\text{-}COO\text{-}Chol]_5[OSiMe_2(CH_2)_3O\text{-}Ph\text{-}COO\text{-}Ph\text{-}Ph]_3$	S_X 114 S_mA 213 I

Three years later, the Laine group at the University of Michigan synthesized various allyl-terminated aromatic diester compounds [15] using an earlier reported method [16]. Some were isotropic and some showed nematic phases and C-LC onset temperatures in the range 160 to 188 °C. Temperature cycling studies were not possible because the compounds underwent Claisen rearrangements upon heating. When one of LC allyl compounds, 4-(4-allyloxybenzoyloxy)biphenyl, was reacted with octahydrido-Si_8O_{12}, both the ratio of the reagents and the ^{29}Si NMR

analysis suggested that a symmetrical tetra-substituted compound may have been formed. This was based on the observation of SiC signals at -67 ppm and -69 ppm, but only one SiH signal at -84 ppm. The size exclusion chromatography (SEC) data were broadly consistent with this. Upon heating, the compound flowed at 90 °C, transitioned to a coarse nematic texture with inversion walls at 133 °C , and showed a clearing point at 184 °C. Upon cooling, the compound transitioned to a nematic Schlieren texture at 178 °C, and transitioned to an inversion wall texture at 134 °C. The remainder of this study concerned model hydrosilylation reactions between silanes and allyl-functionalized small molecule aromatic LC esters, and the various side products formed when different platinum or palladium catalysts were used (see also Section 1.6.2, Chapter 1). Platinum 1,3-divinyltetramethyldisil oxane (Karstedt's catalyst) gave the fewest side-products under the mildest reaction conditions, and an $Si_8O_{12}(H)_8$ >> Et_3SiH > $HMe_2SiOSiMe_2H$ > Ph_2SiH_2 order of reactivity was observed. The use of palladium dibenzylideneacetone-Ph_3P catalyst resulted in oxysilylation with loss of propene.

The same group [17] reported a liquid crystalline methacrylate $Si_8O_{12}(H)_4[(CH_2)_4OPhCOO\text{-biphenyl}]_4$ in 1994 (Fig. 7.3). This material was prepared with the aim of combining the properties of Si_8O_{12} compounds (i.e., good adhesion to surfaces, hardness and thermal stability) with those of rigid rod liquid crystalline (LC) polymers (i.e., toughness, low coefficient of thermal expansion (CTE), good oxidative and photochemical stability) for application as a curable dental composite, where abrasion resistance is achieved at lower filler loadings, and in more easily processed and less viscous materials (see also Section 9.4.2, Chapter 9).

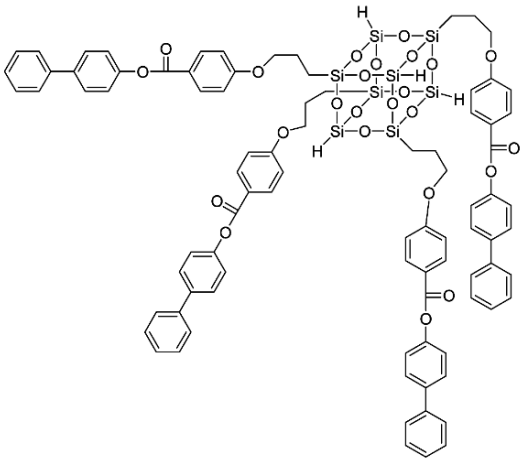

Fig. 7.3 A tetra-substituted LC Si_8O_{12} species [17]

The first Si_8O_{12} species functionalized with a metallomesogen [10] was synthesized by Saez and co-workers at the University of Hull (UK) in 1996. Most metallomesogens are bifunctional and carry two identical functionalized ligands, and are therefore potential cross-linkers; however, a high degree of cross-linking can

cause a loss of liquid crystallinity in polymeric systems. In an attempt to avoid this, a mono-functional (asymmetric) square planar diamagnetic nickel(II) complex (Fig. 7.4) was prepared and reacted with $Si_8O_{12}(OSiMe_2H)_8$ in order to synthesize a free oligomeric LC compound. This hydrosilylation was catalyzed by Karstedt's catalyst and the product was confirmed by elemental analysis. The same compound was also reacted with 1,3,5,7-tetramethyl-cyclotetrahydridosiloxane (D_4H_4). The free Ni(II) complex (Fig. 7.4) melt-transitions to a smectic A phase at 181 °C and clears to the isotropic liquid at 190 °C, and the D_4 cyclic Ni(II) compound melt-transitions to a smectic A phase at 196 °C and clears to the isotropic liquid at 296 °C with some decomposition. Unfortunately, the Ni(II)-functionalized Si_8O_{12} compound was found to be non-mesomorphic, and simply melted with decomposition at 219 °C. A year later, the same group [18] reported a copper analog of the monofunctional nickel mesogen shown in Fig. 7.4.

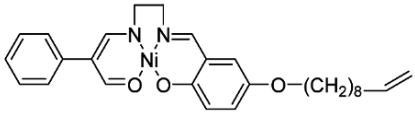

Fig. 7.4 Monofunctional nickel(II) metallomesogen [10]

In 1996, Mehl and Goodby at Hull [19] attached eight cyanobiphenyl units to an Si_8O_{12} core to form the compound Si_8O_{12} $[OSiMe_2(CH_2)_nO$-biphenyl-$CN]_8$ where n = 4, 6 or 11 for the spacer (Fig. 7.5, middle). A lamellar smectic A phase formed, and transition temperatures were observed at 94, 117 and 129 °C for n = 4, 6 and 11, respectively. X-ray diffraction and molecular simulation suggested that the mesogens were packing in two groups of four (Fig. 7.5, top), were forming a rod-like (rather than star-like) molecular shape, and that the rods were packed in disordered layers. Such ABCCBA arrangements (where A is a mesogen, B is a spacer and C is an Si_8O_{12}core) are very common for mesogen-functionalized Si_8O_{12} compounds [19,20,21]. In a later study by Saez and Goodby at Hull in 1999 [22], an analogous n = 11 Si_8O_{12} compound functionalized with 16 cyanobiphenyl units was prepared (Fig. 7.5, bottom) in a convergent synthesis that required five separate hydrosilylation, Grignard or SiCl substitution steps. Interestingly, despite the dense packing of the mesogens around the Si_8O_{12} core, a lamellar mesophase was still preferred over a cubic or a columnar phase, and enantiotropic smectic A and smectic C phases were observed (G -18 °C, S_mC 63 °C, S_mA 92 °C). This compound had a lower clearing point and a lower S_mC to S_mA transition temperature than its linear polysiloxane analog.

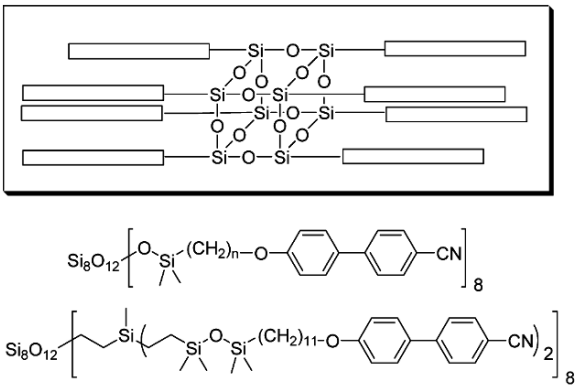

Fig. 7.5 LC Si_8O_{12} compounds carrying cyanobiphenyl mesogens [19,22]

The LC Si_8O_{12} systems discussed above (Fig. 7.5) are useful model compounds because they are monodisperse [11]. Hence they can be used as scaffolds to study the behavior of mesogens without having to consider the variables of polydispersity and tacticity that are unavoidable in studies of side-chain LC polymers. For side-chain LC polymers carrying a given mesogen, phase transition temperatures increase and then plateau out with increasing numbers of repeat units, with the plateau commonly occurring between 12 and 30 repeat units [13]. An Si_8O_{12} core carrying cyanobiphenyl mesogens was compared with tetrakis(dimethylsiloxane) ($Si(OSiMe_2)_4$) star cores, D_4 and D_5 cyclic cores, and a T_{10} polyhedral oligomeric silsesquioxane core. For the standard cyanobiphenyl mesogen on Si_8O_{12}, four or more methylene spacers between mesogen and Si_8O_{12} are required for LC behavior to occur, and a smectic A phase is observed at high temperatures. As the number of methylene spacers increases from four to eleven, the smectic A to isotropization transition temperature increases [19,20]. Analogous compounds with polysiloxane backbones, tetrahedral $Si(OSiMe_2)_4$ star cores and D_4 cyclic cores show the same trend in the transition temperature from smectic A to isotropic. The glass transition temperature of the mesogen-functionalized Si_8O_{12} compounds decreases with increasing spacer length owing to the plasticizing effect of the methylene segments [11]. Isotropization enthalpy and entropy values suggest that the systems become increasingly ordered as spacer length increases. The transition temperatures to smectic A, and also from smectic A to the isotropic phase, increase with the stiffness or the mesogen [9]. Transitioning from smaller to larger polyhedral oligomeric silsesquioxane cores (T_6, T_8, T_{10}) results in an increase in isotropization temperature [9].

Following on from these structure-property studies [9,11], in a much later 2007 study by Kawakami and co-workers at the Japan Advanced Institute of Science and Technology [23], the range of core architectures was extended to include the structures in Fig. 7.6. These were functionalized with 4-allyloxy-4'cyanobiphenyl (somewhat misleadingly classified by the authors as a 'nematic mesogen' C 52 °C,

N 70 °C, I) or cholesteryl-10-undecanoate (classified as a 'cholesteric mesogen' C 52 °C, S 65 °C, cholesteric phase 82 °C, I) by Karstedt-catalyzed hydrosilylation.

The compounds were fully characterized by elemental analysis, MALDI-TOF MS and ^{29}Si NMR. The LC phase behavior was found to be largely independent of the structure of the siloxane core, although the authors did not cite the earlier structure-property studies where core architecture was varied [9,11]. The double-decker compound tetra(dimethylsilanyloxy)octaphenyltetracyclooctasilsesquioxane (DDODMS, Fig. 7.6, bottom right) was an interesting choice of core, since its structure was intermediate between a cyclic siloxane and an open-cage polyhedral oligomeric silsesquioxane. Little work on open-cage cores functionalized with mesogens has been carried out, and the vast majority of work reviewed in this section concerns closed-cage Si_8O_{12} cores. When carrying the cyanobiphenyl mesogen, the DDODMS core gave a T_g of 10 °C, but no mesophases were observed, possibly because of the short spacer, and because of steric hindrance from the phenyl groups interfering with mesogen alignment. When carrying the cholesteryl mesogen, DDODMS showed a cholesteric to isotropic transition at 94 °C, whereas all of the other cholesteryl-carrying cores in Fig. 7.6 showed smectic to isotropic transitions instead. Interestingly D_4 (Fig. 7.6, top right) carrying cyanobiphenyl was reported to have a nematic to isotropic transition at 118 °C, in contrast to earlier studies that had reported smectic mesophases for cyanobiphenyl-functionalized cyclic siloxanes (albeit with longer spacers) [11].

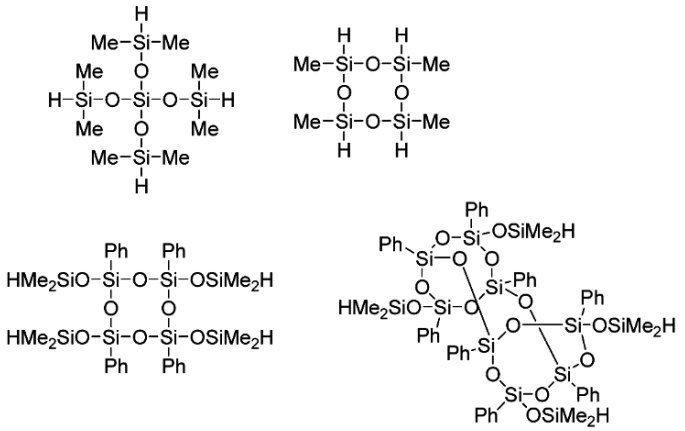

Fig. 7.6 Structures of various cores used to carry cyanobiphenyl or cholesteryl mesogens [23]

In a 2000 University of Hull study [24], two mesogen-functionalized Si_8O_{12} compounds with siloxane (rather than methylene) spacer groups were synthesized, and compared with the starting mesogens, and with related model compounds. (Fig. 7.7) They had lateral rather than end-on functional groups (Fig. 7.7) and were reacted with octavinyl- Si_8O_{12}. These mesogens required multi-step syntheses and were successfully purified by flash column chromatography. The Si_8O_{12} core functionalized with the upper mesogen (Fig. 7.7) showed C 59.5 °C [S_mX 33.1 °C] S_mC 111.3 °C, N 145.8, I, notable for the thermal stability of its mesomorphic state,

with an isotropization temperature ~20 °C higher than that of the free mesogen. The Si_8O_{12} core functionalized with the lower mesogen (Fig. 7.7) showed T_g -19.3 °C, S_mX 37.6 °C, N 50.5 °C, I. In a later 2007 collaboration between the University of Patras (Greece) and the group at Hull University [25], Si_8O_{12} was functionalized with the vinyl analogue of the mesogen [24] shown in the top part of Fig. 7.7 and characterized by XRD, an extension of the earlier POM study [24] of the mesophases. The pure mesogen, the pure mesogen-substituted Si_8O_{12} compound, and mixtures of these two materials at 1:1, 3:1 and 7:1 w/w were studied. The free mesogen formed a nematic phase while the Si_8O_{12} compound and the free mesogen/ Si_8O_{12} mixtures transitioned from a columnar rectangular phase, to a columnar hexagonal phase, to a nematic phase as temperature increased. The columnar phases were destabilized as the amount of free mesogen in the mixture increased. The XRD data suggested that for the columnar hexagonal phase, some free mesogens were located in the inter-columnar space and others were located within the columnar structure (causing an increase in both lattice constant and stacking periodicity), whereas for the columnar rectangular phase all of the mesogens were withinin the columnar structure (causing no significant change in the lattice constant but an increase in stacking periodicity).

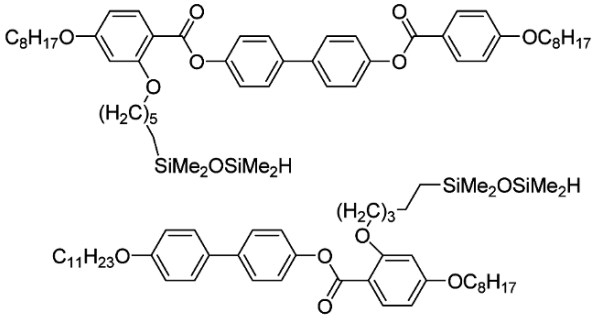

Fig. 7.7 Mesogens for lateral attachment to Si_8O_{12} cores via siloxane spacers [24]

In the 1990s, Saez, Mehl and Goodby at the University of Hull had generally focused upon fully substituted octa-functional LC Si_8O_{12} materials, while the Laine group at the University of Michigan had focused upon partially substituted LC Si_8O_{12} materials [15,26]. In a 2001 University of Michigan study [27], Si_8O_{12} compounds carrying an average of five mesogens per Si_8O_{12} were synthesized in platinum dicyclopentadienyl dichloride-catalyzed hydrosilylation reactions between Si_8O_{12} $(OSiMe_2H)_8$ and allyloxy-functionalized mesogens, following on from an earlier study where a tetra-substituted LC Si_8O_{12} compound had been prepared [15]. The aim of this work was to lower the phase transition temperatures to levels suitable for biological applications (e.g., dental composites, see also Chapter 9). Allyloxy-R mesogens with various spacers were synthesized, where R = $(CH_2)_3$O-Ph-COO-biphenyl (no mesophase), R = $(CH_2)_3$O-Ph-COO-biphenyl-OCH_3 (nematic), $(CH_2)_2O(CH_2)_2$O-Ph-COO-biphenyl (no mesophase), or R= $(CH_2)_2O(CH_2)_2$O-Ph-COO-biphenyl-OCH_3 (no mesophase). Elemental analysis was used to demonstrate the presence of five mesogens per Si_8O_{12}. Interestingly when the latter three

mesogens were attached to Si_8O_{12} cores, the resulting compounds all showed S_mA and N phases, despite the non-mesomorphic nature of some of the starting mesogens. Side-chain LC polysiloxanes show similar behavior, and this has been rationalized in terms of rigid groups being more densely packed and more easily aligned when immobilized on a linear polymer than when free. The Si_8O_{12} materials carrying mesogens with flexible CH_2CH_2O spacers had lower melting and clearing temperatures than the Si_8O_{12} materials carrying mesogens with $CH_2CH_2CH_2O$ spacers. The introduction of OCH_3 end-groups resulted in a general increase in the various phase transition temperatures.

In a 2000 University of Kyoto study [28], the following three mesogens were attached to Si_8O_{12} in hexachloroplatinic acid-catalyzed hydrosilylations between the vinyl-functionalized mesogen and octahydrido- Si_8O_{12}: $(CH_2)_5O$-biphenyl-OCH_3, $(CH_2)_5O$-biphenyl-CN and $(CH_2)_5$-Ph-N=N-Ph-CN. Reaction stoichiometry was set to achieve full mesogen substitution. No mass or elemental analysis data were given for the products; however, the absence of an SiH peak in the ^1H NMR spectrum suggested that highly substituted products had probably been obtained. The three starting mesogens and the three mesogen-functionalized Si_8O_{12} compounds all showed nematic phases by DSC and POM (where the Schlieren texture was observed), but no smectic phase. The nematic phase existed over a much wider temperature range in the Si_8O_{12} compounds than in the starting mesogens. These compounds (synthesized from $Si_8O_{12}(H)_8$) are very closely related to the University of Michigan and University of Hull compounds discussed above (albeit synthesized from Si_8O_{12} $(OSiMe_2H)_8$), although these earlier studies are not cited. Si_8O_{12} $[OSiMe_2(CH_2)_nO$-Biphenyl-$CN]_8$ where n= 4, 6 or 11 shows a smectic phase [19] and $Si_8O_{12}[(CH_2)_2O(CH_2)_2O$-Ph-COO-biphenyl-$OCH_3]_5$ shows both smectic and nematic phases [27]. Nematic phases for mesogen-functionalized POS compounds had only previously been observed at partial substitution [27] or for laterally attached mesogens [9,24] so it is possible that full substitution may not have been achieved in this study.

In 2001, workers at the University of Hull functionalized Si_8O_{12} cores with chiral mesogens to achieve enantiotropic chiral nematic phases that were stable over a wide temperature range [29]. The two chiral alkene-functionalized mesogens shown in Fig. 7.8 (C 111.3 °C, N* 153.5 °C, I and C 101.1 °C, N* 109.2 °C, I respectively) were reacted with Si_8O_{12} $(OSiMe_2H)_8$ in a Karstedt-catalyzed hydrosilylation to give compounds showing G 23.7 °C, N* 116.9 °C, I, and G 11.2°C, N* 72.0 °C, I respectively. POM showed that the chiral nematic phase of the first compound was blue and iridescent in texture (the blue color suggesting a helix with a 0.2 to 0.3 μm pitch). The second compound showed a non-iridescent Schlieren texture. In contrast to the majority of the mesogens reviewed above (where the reactive group was at the 'end' of the rod), in these mesogens 'side-on' or lateral attachment was achieved. A Si_8O_{12} core carrying sixteen laterally attached chiral mesogens [30] was synthesized in a Karstedt-catlyzed hydrosilylation between Si_8O_{12} $[CH_2CH_2SiMe(vinyl)_2]_8$ and the SiH-laterally functionalized mesogen shown in Fig. 7.8. This compound may also be considered as a first

generation dendrimer with an Si_8O_{12} core. Upon cooling, DSC and POM showed an I to N* transition at 107.7 °C, and an N* to Col_{hd} (hexagonal columnar) transition at 102.3 °C. The hexagonal columnar phase had a characteristic fan-like texture. Upon further cooling, POM showed a texture change that was tentatively assigned as a rectangular columnar phase, although no associated thermal transition was observed by DSC. The columnar phases suggested the molecules had a disc-like shape, and the structural organization of the mesogens was further investigated by molecular modeling. In the earlier study discussed above [22], sixteen ‘end-on’ cyanobiphenyl groups had been attached to an Si_8O_{12} core (Fig. 7.5) and had formed S_mA and S_mC phases. Columnar phases for mesogens laterally attached to Si_8O_{12} cores were also observed in later studies [25].

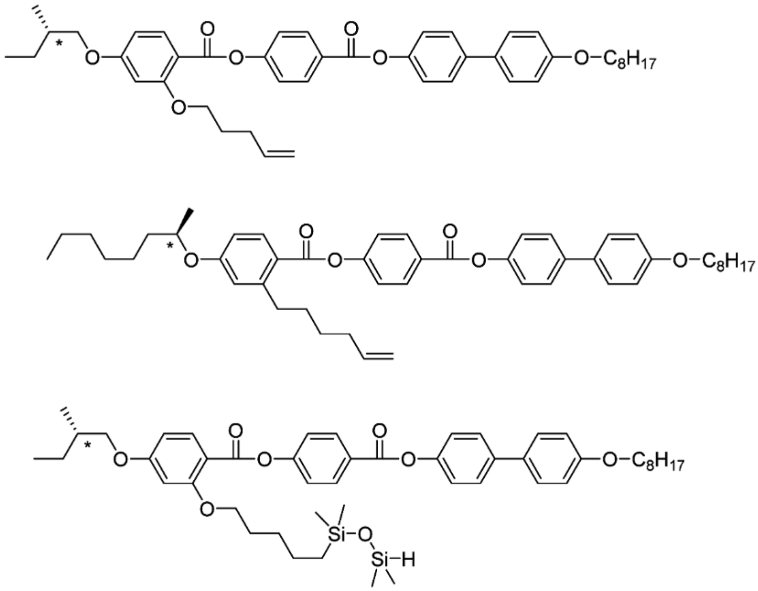

Fig. 7.8 Chiral mesogens used to functionalize Si_8O_{12} cores and create chiral nematic phases [29] and hexagonal columnar phases [30]

The effect of attaching a bent-core mesogen (Fig. 7.9) to an Si_8O_{12} core by hydrosilylation (Karstedt catalyst) at various substitution levels (3.5, 5 and 8 mesogens per Si_8O_{12}) was studied [31] by Fan, Shen, Zhou and co-workers at Beijing National Laboratory in 2008, with the aim of tailoring ferroelectric and antiferroelectric behavior. In bent-core systems, the symmetry is broken using an achiral molecule with a bent-core structure instead of using a mesogen with a chiral center (as in Fig. 7.8) [29,30,32]. Characterization by DSC and one-dimensional WAXD showed that the product carrying 8 mesogens formed two bilayer smectic C phases, while the products carrying 3.5 mesogens and 5 mesogens formed a single monolayer antiferroelectric smectic C phase.

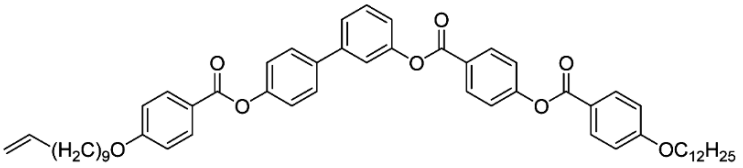

Fig. 7.9 Bent-core mesogen [31]

The discussion above covers Si_8O_{12} cores either partially or fully substituted by mesogens. When the substitution level is very low and the Si_8O_{12} core carries only one mesogen (Fig. 7.10), it may also be considered as an asymmetric molecular dyad, i.e., a dumbbell-shaped molecule in which two different entities are linked by a spacer. Dyads are of particular interest when the two components have complementary properties, e.g., they may be electron-donor acceptor pairs. In 2006 and 2007 University of Connecticut studies [33,34], the behavior of an Si_8O_{12}-discotic mesogen dyad was investigated (Fig. 7.10). This was synthesized by reaction between Si_8O_{12} (*i*-Bu)$_7$(CH$_2$)$_3$OH and a carboxylic acid-functionalized triphenylene (in an interesting departure from hydrosilylation chemistry), and the pure material and its 1:1 mol/mol mixture with POS were studied by DSC, two-dimensional XRD and TEM. Both compositions were nanophase-separated. The discotic triphenylene groups formed a bilayer LC lamella sandwiched between Si_8O_{12} lamellar crystals in the pure dyad, and in the 1:1 blend, the discotic triphenylene groups were interdigitated. No evidence of columnar mesophases was observed. The isotropization of the LCs and the melting of the Si_8O_{12} both occurred at 66 °C. In a more recent University of Connecticut study [35], analogous Si_8O_{12} compounds carrying eight triphenylene groups were synthesized via amidation. A number of variants were studied, with triphenylene alkyl groups of either 5 or 12 carbons, and with spacers of either 2, 6 or 10 carbons, and various columnar phases were characterized by XRD and TEM.

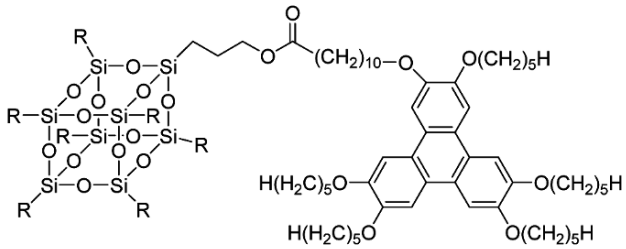

Fig. 7.10 An Si_8O_{12}-discotic mesogen dyad [33]

The materials reviewed above all have architectures where an Si_8O_{12} core carried one or more mesogens, but in an alternate approach, an Si_8O_{12} core carrying LC polymer arms was studied [36]. Atom transfer radical polymerization (ATRP) was used to grow eight arm star poly{2,5-bis[(4-methoxyphenyl)oxycarbonyl] styrene} (PMPCS) from an octafunctional Si_8O_{12} core, and the liquid crystalline

phase behavior of the star polymers was studied. Si_8O_{12} $(OSiMe_2(CH_2)_3O(C{=}O)CMe_2Br)_8$ was used as an initiator, and 2,5-bis-4-methoxyphenyloxycarbonylstyrene (MPCS) was used as monomer in the presence of copper(I) bromide, an amine and chlorobenzene. This monomer was the precursor to a lateral jacketed LC polymer (Fig. 7.11). Products with PMPCS arms of various lengths (and various total molecular masses) were prepared and characterized by GPC, DSC, one-dimensional WAXD and POM. In addition, the Si_8O_{12} core was destroyed using hydrofluoric acid in order to release and characterize the arms, and to gain insight into what had occurred during the ATRP reaction (e.g., intramolecular coupling of arms and/or intermolecular coupling of stars). The T_g of the star increased with molecular mass, and plateaued at 116 °C when M_n exceeded 38,000. At $M_n < 45{,}000$, only amorphous phases were observed, but above this mass, columnar hexagonally-packed nematic phases with star-like textures were observed. Relative to their linear analogs, the star polymers required fewer repeat units per arm to stabilize the LC phase.

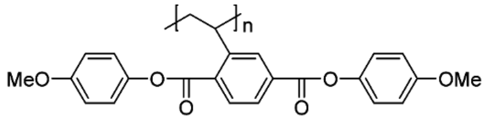

Fig. 7.11 Structure of lateral jacketed LC polystyrene derivative [36]

In contrast to the various Si_8O_{12} core species discussed above, an alternate class of LC Si_8O_{12} materials [37] are based on an architecture where conventional linear main-chain LC polymers are end-capped with Si_8O_{12} (Fig. 7.12). These materials were studied in an attempt to overcome the poor adhesion of LC polymers to metal surfaces, to other polymers and to themselves. In a 1996 study [37], a US Air Force Research Laboratory (AFRL) group reacted an Si_8O_{12}(cyclohexyl)$_7$Cl end-capper with carboxylic acid-terminated LC polymer to give the structure shown in Fig. 7.12. DSC showed that both the starting LC polymer and the Si_8O_{12}-terminated LC variant had a T_g of ~95 °C and a nematic to isotropic transition at ~235 °C. In a 2004 Case Western Reserve University (USA) study by Schiraldi and co-workers, side-chain and main-chain LC species were combined by formulating 2.5 wt % cyanobiphenyl-functionalized Si_8O_{12} nano-additive into several main-chain LC polyesters [38]. The aim of this work was to improve the performance of the polyesters in fiber and high barrier packaging applications. Main-chain LC polymers with Si_8O_{12} fillers have also been patented as improved dielectric materials for electronic circuits [39].

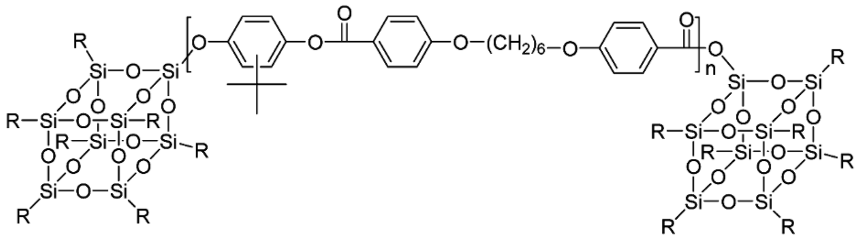

Fig. 7.12 An Si_8O_{12} end-capped main chain LC polymer [37]

In a further example of an unusual Si_8O_{12} LC architecture [40], a Kyoto University group prepared linear polymethacrylates carrying various levels of pendant Si_8O_{12} and pendant cyanobiphenyl mesogen. These polymers were prepared from mixtures of Si_8O_{12}-functionalized methacrylate monomers and cyanobiphenyl-functionalized monomers in an azobisisobutyronitrile (AIBN)-initiated free radical polymerization. The materials did not show any LC behavior until a composition of 90% cyanobiphenyl /10% POS was reached, and a smectic phase was observed by POM and DSC. Relative to the 100% pendant cyanobiphenyl polymethacrylate, the 90% cyanobiphenyl material showed improved thermal stability, and an LC phase that was stable over a wide temperature range. For cyanobiphenyl levels below 90%, no glass transitions or LC transitions were observed.

Most recently Si_8O_{12} species have been used to induce spontaneous vertical alignment in liquid crystal cells [41], thus eliminating the need for a conventional vertical alignment layer [42,43,44]. Many kinds of commercial LC display require that a nematic LC be aligned at an intermediate pre-tilt angle. A desirable decrease in switching time occurs as pre-tilt alignment angle increases from 0° to near 90°, and extremely fast response times of less than 1 ms have been achieved for some displays (e.g., no bias bend (NBB) displays). Cells were made from indium tin oxide (ITO)-coated substrates with a polyimide layer that could induce a near-horizontal pre-tilt angle of 2° for nematic LC molecules. When aminoalkyl-functionalized Si_8O_{12} was added to the LC molecule and injected into the cell, it was found that the pre-tilt angle could be controlled from 0° to 90° by varying the loading of Si_8O_{12} compound from 0 to 2 wt % [41]. This resulted from the contributions from the polyimide (imposing a pretilt angle of 2°) and from the Si_8O_{12} compound (imposing spontaneous vertical alignment after its adsorption on the inner surface of the ITO substrate). Alignment can also be achieved by doping the LC material with an azo-dye (e.g., methyl red) that adsorbs to the substrate surface when irradiated with light of an appropriate wavelength and intensity. When this approach was combined with the Si_8O_{12} approach, and both Si_8O_{12} compound and methyl red were added to the LC compound, homogenous alignments were achieved [45].

Si_8O_{12} compounds were also used to improve the response time of a holographic polymer dispersed liquid crystal (HPDLC) system [46], of importance in applications such as switchable windows, shutters and displays. HPDLCs have a periodic structure of alternating LC-rich and polymer-rich layers analogous to a diffraction grating, and can thus display volume holographic properties. They are fabricated by irradiating a mixture of LC and photosensitive monomer. A periodic composition is achieved because monomers are consumed in the irradiated areas while LCs are driven into the dark areas. Diffraction efficiency increases as the difference between the refractive index (RI) of the polymer and the LC increases, and also as the phase separation between the LC and the polymer improves. Octavinyl- Si_8O_{12} was added to a HPDLC system to obtain a fast response time, a low driving voltage, a high diffraction efficiency and a low shrinkage. SEM and AFM showed that Si_8O_{12} moieties were located at the LC-polymer interfaces.

7.2 Polyhedral Oligomeric Silsesquioxanes in Electroluminescent (EL) Materials and Light Emitting Devices (LEDs)

In 1962, blue light emission was demonstrated when anthracene was subjected to high voltages (>400 V) [47], and in 1990, a group at Cambridge [48] reported π-conjugated green light-emitting poly-*p*-phenylene-vinylene (PPV) polymers (Fig. 7.13). Some conjugated polymers were found to have electroluminescent properties [49], i.e., they emit light in the presence of an applied electric field or current, and LEDs based on low molecular mass organics (OLEDs) and polymers (PLEDs) have been widely studied [50]. Such devices comprise a cathode, an electron transport layer (ETL), an emissive layer, a hole injection layer (HIL) and an anode. Typical cathodic materials are aluminum or calcium, having suitably low work functions and low susceptiblities to oxidation. Typical anodic materials are ITO-coated glass with an ultra-high quality surface, PANI (polyaniline) and PEDOT (poly-2,3-ethylenedioxythiophene), Fig. 7.13. ITO is an important material because it is both transparent and electrically conducting. In addition, 2-(4'-*t*-butylphenyl)-5-(4'-diphenyl)-1,3,4-oxadiazole (PBD) is often used as an electron transport material and poly-N-vinylcarbazole (PVK) is often used to raise the highest occupied molecular orbital (HOMO) level in order to achieve a closer match to the HOMO level of PEDOT. Electrons come from the cathode, holes come from the anode, and electron-hole pairs form (excitons) in the emissive layer. Excitons create excited states that decay by emission of a photon. The emissive layer is of key interest, and

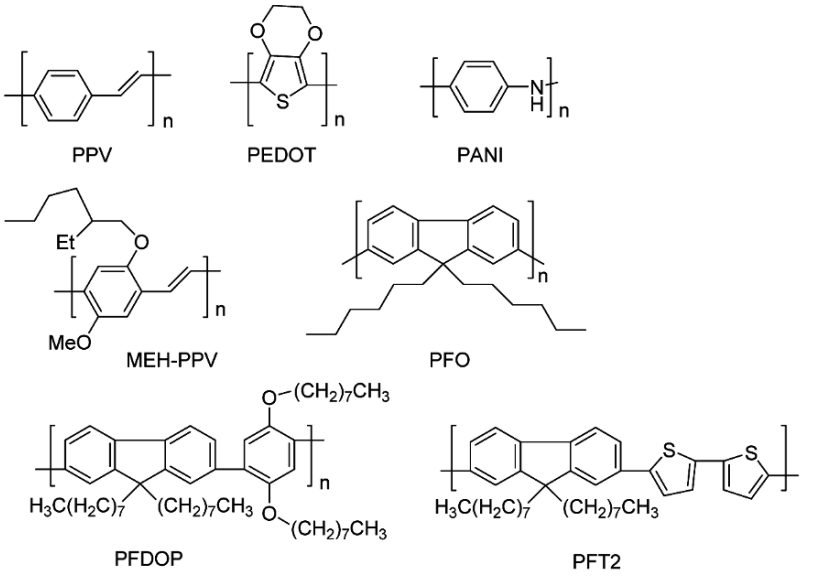

Fig. 7.13 Polymers commonly used in light emitting devices

the use of Si_8O_{12} hybrid materials to improve its performance, lifetime, stability and color balance is covered in this section [51]. Common EL polymers used in the emissive layer include poly(9,9'-dihexylfluorenyl-2,7-diyl (polyfluorene, PFO, a blue emitter [52] and poly-2-methoxy-5-[2-ethylhexyloxy]-1,4-phenylenevinylene (MEH-PPV, a yellow emitter) (Fig. 7.13). EL polymer architectures may include Si_8O_{12} as an endcapping group, as a pendant group and as a star core, and Si_8O_{12} compounds have also been introduced into these polymers as physical additives.

LEDs are currently being applied in flat display panels, and in flexible and rollable screens, leading to concepts such as 'electronic paper' (since LEDs do not require backlighting); however, coating large areas without defects in the fabrication of larger displays remains a challenge. In contrast to LCD devices, LEDs have far higher image quality, resolution and brightness (>2000 cd m^{-2}), plus better viewing angles (approaching 180°) and faster switching speeds (0.01 ms and 10 kHz refresh rate). LEDs are also used as low-power white light sources, where the emissions of two or more materials that emit at different wavelengths are combined to produce white light. White light emitting diodes are of interest for full-color displays (via color filters), as backlights for liquid crystal displays, and as light-emitting sources. Some white light emitting devices require complex fabrication one layer (i.e., one color) at a time. OLED performance parameters include wavelength (color of light emitted), luminance (a brightness greater than 10,000 cd m^{-2} is desirable), EQE (external quantum efficiency, probability that one electron will result in the emission of one photon, greater than 10% is desirable), Commision International de l'Eclairage (CIE) coordinates (relative intensities of red, green and blue emission), turn-on voltage, drive voltage and luminescence half life (greater than 10,000 hours is desirable).

Semi-conducting polymers have been widely studied for use in electroluminescent displays, solar cells, photovoltaics, sensors, thin film organic transistors, lasers and light-emitting electrochemical cells. However, the formation of aggregates, excimers and polaron pairs can degrade performance in these applications. Strategies to address this include increasing the molecular mass of the polymer, decreasing its polydispersity, introducing asymmetry (e.g., *cis*- or *meta*-linkages), or end-capping with a bulky group such as Si_8O_{12}. The introduction of Si_8O_{12} is known to stabilize color at high temperatures [53,54,55]. This is important since device temperatures can go up to 90 °C. Blue light emission has been the most problematic area in conjugated polymer organic light emitting device (OLED) research. PFO (Fig. 7.13) and its derivatives are widely used as blue light emitters because they have high solid-state quantum yields, good solubility, and good chemical and thermal stability. However PFO also has low energy emission bands resulting in the emission of undesirable blue-green light, and in quenching. Blue-green emission is caused by chain aggregation and formation of lower wavelength emitting excimers, and also by fluorenone defects. Many attempts have been made to stabilize PFO, and one approach has been to introduce Si_8O_{12} into the structure, where the enhanced thermal stability conferred by the presence of Si_8O_{12} reduces the tendency of fluorenone defects to form at higher temperatures.

7.2.1 Polyhedral Oligomeric Silsesquioxane End-capped EL Polymers

Heeger and co-workers [56] at the University of California (Santa Barbara) first introduced Si_8O_{12} onto the chain ends of PFO and MEH-PPV, two well-established EL polymers (Fig. 7.13), in 2003. Si_8O_{12}-endcapped MEH-PPV (DP=2000) and Si_8O_{12}-endcapped PFO (DP=500) were prepared with molecular masses in the region of 100,000, determined by both elemental analysis for silicon and by size exclusion chromatography (SEC). The Si_8O_{12}-MEH-PPV polymer was prepared by reaction between aryl chloride monomer and aryl chloride-functionalized Si_8O_{12} in the presence of potassium *t*-butoxide, and the Si_8O_{12}-PFO polymer was prepared in a Yamamoto coupling reaction between aryl bromide PFO monomer and aryl chloride functionalized Si_8O_{12} in the presence of bis(1,5-cyclooctadiene)-nickel(0) catalyst. Thermogravimetric analysis (TGA) showed that the presence of Si_8O_{12} end groups improved thermal stability by 50 °C. Solubility in organic solvents was also improved. The Si_8O_{12} end-capped materials and their Si_8O_{12}-free analogs had identical EL spectra. At 100 mA cm^{-2} in an ITO/PEDOT/polymer/Ca/Ag device, MEH-PPV- Si_8O_{12} gave a luminance of 1320 cd m^{-2} while MEH-PPV alone gave a luminance of 230 cd m^{-2}. These performances were rationalized in terms of better injection and transport of charge carriers. The Si_8O_{12} materials had improved coating quality, fewer pinholes and showed better adhesion to the substrate. The PFO - Si_8O_{12} polymer gave reduced excimer emission (i.e., the undesired blue-green color at 525 nm) relative to PFO itself. The same group filed a 2003 American Dye Sources, Inc. patent of broad scope that covered conjugated optoelectronic polymers (e.g., polypyrroles, polyacetylenes, polyphenylenes, polyphenylenevinylenes, polythiophenes, polyfluorenes and polyanilines) with bulky groups (organic or inorganic) in the polymer backbone or pendant to the backbone, with at least one silsesquioxane moiety serving as an anchor for the polymer [57].

Blue-emitting devices based on an Si_8O_{12} end-capped PFO (poly-9,9'-dioctylfluorene variant) were also reported by another group four years later [58]. The devices had an ITO/PEDOT:PSS/PVK/PFO-Si_8O_{12}/LiF/Al structure. The effect of plasma treatment and/or heat treatment upon the ITO surface was studied by atomic force microscopy (AFM). The best luminance and current density values were obtained when both plasma treatment and heat treatment were carried out (486 cd m^{-2} and 0.55 cd A^{-1}), and plasma treatment was shown to contribute more to performance than heat treatment. The presence of a PVK hole injection and transport layer resulted in a reduction of the intensity of undesirable PFO excimer emission. The ITO substrate is commonly treated with hydrogen peroxide-ammonium hydroxide-water (1:1:5 v/v) followed by ultrasonic cleaning with isopropanol and water, and polymer layers are applied by spin-coating and inorganic layers are applied by chemical vapor deposition. Further work [59] was reported on Si_8O_{12}-endcapped poly(9,9'-dioctylfluorenyl-2,7-diyl) in a study of current-voltage and luminance current characteristics of devices in which aluminum(III) tris(8-hydroxyquinoline) (Alq3) was assessed as an electron transport layer directly below

an uppermost Mg:Ag/Ag layer.

7.2.2 EL Polymers with Pendant Polyhedral Oligomeric Silsesquioxane Groups

The first example of a conjugated polymer carrying a pendant Si_8O_{12} group [60] was reported in 2004 by Shim and co-workers at the Korea Advanced Institute of Science and Technology. A PFO carrying pendant Si_8O_{12} groups was synthesized in a nickel(0)-mediated Yamamoto coupling reaction using a Si_8O_{12}-functionalized monomer (Fig. 7.14, monomer **1**). The Si_8O_{12}-functionalized monomer was itself prepared in a hydrosilylation reaction between $Si_8O_{12}(cyclopentyl)_7H$ and a diallyl-functionalized aryl bromide monomer. Poly-9,9'-dihexylfluorene-poly-9,9'-di- Si_8O_{12}-fluorene copolymers of various compositions (1, 2, 5, 10 and 20% Si_8O_{12} units) were then prepared. They have good solubility in organic solvents and could be readily spin-coated into high quality thin films. Photoluminescene spectroscopy on polymer-coated quartz substrates showed reduced aggregation and excimer formation, resulting from the large Si_8O_{12} group causing steric hindrance and reducing inter-chain interactions. Higher quantum yields and improved stability after thermal annealing (up to 150 °C) relative to PFO were also observed. A stable blue-emitting device was fabricated with the layer structure: ITO/PEDOT-PSS (40 nm)/pendant Si_8O_{12}-polyfluorene 20% (80 nm)/Ca(500 nm)/Al(800 nm). No green emission (500-600 nm) was observed. The HOMO and LUMO energy levels of the polymers were determined by cyclic voltammetry, and it was shown that the presence of Si_8O_{12} did not affect the redox properties of the polymers. In this study [60] each C9 position carried two Si_8O_{12} groups (Fig. 7.14). In a study by the same group published the following year, PFOs with one Si_8O_{12} group and one hexyl group at the C9 position were synthesized using an analogous synthetic route, and copolymers containing 5, 10 and 20% Si_8O_{12}-carrying repeat units were prepared [50]. In another 2005 study [61], the Shim group attached pendant Si_8O_{12} groups to photoluminescent blue-emitting poly-9,9'-dioctyl-2,7-fluorene-*alt*-2,5-bis(octyloxy)-1,4-phenylene (PFDOP) and poly-9,9'-dioctylfluorene-*alt*-bithiophene (PFT2) polymers (Fig. 7.13) in palladium-catalyzed Suzuki coupling reactions using Si_8O_{12}-functionalized aryl bromide monomers [61]. Once again, chain aggregation decreased, quantum yields were enhanced, thermal color stability increased and brighter devices were fabricated.

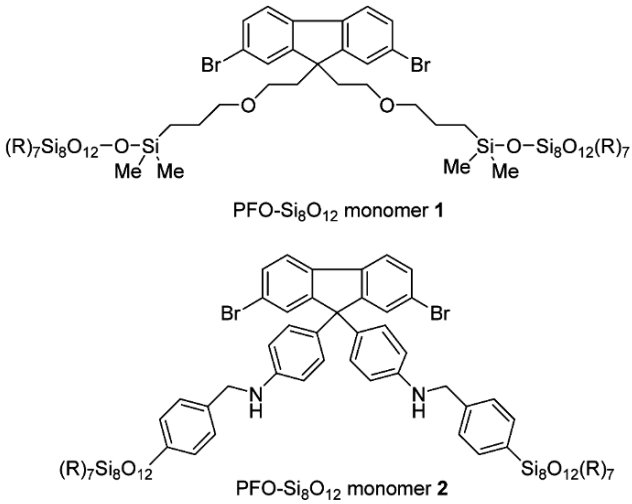

Fig. 7.14 PFO- Si_8O_{12} monomer **1** [60] and PFO- Si_8O_{12} monomer **2** [55]

Six months after the 2004 Shim study discussed above, an alternative PFO with C9-pendant Si_8O_{12} groups (Fig. 7.14, monomer **2**) was reported by Wei and co-workers [55] at National Chiao Tung University (Taiwan); hence both the Shim and Wei materials have been claimed as the first pendant- Si_8O_{12} PFOs. The Wei polymer was prepared in a palladium-catalyzed Suzuki coupling, where $Pd(PPh_3)_4$ and Si_8O_{12}-functionalized aryl bromide monomers were used. Once again, the presence of Si_8O_{12} reduced inter-chain aggregation and prevented the formation of keto defects. In PFO, the C9 position is most readily modified to enhance solubility in organic solvents. In this structure (Fig. 7.14), undesirable C9-benzyl- Si_8O_{12} links prone to photoxidation are avoided. Molecular mass decreased as the proportion of POS-functionalized monomer in the polymer increased (M_n = 27,000 for PFO versus M_n=12,000 at 10% pendant- Si_8O_{12} PFO copolymer). This was attributed to steric hindrance during polymerization. PFO had a T_g of 62 °C while no T_g was observed for the 10% pendant- Si_8O_{12} copolymer. The photoluminescence maxima for PFO and 10% pendant- Si_8O_{12} PFO copolymer were the same, but the quantum yield for 10% Si_8O_{12} copolymer was 54% higher than that of pure PFO.

The following year, Wei and co-workers carried out a second study [54] comparing a pendant- Si_8O_{12} EL polymer with the Si_8O_{12}-free EL polymer. In this case, pure MEH-PPV (Fig. 7.13) was compared with pendant-POS-PPV-*co*-MEH-PPV, a copolymer of poly-*p*-phenylenevinylene with pendant Si_8O_{12} units and MEH-PPV. The former had a quantum yield of 0.19 while the latter had a quantum yield of 0.85. With 10% Si_8O_{12}-PPV content, an ITO/PEDOT/polymer/Ca/Al device was five times brighter than the MEH-PPV control device (2196 cd m^{-2} versus 473 cd m^{-2}). As before, Si_8O_{12} was introduced by using an Si_8O_{12}-functionalized monomer, but on this occasion a Gilch polymerization route was followed, using

benzyl bromide monomers and potassium *t*-butoxide. Introduction of 10% Si_8O_{12} units lowered M_n from 61,000 (pure MEH-PPV) to 39,000. Both MEH-PPV and the 10% pendant- Si_8O_{12} copolymer resulted in devices with a yellow EL emission peak at 590 nm.

In 2005, Takagi and co-workers (Nagoya Institute of Technology, Japan) reported another PFO variant carrying pendant Si_8O_{12} groups [62], where the C9 position carried two Ph-O-Ph-CH_2CH_2- Si_8O_{12}(cyclopentyl)$_7$ groups, and the polymer was prepared in another palladium-catalyzed Suzuki coupling reaction. These polymers were compared to PFO variants carrying C9 trimethylsilyl groups. The Si_8O_{12} polymers maintained strong blue emission even after thermal annealing, whereas the trimethylsilyl polymers showed an undesirable green emission that became stronger after annealing. In 2006, Fan, Huang and co-workers (Fudan University, Shanghai) made hybrid Si_8O_{12}-tethered polyfluorenylene-ethynylene (PFE) materials [63] in Sonagashira coupling reactions using di-bromo-fluorene monomers carrying two pendant Si_8O_{12} groups (as per Fig. 7.14). WAXD showed that introduction of Si_8O_{12} increased the interchain distance, and quantum yields and thermal stability were improved relative to the Si_8O_{12}-free PFE analog.

Recently, the introduction of Si_8O_{12} into a hyperbranched EL polymer architecture [64] has also been reported to improve electroluminescence, photoluminescence quantum yield and thermal stability relative to a linear Si_8O_{12}-free EL polymer analog. Iron(III) chloride oxidative polymerization was used to combine 4,7-bis(3-ethylhexyl-2-thienyl)-2,1,3-benzothiadiazole and octa(3-ethylhexyl-2-thienyl-phenyl)- Si_8O_{12} monomers to give a hyperbranched architecture, and both the linear and HB polymers in this study gave an EL maxiumum at 660 nm.

In many of the nickel (Yamamoto) and palladium (Heck or Suzuki) coupling chemistries above, it is worth noting the importance of removing any residual metal catalyst, since metal residues are detrimental to OLED performance; in this respect, small organics that can be purified by flash column chromatography are advantageous (see later sections).

7.2.3 EL Star Architectures with Polyhedral Oligomeric Silsesquioxane Cores

A number of electroluminescent star species with Si_8O_{12} cores have been described in the literature, and the use of this architceutre in EL, optoelectronic and photovoltaic applications has recently been reviewed [65]. In 2001 the Laine group at the University of Michigan filed a patent claiming hybrid LED materials where hole transport groups, electron transport groups or emissive moieties were attached to an Si_8O_{12} core [66], and in 2004 Jabbour (Arizona State University) and co-inventors filed a patent [67] claiming one or more luminophores (e.g., 2,7-bis-(2,2-diphenylvinyl)fluorene for blue emission or pyran-4-ylidene malononitrile for red emission) attached to a nanoparticle core (e.g., Si_8O_{12}) for the purpose of achieving

white light-emitting devices. In this section, Si_8O_{12} cores functionalized with EL polymers and Si_8O_{12} cores functionalized with small aromatics are reviewed.

In 2004, Chen and co-workers at National Taiwan University (Taipei) synthesized a star polymer with an Si_8O_{12} core and PFO arms in an attempt to produce an EL material with higher Si_8O_{12} content than a Si_8O_{12} end-capped linear EL polymer [53]. High molecular mass is desirable in a linear EL polymer, but such polymers only have 1 wt % POS content [56]. However, when PFO is attached to the eight corners of POS in a star architecture, 3.8 wt % content is possible. Another Yamamoto bis-1,5-cyclooctadiene-nickel(0)-catalyzed coupling reaction was used, this time between octa(2-(4-bromophenyl)ethyl)octasilsesquioxane ($POS(CH_2CH_2PhBr)_8$) and aryl bromide-terminated polydioctylfluorene [53]. When used in a device, the star polymer had a quantum yield and a maximum luminescence intensity twice as large as the pure PFO control (5430 cd m^{-2} versus 2510 cd m^{-2}). Since both the linear polyfluorene and the octa-functional Si_8O_{12} carried aryl bromide functionality, the structure of the resulting material was ambiguous (i.e., the number of arms per Si_8O_{12} and the molecular mass of the arms were undefined); however approximately 75% of the crude product was soluble, making it possible for devices to be fabricated by spin-coating the EL layer from xylene.

In 2008, a University of Nantes (France) group made green-emitting hybrid Si_8O_{12}-DP-PPV materials [68]. An ITO/PEDOT:PSS/Si_8O_{12}-DP-PPV/Ca/Al device was fabricated [69], where Si_8O_{12}-DP-PPV was poly-2,3-diphenyl-1,4-phenylenevinylene (Fig. 7.13) grown from an Si_8O_{12} core. This was then studied by charge-based deep-level transient spectroscopy (Q-DLTS), a technique for observing defect states and traps in LED devices. Traps associated with the inorganic or the organic parts of the hybrid Si_8O_{12}-DP-PPV material were assigned on the basis of their capture cross sections.

However, the majority of Si_8O_{12} star species are comprised of an Si_8O_{12} core functionalized with small organic emitters rather than polymeric arms [53]. Since free aromatics have a tendency to assemble into π-stacks (causing excimer emission, and impacting electronic and photonic performance), the original rationale for producing Si_8O_{12}-aromatic stars was to keep the aromatics apart, and to prevent aggregation [70,71,72]. In 2004, He and co-workers (Institute of Materials Research and Engineering, Singapore) [70] claimed the synthesis of the first luminescent organic clusters displaying the same properties as inorganic quantum dots (Fig. 7.15, top left and top right), but without the disadvantage of dot size distribution resulting in line-broadening. These were synthesized from $Si_8O_{12}(PhBr)_8$ and the appropriate brominated aromatics in palladium-catalyzed coupling reactions, and thin films of the Si_8O_{12} compounds showed enhanced photoluminescence (PL) quantum yields relative to the analogous free aromatics. Si_8O_{12} was selected as a scaffold because of its thermal stability, low dielectric constant (~2.7) and its high band gap (6.0 eV absorption and 4.2 eV emission). Later quantum dot compounds [73] incorporating longer sequences of phenyl groups (Fig. 7.15, bottom left) also showed enhanced PL quantum efficiency and improved film forming properties. In 2005, the Laine group at University of Michigan reacted bromophenyl- Si_8O_{12} with various aryl-

boronic acids, $(HO)_2B$-Ar, in $Pd(PPh_3)_4$-catalyzed coupling reactions [71]. In this way, phenyl, biphenyl, naphthyl, thiophene and 9,9-dimethylfluorene were attached to Si_8O_{12} cores. MALDI-TOF spectra showed that these compounds had a distrubtion of compositions corresponding to the distribution (varying numbers of bromine atoms) in the bromophenyl- Si_8O_{12} starting materials. The absorption and emission spectra of these materials showed them to behave as conventional organic aromatics rather than quantum dots [70], and this was attributed to the distribution of compositions, although the distribution of compositions of $Si_8O_{12}(PhBr)_8$, or possible lack thereof, was not reported in He's 2004 study [70]. The effect of an Si_8O_{12} substituent on the absorption and emission wavelengths of the aromatic was unclear in the 2005 University of Michigan study [72], with a red shift being reported for the aromatics above, but a blue shift being reported for stilbene. Recently a Korean group synthesized an EL Si_8O_{12} material carrying eight anthracenenaphthyl groups via hydrosilylation between $Si_8O_{12}(OSiMe_2H)_8$ and the allyl-functionalized aromatic, and used the material to fabricate a blue-emitting device [74].

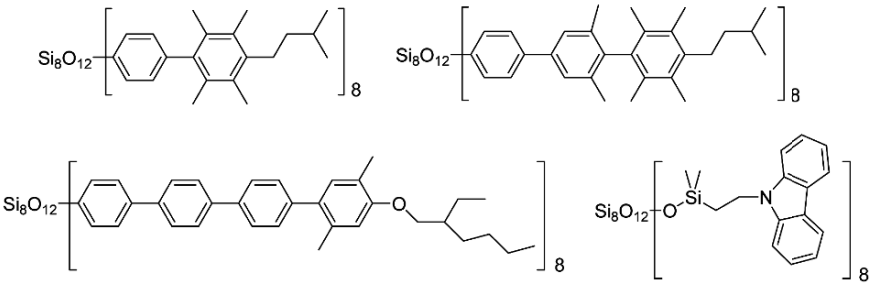

Fig. 7.15 First Si_8O_{12} 'quantum dot' compounds (top) [70], a later dot (bottom left) [73], and a carbazole-functionalized Si_8O_{12} (bottom right) [75]

Another early example of a small molecule star species with an Si_8O_{12} core [76] was synthesized by the Laine group at the University of Michigan in 2005. In contrast to the Si_8O_{12}-PFO star species above [53] that carried oligomeric PFO arms, in this material a small organic aromatic hole transport compound, FL03 (*N*4-(9,9-dimethyl-9*H*-fluoren-7-yl)-*N*4'-(9,9-dimethyl-9*H*-fluoren-2-yl)-*N*4,*N*4'-diphenylbiphenyl-4,4'-diamine), was coupled to octavinyl- Si_8O_{12} in a Heck reaction with a monobromo-FL03 derivative and a $Pd(P(t\text{-}Bu)_3)$ catalyst (Fig. 7.16, top). Small organics can be obtained with greater purity than polymers, but require vacuum deposition techniques to fabricate displays. Vacuum deposition is expensive and is only practical for small displays. Polymers can be deposited from solution using efficient and industrially scalable techniques such as ink-jet printing to form large surface area displays, but are less pure than small organics. Hence the rationale of this study was to achieve a solution-processable but high purity (monodisperse) OLED material by attaching a small organic OLED entity to an Si_8O_{12} core via a rigid link. Flexible links have been used to attach mesogens to Si_8O_{12} cores in liquid crystalline materials [15,27,30] (as discussed in the previous section) but crystalline domains are undesirable in OLED materials because they result in charge trapping.

The resulting Si_8O_{12}-FL03 star carried 3 to 10 FL03 units per Si_8O_{12} (i.e., some double Heck reactions took place), and exhibited intense blue photoluminescent emission at ~430 nm. When devices fabricated using Si_8O_{12}-FL03 were compared to devices fabricated using pure FL03, the Si_8O_{12}-FL03 devices were brighter and had higher external quantum efficiencies. In another 2005 study [75] by Kawakami and Imae (Japan Advanced Institute of Science and Technology, Ishikawa), Si_8O_{12} was functionalized with carbazole (a photoactive and electroactive π-chromophore, Fig. 7.15, bottom right) in a hydrosilylation reaction between octahydrido- Si_8O_{12} and *N*-vinyl carbazole. Elemental analysis showed it to be a pure octa-substituted compound, in contrast to the mixed compositions above [76]. The Si_8O_{12}-carbazole compound showed a single strong emission peak in the solid state, and no excimer emission.

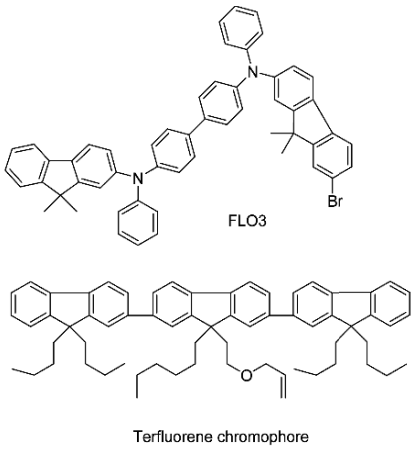

Fig. 7.16 FL03 reagent [76] and terfluorene chromophore [77] used to prepare POS-cored star species

In 2006, Shim and co-workers [77] at the Korea Advanced Institute of Science and Technology synthesized a blue-emitting Si_8O_{12} with terfluorene (FL3) chromophores on each of the eight corners (Fig. 7.16, bottom). This Si_8O_{12}-FL3 star was then doped into PFO. Si_8O_{12}-FL3 was prepared in a platinum-catalyzed hydrosilylation reaction between octakis(dimethylsiloxy)- Si_8O_{12} and allyl-functionalized terfluorene (Fig. 7.16, bottom) which itself required a six step synthesis [77]. This compound also showed good solubility and thin film-forming abilities. The maximum blue emission wavelength of Si_8O_{12}-FL3 (394 nm in THF solution) overlaps well with the maximum absorption wavelength of PFO (391 nm in THF solution), making it suitable for use as a dopant for blue light emitting polymers, and increasing quantum efficiency via energy transfer. This also applies in the solid state. EL devices (analogous to those described above) fabricated from Si_8O_{12}-FL3-doped polyfluorenes showed a four- to eight-fold increase in quantum efficiency relative to the non-doped PFO EL device. This was explained in terms of Si_8O_{12} disruption of terfluorene aggregation in this system. It is notable that an energy transfer from a shorter-wavelength blue emissive material to a longer-

wavelength blue emissive material is being reported.

By 2007, a light-emitting pyrene-functionalized Si_8O_{12} had been reported with an external quantum efficiency (EQE) of 2.6% [78]. In addition an Si_8O_{12} core had been functionalized with two different emitters in a controlled ratio, and multiple-wavelength emitting Si_8O_{12} materials had been synthesized [79]. Si_8O_{12} cores functionalized with a combination of hole transport groups, electron transport groups and at least one cross-linkable group, and light-emitting devices incorporating these Si_8O_{12} compounds were also claimed in a 2007 patent [80].

7.2.4 Polyhedral Oligomeric Silsesquioxane Iridium Complexes

An important subset of EL Si_8O_{12}-cored star species are those functionalized with iridium complex emitters. Heavy metal ions such as osmium, iridium and platinum are used in phosphorescent LEDs because they facilitate singlet to triplet intersystem crossing (ISC) via spin-orbit coupling, and can harvest singlet and triplet excited states. Cyclometalated iridium complexes have been used to produce high efficiency systems where wavelength tunability across the visible spectrum has been achieved by varying the cyclometalating ligand.

In 2009, Jabbour (Arizona State University), Mochizuki (Nitto Denko Corporation) and co-workers reported a system where carbazole hole transporters and iridium complexes (Fig. 7.17) were attached to the same Si_8O_{12} scaffold in hydrosilylation reactions between vinyl-functionalized iridium complexes and SiH-functionalized Si_8O_{12} species [81]. Two series of materials were prepared. In the first series, monochromatic emitters were based on an Si_8O_{12} core carrying seven cyclopentyl groups and one iridium complex (Fig. 7.17). White-emitting devices were then fabricated by combining three Si_8O_{12} (cyclopentyl)$_7$(iridium) compounds of this type, carrying the three different iridium complexes, Ir-(fppy)$_2$- Si_8O_{12} (blue, 470 nm), Ir-(ppy)$_2$- Si_8O_{12} (green, 500 nm) and Ir-(pq)$_2$- Si_8O_{12} (red, 587 nm). In the second series, emitters based on an Si_8O_{12} core carrying one iridium complex and seven carbazole groups were prepared by stepwise stoichiometric hydrosilylation with a one equivalent of vinyl-functionalized iridium complex followed by seven equivalents of *N*-allylcarbazole. A distribution of products was obtained, but these could be separated chromatographically. The mononchromatic OLEDs had EQEs of 5 to 9% and the white light-emitting OLEDs had EQE's of 8%. In 2009, the same group [82] synthesized an electroluminescent Si_8O_{12} star compound carrying an iridium complex (Fig. 7.18) and used it in an ink-jet fabrication of an LED device that had a peak luminance of 10,000 cd m^{-2} and a peak quantum efficiency of 2.5%.

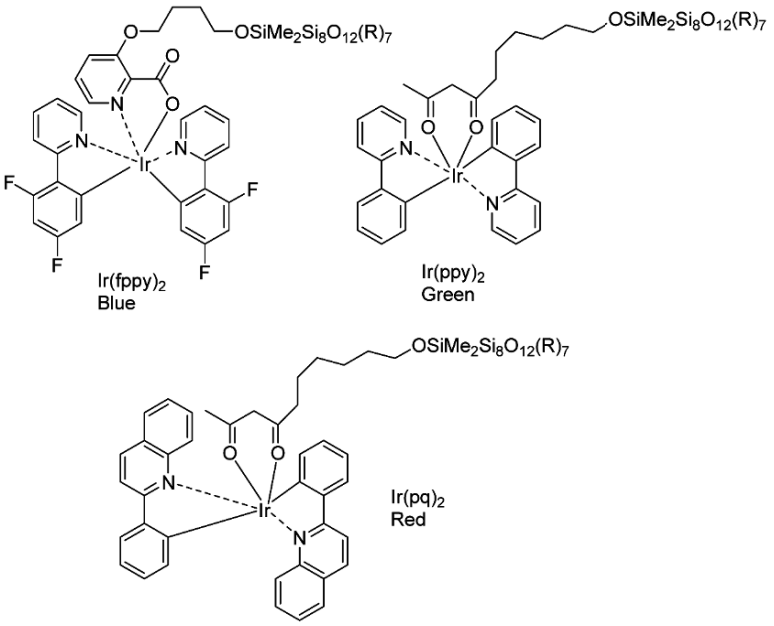

Fig. 7.17 Si_8O_{12} functionalized with various iridium complex emitters [81]

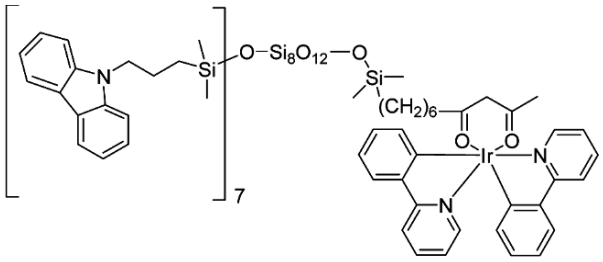

Fig. 7.18 Iridium-based Si_8O_{12} star dye used in ink-jet fabrication process [82]

In an earlier 2006 study, Hsu and co-workers (National Chiao Tung University, Taiwan) reported an Si_8O_{12} core functionalized with iridium(III) bis(2-phenylpyridine-C2-N')(13-terdecenylacetonate) had been added to CBP (4,4-*N*,*N*'-dicarbazole-biphenyl) and TPBI (1,3,5-tris-2-*N*-phenylbenzimidazoylbenzene), and used in an OLED device [83]. Three Si_8O_{12}-cored star light-emitting materials were prepared by reacting octasilane-POS with three allyl-functionalized conjugated light-emitting moieties (Fig. 7.19) in hydrosilylation reactions. SEC data suggested that five to eight chromophores were attached to the Si_8O_{12} core. All three materials had good solubility in organic solvents and could be spin-coated to form high quality films, and to fabricate devices (Table 7.2). The triplet Si_8O_{12}-**3** material (Fig. 7.19) was blended with a 4,4-*N*,*N*'-dicarbazole-biphenyl (CBP) host to prevent

quenching.

Table 7.2 Characteristics of various devices incorporating Si_8O_{12}-star EL species [83]

Device	Color / λ^{EL}_{max} (nm)	Maximum brightness (cd m^{-2})	Maximum current yield (cd A^{-1})
ITO/PEDOT/ Si_8O_{12}-**1**/Ca/Al	496 (Green)	115	0.07
ITO/PEDOT/ Si_8O_{12}-**1**, 0.8 wt % PBD/Ca/Al	496	1469	0.8
Si_8O_{12}-**2**	476 (Blue-green)	70	0.02
Si_8O_{12}-**2** + 0.8 wt % PBD	476	1102	0.88
Si_8O_{12}-**3**	524 (Green)	1008	1.04
Si_8O_{12}-**3** + 18 wt % CBP	524	1172	3.99

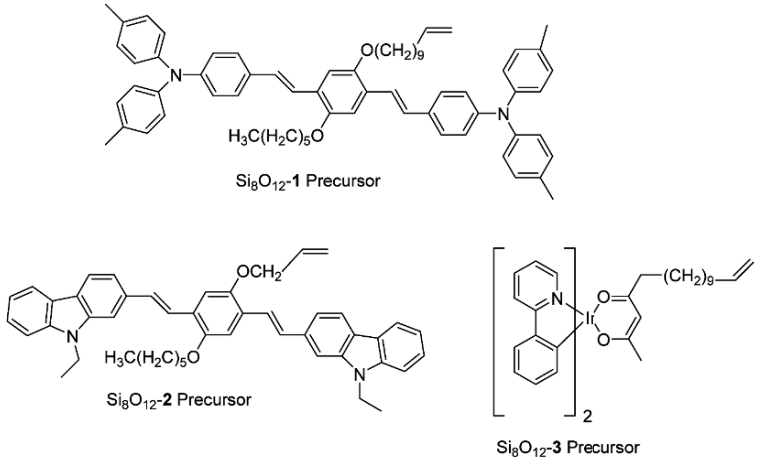

Fig. 7.19 Allyl precursors used to prepare Si_8O_{12}-cored stars [83]

In 2005, Peng and co-workers at South China University of Technology (Guangzhou) co-doped a blue emitting Si_8O_{12}-terminated PFO host (EL at 424 nm) with two phosphorescent iridium complex guests, green-emitting $Ir(Bu\text{-}ppy)_3$ (EL at 510 nm, where Bu-ppy denotes 2-4'-*t*-butylphenylpyridine) and red-emitting $(Piq)_2Ir(acaF)$ (EL at 610 nm, where acaF denotes 1-trifluoro acetylacetonate) in order to fabricate a white light-emitting diode [84]. The EL peaks appeared at slightly different wavelengths than those observed in the EL spectra of the individual emitters. In 2006, in another South China University of Technology study [85], the iridium complex $Ir(1\text{-}piq)_2pt$ was synthesized, where 1-piq denotes 1-phenylisoquinoline and pt denotes 3-(pyridin-2'-yl)-1*H*-1,2,4-triazole. This complex was added to an Si_8O_{12}-terminated PFO host polymer, and an ITO/PEDOT/

PVK/2% Ir complex-PFO- Si_8O_{12}-PBD/Ba/Al electrophosphorescent device was fabricated that had red emission at 605 nm, a quantum efficiency of 10.4% and a luminous efficiency of 9.4 cd A^{-1} at 10.8 mA cm^{-2}.

It is also interesting to note that luminescent iridium-Si_8O_{12} compounds have been used in oxygen sensing (see also discussion of sensor applications in Section 7.5). An Si_8O_{12} core carrying eight Ir(ppy)$_2$(cs-acac) groups was synthesized via reaction of the cs-acac (non-8-ene-2,4-dione) alkene groups, and different luminescent responses in the presence of nitrogen and oxygen were observed [86].

7.2.5 Physical Blending of Polyhedral Oligomeric Silsesquioxanes into EL Polymers

Si_8O_{12} has also been introduced into the EL layers of devices by physical blending (rather than by chemical attachment to EL materials, as per Sections 7.2.1 to 7.2.4), following work where silica or titanium dioxide nanoparticles were introduced into PPV films in OLEDs [87,88,89]. Physical blending has the advantage of being simple relative to the chemical introduction of Si_8O_{12}, where multistep synthetic and purification procedures are often required. In a 2006 study by Gong and co-workers at the University of California at Santa Barbara [90], Si_8O_{12} carrying one chloro group and seven cyclohexyl groups was physically blended into MEH-PPV at 0.5 wt %, and the resulting ITO/PEDOT:PSS/MEH-PPV:POS/Al device had a luminous efficiency of 1 cd A^{-1}. The improvement in performance was attributed to enhanced electron injection into the emissive layer associated with ionic conductivity contributed by Si_8O_{12}, although the identity of the ions and mechanism of conduction were not clearly defined. An ITO/PEDOT:PSS/MEH-PPV- Si_8O_{12}/Al device was used as a control, where Si_8O_{12} was present as a chemically bound end group on MEH-PPV rather than as a physical additive.

In a later 2007 study [91] by Lee and Lai at National Yunlin University (Taiwan), $Si_8O_{12}(OSiMe_2CH_2CH_2Ph)_8$ was physically blended with MEH-PPV at 5, 10 and 30 wt % Si_8O_{12} to fabricate composite films that were characterized by AFM and evaluated in devices (Table 7.3). It was shown that POS and MEH-PPV were highly compatible, and that surface roughness increased with increasing Si_8O_{12} content. Thus the interfacial area between the light-emitting layer and the cathode was increased, resulting in enhanced electron injection from the cathode, increased electron-current density and improved current efficiency. The presence of Si_8O_{12} also resulted in deceased hole-current density, showing that Si_8O_{12} compounds functioned as hole-trappers. The EL emission wavelength at 590 nm remained constant with varying Si_8O_{12} content, but intensity decreased with increasing Si_8O_{12} content. The intensity of excimer emission at 630 nm decreased with increasing Si_8O_{12} content. At high Si_8O_{12} contents thickness decreased and current leakage increased.

Table 7.3 Characteristics of various devices incorporating physically blended Si_8O_{12} species in the EL layer [91]

Device	Color / λ^{EL}_{max} (nm)	Maximum brightness (cd m^{-2})	Maximum current yield (cd A^{-1})
ITO/PEDOT/MEH-PPV 0% Si_8O_{12}/Ca/Al	593	2946	0.78
MEH-PPV 5% Si_8O_{12}	592	2376	0.83
MEH-PPV 10% Si_8O_{12}	592	1962	1.06
MEH-PPV-30% Si_8O_{12}	590	1693	1.10

Hence the use of Si_8O_{12} to improve the stability and electroluminescent properties of LEDs has become so well established that Si_8O_{12} materials are used as the default when other materials and variables associated with LED performance are being studied [59,69,85], and Si_8O_{12}-terminated PFO is now so successful as a blue EL material that it is commercially available from companies such as American Dye Sources, Inc. (Quebec, Canada).

7.3 Polyhedral Oligomeric Silsesquioxanes in Non-linear Optic (NLO), Optical Limiting (OL) and Laser Applications

Despite the extensive work done on Si_8O_{12} in LC and EL applications (Sections 7.1 and 7.2), very little work has been done in the related area of non-linear optical (NLO) materials. Sol-gel techniques have been used to prepare NLO hybrid materials comprised of an NLO component, e.g., an azo dye [92,93], a Disperse Orange 3 chromophore [94,95], nitroanilines [96] or *N*-4-nitrophenol-L-prolinol [97], and either a silsesquioxane or TEOS-derived silica component [98,99], with the aim of maintaining NLO properties while improving thermal post-poling orientation stability. Poling is carried out by exposing the material to an electric field (2-5 kV cm^{-1}), and the dipoles of the chromophores align in the direction of the field. In hybrid silsesquioxane-organic materials, refractive index and optical loss can be reduced with increasing silsesquioxane content [100]. A ladderlike polysilsesquioxane carrying stilbene chromophores (Me_2N-Ph-CH=CH-Ph-NO_2) was poled in-situ during film formation, and the film was found to have more stable poling-induced orientation than the analogous linear polysiloxane [101]. Stilbene chromophores were attached side-on (at a C=C group) or end-on by hydrosilylation with polyhydridosilsesquioxane. The less mobile the orientated NLO groups are, the greater the thermal stability of the second order non-linear response will be. This has been achieved by poling before or during cross-linking and then stabilizing

the orientation after complete cross-linking has occurred. Hence sol-gel chemistry offers one route to cross-linking and 'fixing' chromophores in position.

Another area of increasing importance is that of optical limiting (OL) materials [102,103], a class of NLO materials that are transparent under normal conditions, but become opaque in response to high energy laser pulses. These materials are useful for protecting the human eye, and also various optical sensors, from laser damage, and exhibit a decrease in transmission when the energy of an incident laser pulse increases above a certain threshold. The ideal OL material responds rapidly over a wide range of wavelengths and has a high damage threshold. Structures with π-conjgation (e.g., carbon nanotubes, fullerenes, porphyrins, phthalocyanines, various organic dyes, chromophores and organometallics) may be used as optical limiting (OL) materials [104]. However many such materials have poor solubility, processability and low thermal stability, issues that are also encountered in the EL polymer field (as discussed in Section 7.2). A series of inorganic Si_8O_{12}-organic (azobenzene) hybrid materials was prepared in order to achieve good OL properties in combination with improved solubility in organic solvents and thermal stability [105]. Three different target material architectures were prepared in hydrosilylation reactions between the di-functional azobenzene monomer and octahydrido- Si_8O_{12}. The monomer was prepared in a four-step convergent synthesis. The first was a dumbbell molecule prepared by reaction between two equivalents of $Si_8O_{12}(H)_8$ and one equivalent of monomer. The second was a linear 'bead' polymer with POS units ('beads') within the backbone and pendant azobenzene groups, prepared using a one to one molar ratio of $Si_8O_{12}(H)_8$ and monomer. The third was a network of Si_8O_{12} units connected by spacers with pendant azobenzene groups, prepared using a two to one molar ratio of monomer to $Si_8O_{12}(H)_8$. Platinum dicyclopentadiene catalyst gave soluble products in moderate yields, while platinum divinyltetramethyldisiloxane catalyst (Karstedt's catalyst) gave cross-linked gels. For all products, mixtures of α- and β-adducts were obtained, and the highest proportions of β-adducts were observed for the highest monomer molar ratios. The products were characterized by GPC, IR, ^{1}H and ^{29}Si NMR. Incorporation of the chromophores into the various Si_8O_{12} architectures did not change their UV-visible spectra or impact their OL performance. TGA showed that the hybrids decomposed at temperatures 65 to 85 °C higher than the free chromophores (5 wt % loss). Interestingly the 'bead' materials had higher thermal stability than the dumbbells or the networks, and this was attributed to their more ordered structures. OL performance was studied using 13 ns optical pulses at 532 nm with a repetition of 1 Hz from a frequency doubled Q-switched mode locked ns/ps Nd:YAG laser, and incident and transmitted laser pulses from samples in solution in a quartz cell were monitored. Non-linear optical properties were measured using a Z-scan technique and the same laser system and sample solutions. This showed that the nitro materials had non-linear absorption and non-linear refraction, while the H and methoxy materials only had non-linear refraction. Recently the same Donghua University (Shanghai) group reported an Si_8O_{12} core functionalized with eight stilbene groups that was prepared in a hydrosilylation of octahydrido- Si_8O_{12} [106]. When compared with stilbene

control OL materials, the hybrid material had comparable OL performance, but had improved thermal stability, with thermal decompositions temperatures 20 to 60 °C higher than the stilbenes.

Another example of a covalently bonded Si_8O_{12}-conjugated aromatic system used to make improved OL materials is Si_8O_{12}-metallophthalocyanine, with either cobalt(II), copper(II) or zinc(II) [107]. Two equivalents of mercaptopropyl-Si_8O_{12}(*i*-Bu)$_7$ were reacted with 4,5-dichloro-1,2-dicyanobenzene in the presence of potassium carbonate as base, in a nucleophilic aromatic substitution at the two aryl chloride sites. The product was used to synthesize the three metallophthalocyanines. Tetramerization to form the planar phthalocyanines resulted in structures carrying eight peripheral Si_8O_{12} units. The copper phthalocyanine showed significant non-linear absorption in a Z-scan measurement and promising OL performance, while the cobalt and zinc phthalocyanines showed no non-linear absorption.

Polyhedral oligomeric silsesquioxane compounds have also been used to improve the performance of laser dyes. When Si_8O_{12}(methylmethacryl)$_8$ was added to an ethyl acetate solution of the laser dye PM567, the laser action was significantly enhanced [108].This was attributed to weak optical scattering from the Si_8O_{12} compound (despite its nanometer dimensions), resulting in a phenomenon known as 'lasing with intensity feedback'. Hence the addition of the Si_8O_{12} compound at 1 wt % was reported to improve the dye laser efficiency by 65%. Similar enhancements in laser performance were seen when the same Si_8O_{12} structure was present in PM567-doped polymethyl methacrylate (PMMA) with no degradation in laser output after 100,000 pump pulses [109]. Si_8O_{12}(methylmethactyl)$_8$ and Si_8O_{12}(*i*-Bu)$_8$ were also found to enhance the laser action of other laser dyes such as Rhodamine 6G, Rhodamine 640, Sulforhodamine B and Perilene Red.

7.4 Polyhedral Oligomeric Silsesquioxanes in Lithographic Applications

Lithography has much in common with photography; a pattern is formed by exposing a chemically reactive surface to radiation, and then the pattern is fixed and stabilized in a series of additional processes [110]. The use of a polymeric resist is the most important method for the fabrication of patterns on the nano-scale, although other approaches besides nanolithography have been reviewed (e.g., imprinting and self-assembly) [111,112]. Lithography is also the method preferred by industrial fabricators of electronic and optical devices. Resists have played a key role in the steady decrease in feature size, and in the increase in memory capacity predicted by Moore's law. In a typical process, a substrate is coated with a continuous layer of resist material, and the resist is exposed to radiation through a mask having transparent and opaque regions that confer the desired pattern. The regions of the resist that are irradiated (corresponding to the transparent regions of the mask) undergo a chemical change, while the regions of the resist that are not

irradiated (corresponding to the opaque regions of the mask) remain unchanged. The unexposed regions of the resist may then be removed (in a positive process) or the exposed regions may then be removed (in a negative process). The removal of the resist is termed the development stage, as in the processing of photographic film. The surface-patterned resist may be irradiated by exposure to UV-visible wavelengths in the range 13 to 436 nm, or by exposure to X-rays, electron beams, ion beams or plasma. Hence resists must be polymeric, in order to be spin-coated into films, although film-forming molecular glasses based on lower mass species have been reported [113]. Resists must also be thermally stable, and have suitable photochemical properties such that they change their solubility upon exposure to radiation. In the chemical amplification method, exposure generates the formation of a catalyst (normally a protic acid resulting from a photoacid generator, PAG, precursor) which then catalyzes the post-exposure bake (PEB) reaction resulting in the solubility change of the resist polymer. Important parameters associated with lithographic processes include sensitivity, that is inversely related to the mJ cm^{-2} dose of radiation required to achieve exposure without loss of resolution, and line edge roughness (LER), where low LERs are desirable and are associated with good quality pattern transfer.

The irradiation wavelength favored by the semiconductor industry has gradually decreased from 436 nm, to 365 nm, to 248 nm, to 193 nm, where 90 nm resolution could be achieved at 193 nm in 2006, and 65 nm resolution could be achieved in 2009. Each new wavelength required the development of new resists with appropriate transparency at the wavelength of interest. For example, conventional aromatic polymers are unsuitable for 193 nm applications despite their chemical and thermal stability, although polyaromatics have not been ruled out owing to the lower wavelength (red shift) of their absorbance. Currently devices with 65 nm critical dimensions are being produced, and new technologies with target critical dimensions of 45, 32 and 22 nm are in development. These targets will require thinner resist films (50-100 nm) in order to maintain reasonable aspect ratios; however, thinner films have higher defect densities, and different glass transition temperatures and LERs than bulk films of the same chemical composition [110]. 157 nm lithography and 193 nm immersion lithography were both considered as the successors of 193 nm lithography in the next step toward increased resolution and ever smaller features, but 193 nm has emerged as the front runner for 45 nm and 32 nm features because of technical obstacles encountered during the development of 157 nm resists. For 22 nm features, the current favored technology is EUV (13 nm) using polycarbocyclic organic resists. In immersion lithography, an immersion fluid is used between the lens and the photoresist layer, where the immersion fluid medium confers higher resolution than air. The drawback of immersion lithography is that components of the resist may leach out into the immersion fluid, or that the immersion fluid may contaminate the photoresist.

Lithographic resist materials used for the fabrication of sub-100 nm features (e.g., 193 nm, 157 nm, 13 nm for EUV) must meet very demanding performance requirements [110]. Fluoropolymers and siloxane polymers are useful in 157 nm

systems because of their high transparency and low absorbance at this wavelength, although siloxane polymers are prone to fragmentation and to undesirable outgassing that can damage the lens. Hence polyhedral oligomeric silsesquioxanes are promising resist materials because of their transparency and increased chemical stability relative to polysiloxanes. An Si_8O_{12} cage architecture is also preferable to a polysilsesquioxane architecture because of the Si_8O_{12} monodispersity and precisely defined structure. In addition, polysilsesquioxanes carry residual SiOH functionality that can undergo condensation reactions, decrease shelf life and result in negative tone chemistry, whereas Si_8O_{12} does not. The Shipley Company (Marlborough, USA) studied the effect of polymer architecture on silicon outgassing in bilayer silicone resists in ArF and F_2 lithography [114], and it was found that an Si_8O_{12} moiety in the silicone backbone gave a high silicon content for superior etch resistance, no outgassing, and successful pattern resolution below 100 nm.

The use of Si_8O_{12} compounds as lithographic resists was originally suggested in a 1985 Russian report by Korchkov and Martynova [115], particularly as negative resists for electron and X-ray lithography. From 2000 onward [116], various resists comprised of Si_8O_{12}-acrylate copolymers (see for example Fig. 7.20) have been studied, primarily by groups at the University of Connecticut (USA) and at the Institute of Microelectronics (Athens, Greece) [116-125]. Structures and monomer ratios have been varied in order to achieve optimum properties for lithographic resists, and in some cases a combinatorial approach has been used [116]. Such copolymers have the potential disadvantage that incorporation of an Si_8O_{12} moiety changes the morphology (i.e., Si_8O_{12} domains form and phase separation occurs) relative to the Si_8O_{12}-free acrylate polymer (see Chapter 4), and thus the physical properties of the resist are affected [126]. An x-ray photoelectron spectroscopy (XPS) study showed that a 1.5 nm layer at the surface of an Si_8O_{12}-acrylate copolymer resist was rich in Si_8O_{12} relative to the bulk material below [127], and when an Si_8O_{12} copolymer was treated with oxygen plasma, ellipsometry and XPS showed that a silicon oxide layer formed at the surface [128]. This concept is further explored in Chapter 8, where Si_8O_{12} copolymers are used in space applications requiring resistance to atomic oxygen (instead of oxygen plasma).

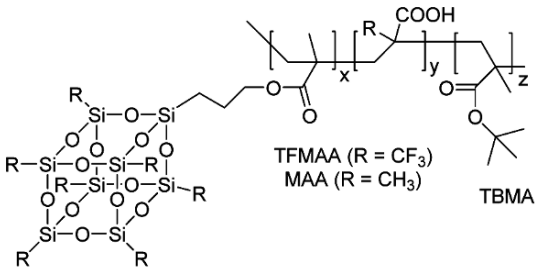

Fig. 7.20 An Si_8O_{12}-acrylate terpolymer evaluated as a resist for 193 nm bilayer lithography [129]

In a 2004 Greek-French collaboration by Argitis and co-workers [130], positive tone Si_8O_{12}-functionalized methacrylate photoresists were prepared from

acrylate-Si_8O_{12} monomers copolymerized with various combinations of other acrylate monomers (methacrylic acid, MAA, *t*-butylmethacrylate, TBMA, *t*-butyl trifluoromethylacrylate, TBTFMA, itaconic anhydride, IA and 2-(trifluoromethyl) acrylic acid, TFMAA). TBMA and TBTFMA undergo acid catalyzed deprotection reactions (where acid comes from a perfluorooctylsulfonate photoacid generator PAG) to form the carboxylic acids that undergo positive tone lithography and dissolve in basic solution, while MA and IA are hydrophilic and enhance adhesion and solubility in base. TFMAA was also selected to decrease absorbance at 157 nm. Thin films of Si_8O_{12} copolymer were spin coated from MIBK (methyl isobutyl ketone) or PGME (propylene glycol methyl ether) onto a novolac epoxy resin substrate and etched by oxygen plasma. XPS showed that undesirable aggregation of Si_8O_{12} at the surface occurred most with the Si_8O_{12}-TBMA copolymers. The best copolymers (comprised of the multiple copolymers above) were found to have high sensitivity at 157 nm (less than 10 mJ cm^{-2}), no silicon outgassing, and sub-100 nm resolution.

In a 2006 study by the same group from Athens and collaborators at Interuniversity Microelectronic Center (Leuven, Belgium), similar Si_8O_{12}-methacrylate resists were assessed in 193 nm bilayer lithography [129]. These were terpolymers prepared from methacrylate POS, TFMAA or MAA (to control degree of fluorination), and TBMA (Fig. 7.20). IA was not used as a monomer because its tendency to hydrolyze was detrimental to shelf life. Although TFMAA was not required to reduce absorbance at 193 nm (in contrast to the 157 nm case above [130]), it was found that terpolymers with high TFMAA content gave resists with the best homogeneity. A partially fluorinated terpolymer was the first example of an Si_8O_{12} resist that could be directly incorporated into the standard industrial process using tetramethyl ammonium hydroxide developer. In some cases cyclopentyl groups were used as the other (blocking) groups on Si_8O_{12} [117,121] but in this study ethyl groups were used to confer higher etch resistance and lower surface roughness [120,131]. The best homogeneity was obtained when a hydrophobic PAG anion with a long fluorinated tail was used in order to achieve the best compatibility with the terpolymer matrix. The best-performing resists had a sensitivity of 10 mJ cm^{-2}, and the most suitable substrate was found to be a novolac resin.

In a 2006 Korean study by Kim and co-workers [132], an Si_8O_{12} molecular resist carrying diazoketo groups (Fig. 7.21) was reported for use in deep UV lithographic processes. This work was carried out to avoid the use of chemically amplified resists and the associated PAGs, since PAGs are environmentally unfriendly aromatic compounds, and have poor compatibility with photoresist polymers, resulting in poor resolution. Diazoketo groups were selected to achieve deep UV photobleaching and polarity change upon exposure (where a Wolff rearrangement occurs and carboxylic acid groups are generated), and once again Si_8O_{12} was selected for its thermal and chemical stability. The polycyclic cholate moiety (Fig. 7.21) was selected because its amphilicity conferred good film-forming ability. The Si_8O_{12} molecular resist was evaluated in a single layer (positive tone) process and in a bilayer process. Spin-coating of silicon wafers was carried out from propylene glycol methyl ether, and

the exposed regions of the resist film were developed using industry standard 2.38 wt % tetramethylammonium hydroxide solution.

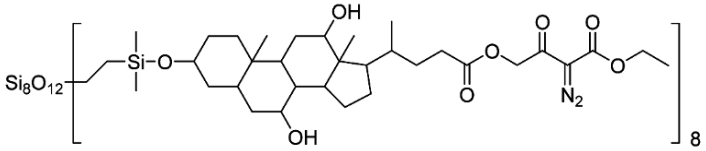

Fig. 7.21 Diazoketo Si_8O_{12} molecular resist for use in lithographic processes without photoacid generators (PAGs) [132]

In an attempt to avoid the post-exposure bake (PEB) step in conventional lithographic processes, a molecular resist comprised of Si_8O_{12} functionalized with trimethoxysilyl groups was designed [133], taking advantage of the fact that acid-catalyzed cross-linking of $Si(OMe)_3$ occurs readily at room temperature.

As well as the resist itself, Si_8O_{12} has also been used in topcoat materials for resists. A 2006 IBM Corporation patent claimed T_8, T_{10} and T_{12} polyhedral oligomeric silsesquioxane cores functionalized with groups soluble in aqueous bases (e.g., COOH, SO_3H, amides, ureas and so on) as topcoats for photoresists used in photolithography or immersion lithography [134]. The function of the topcoat was to prevent interactions between the photoresist material and the immersion fluid (see description of immersion lithography above), while being soluble in base developer and transparent at the irradiation wavelength. The materials were prepared in hydrosilylation reactions between hydrido- Si_8O_{12} species and various unsaturated cyclic aliphatics.

In a 2007 University of Texas (Austin) study [135], Si_8O_{12} functionalized with a mixture of photosensitive acrylate groups and thermally curable benzocyclobutane (BCB) groups (Fig. 7.22) was used in a step and flash imprint lithography reverse tone (SFIL-R) process. SFIL was developed in order to reduce the number of steps in the dual damascene process used to fabricate copper interconnects, where SFIL was an alternative to optical lithography [136]. In SFIL-R [137], a topcoat is applied on top of an organic imprinted layer. The topcoat must be a low viscosity and non-volatile liquid (for efficient 'filling' of the imprinted layer beneath) with a high silicon content for etch resistance, and must carry curable functional groups. In addition, in order to be compatible with a low-κ manufacturing process, the imprint material must have a low dielectric constant, thermal stability at 400 °C, high modulus, low shrinkage upon cure and low coefficient of thermal expansion (CTE).

In 1996, Laine and co-workers (University of Michigan) had reported that liquid Si_8O_{12} compounds functionalized with epoxy groups could be used as photochemically curable materials [138], and thus had potential for use in an SFIL process. In the 2007 Texas work [135], an Si_8O_{12} starting material was synthesized with long flexible arms that conferred liquid character, $Si_8O_{12}(OSiMe_2OSiMe_2H)_8$. This compound is an interesting variant of the more commonly used, $Si_8O_{12}(OSiMe_2H)_8$ mentioned elsewhere in this chapter, and is synthesized as shown in Fig. 7.22. The octasilanol-Si_8O_{12} intermediate (Fig. 7.22, top center) is a surprisingly

stable white solid that can be stored long-term without self-condensation of the silanol groups, and that maintains its solubility over time [139]. In the final product (Fig. 7.22, bottom), a ratio of 5:3 BCB to acrylate was shown to give the optimum combination of properties for SFIL.

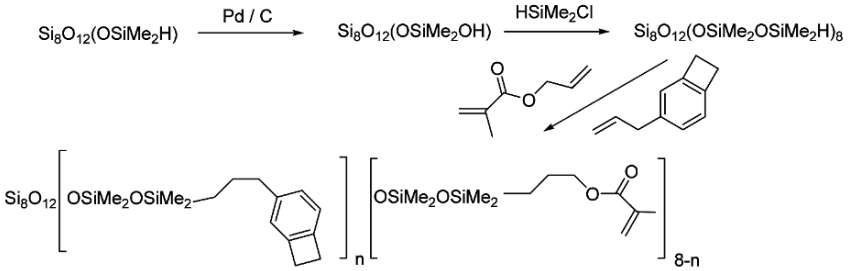

Fig. 7.22 Synthesis of a long-arm POS material for an SFIL process [135]

Recently four-beam interference lithography was used to fabricate three-dimensional porous Si_8O_{12} microstructures with high periodicity that could be used as templates for fabrication of various photonic crystals, phononic crystals, micro- and opto-fluidic devices and sensors [140]. Multibeam interference lithography is the most widely used technique for the fabrication of large-area 0.3 to 6 micron periodic structures, although this can only be used to create periodic structures from photosensitive materials. However, if a 3D periodic material is used as a template, it can be back-filled with an almost unlimited range of other (non-photosensitive) materials, and then the template can be removed by decomposition or dissolution to obtain an inverse 3D periodic structure. In some cases this structure is then used itself as a template in a second templating process. Si_8O_{12} is a good 3D template material because it is compatible with photolithographic processes (see earlier discussion), thermally and dimensionally stable above 400 °C and soluble (i.e., removable by dissolution) at room temperature. An epoxycyclohexyl polyhedral oligomeric silsesquioxane cage mix (T_8, T_{10}, T_{12}) was used as the negative-tone resist precursor [141], and exposed in the presence of 1 wt % PAG to form a 3D silica-like structure. This was then calcined, either by heating in argon to 500°C, or by exposure to oxygen plasma. Cracking was found to occur upon thermal treatment in oxygen, and crack resistance was associated with the presence of residual carbon in the calcined material. The 3D structure was stable when heated up to 1100 °C, and when oxygen plasma was used for calcinations, the volume fraction of pores could be controlled by varying the plasma etch time and power. Because Si_8O_{12} is transparent at UV-visible wavelengths, thicknesses of 30 micron were possible, in contrast to less transparent substrates used for multibeam lithography, where thicknesses of 5 micron are obtained [142]. The 3D structures were filled with elastomeric polydimethylsiloxane (PDMS) and then the Si_8O_{12} component was removed using hydrofluoric acid at room temperature. This resulted in a high fidelity PDMS replica of the periodic 3D structure that could be used as a flexible photonic crystal. Because PDMS has a low modulus and is easily deformed, it is possible to use it to fabricate tunable photonic crystals [142]. Hence the color of

the PDMS photonic film in this study was a function of strain, and its behavior was reversible, i.e., the same color changes were observed as strain values were varied over multiple cycles between 0 and 23%.

7.5 Polyhedral Oligomeric Silsesquioxanes in Sensor Systems

Sensors have a transducer element that converts one stimulus or form of energy (input) into another form of energy (output signal). Inputs may be physical (e.g., temperature, pressure) or chemical (e.g., vapors, liquids). A sensor behaves reversibly, i.e., it should return to its original state after the sensing event (stimulus) has occurred. Sensors should not be confused with assays, which are irreversible, nor with actuators, which convert energy into motion (e.g., muscles). In this section, the use of Si_8O_{12} materials in sensor systems that change their fluorescent, optical, piezoelectric, resistive or electrochemical properties in response to an analyte in the vapor or liquid phase is reviewed. In some cases, single sensors are used, and in other cases arrays of sensors are used (Fig. 7.23). Sensor arrays for vapor detection are often termed 'electronic noses' and their liquid phase counterparts are termed 'electronic tongues'. Sensors may function according to a lock-and-key model, or according to a cross-reactive array model. Array systems are 'cross-reactive' when one component in the array responds to multiple analytes, and a particular analyte causes a number of components in the array to respond. This is in contrast to lock-and-key sensor arrays where each component is specific to a given analyte or to a class of analytes. The cross-reactive array-based vapor sensor systems incorporating Si_8O_{12} that are covered in this section include chemically responsive dyes (giving on-off fluoresence intensity changes, or wavelength changes in absorption or fluorescence emission), surface acoustic wave (SAW) sensors (giving changes in acoustic frequency) and carbon-polymer composite sensors (giving changes in volume and in resistivity).

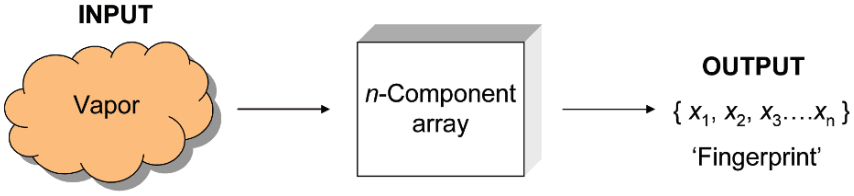

Fig. 7.23 Response of an *n*-component sensor array to a vapor input. Output *x* may be a set ('fingerprint') of *n* resistance, conductivity, frequency, wavelength or other values

Interestingly, in the light of the earlier discussion of predominantly aromatic liquid crystal Si_8O_{12} materials (Section 7.1) and electroluminescent Si_8O_{12} materials

(Section 7.2), many of the sensor materials reviewed in this section are also based on architectures where an Si_8O_{12} core is functionalized with aromatic groups. Most of these aromatic groups are fluorophoric. Apart from sensors, the other main application of fluorophore-functionalized Si_8O_{12} compounds is as fluorescent colorants for plastics or inks, e.g., a 2008 Ciba patent reports that POS has been functionalized with the *N*-(2'-ethylhexyl)-3,4,9,10-perylenetetracarboxylic monoimide monoanhydride chromophore to make fluorescent colorants for addition to thermoplastic or thermoset polymer formulations, or to formulate fluoresecent inks [143].

7.5.1 Fluorophore-Functionalized Polyhedral Oligomeric Silsesquioxanes as Sensors

In 2008, the use of fluorophore-functionalized Si_8O_{12} cores in various sensor applications was reported in three separate studies [144-146]. In the first 2008 study by Hartmann-Thompson and co-workers at Michigan Molecular Institute [144], a set of polyhedral oligosilsesquioxane nanosensors designed to change their wavelength of fluorescence emission upon interaction with analytes was synthesized, characterized and assessed in a remote detection application (Fig. 7.24). In remote detection, information may be obtained from a remote location either by passive detection of waves emitted from remote objects (e.g., passive FTIR), by actively sending a wave to a remote object, and obtaining information by analyzing the wave(s) returning from the object (e.g., Laser Detection and Ranging, LIDAR) or by introducing a sensor at the remote location that can send back information (e.g., use of metal nanoparticles on a remote surface to send back enhanced Raman data). In this study, the nanosensors deployed at the remote location were based upon Si_8O_{12} cores carrying various wavelength-shifting fluorophores more commonly used in the life sciences field (e.g., for multiphoton excitation microscopy and for fluorescence labeling of cells and tissues), where the wavelength of fluorescence emission is a function of the polarity of the chemical environment around the fluorophore. The Si_8O_{12} nanosensors were easily synthesized from commercially available fluorescent labels that had been designed to react readily with amino groups in amino acids; hence the labels were also able to react with amino- Si_8O_{12} compounds under mild conditions. A four-component cross-reactive array of nanosensors was used to generate fluorescence data sets (fingerprints) for a number of analytes including chemical warfare agent (CWA) simulants and toxic industrial chemicals (TICs) by measuring the one-photon fluorescence spectra of nanosensor-analyte pairs in solution (Fig. 7.24). The feasibility of using the nanosensor array for the remote detection of analytes in clouds and on surfaces was then demonstrated in collaboration with the Dantus laser research group at Michigan State University. A femtosecond laser was used to interrogate the array and induce two-photon fluorescence in the nanosensors, and a remote fluorescence probe was used to record

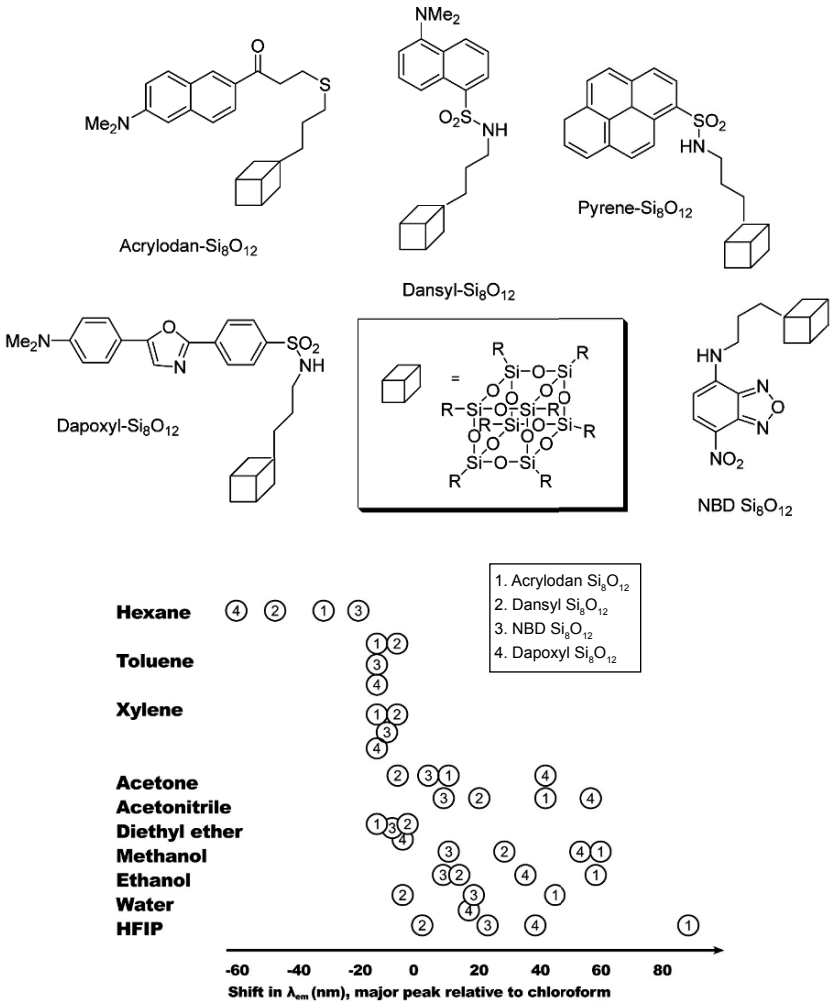

Fig. 7.24 An array of fluorophore-functionalized Si_8O_{12} compounds and the response of the array to various analytes [144]

the responses of the nanosensors [144].

It is interesting to note that the environmentally sensitive NBD (7-nitrobenz-2-oxa-1,3-diazole-4-yl) fluorophore (Fig. 7.24) has also been used in bridged silsesquioxane sensors, as well as in the discrete Si_8O_{12} nanosensors discussed above. These bridged silsesquioxane sensors were described in a 2006 study by Edmiston and co-workers at the College of Wooster (Ohio), and were based on molecularly imprinted sol-gels originating from bis(trimethoxysilylethyl)benzene and an additional fluorene-functionalized trimethoxysilyl compound (Fig. 7.25). The fluorene groups were removed from the sol-gel matrix via carbamate cleavage

leaving fluorene-shaped voids (i.e., fluorene-specific binding sites) and an NBD fluorophore was placed in the void by reacting a free amino group with NBD chloride [147]. The aim of this study was to fabricate a chemical fluorescence sensor specific to fluorene. Molecular imprinting of polymeric substrates is an established way to achieve such specificity. Sol-gel films on glass slides were tested by immersion in 0.5 to 100 ppb aqueous fluorene solutions or by exposure to solid fluorene (and resultant vapor). Non-imprinted sol-gels were used as controls [148]. In this study changes in fluorescence intensity at a given wavelength (540 nm) were monitored rather than changes in fluorescence wavelength [144]. For the NBD fluorophore, both wavelength and intensity of fluorescence are highly solvent-dependent, and quantum yield is particularly low in water. Fluorescence intensity was found to increase with concentration of fluorene test solutions, and this was rationalized in terms of displacement of water by fluorene near NBD rather than direct interaction between fluorene and NBD fluorophore. Response times were less than 1 minute and the limit of detection was estimated to be 1 ppt, but the responses were not reversible, and rinsing with water or non-polar solvents (or flushing with air or nitrogen) failed to remove fluorene from the matrix, or to decrease the fluorescence intensity to its baseline value. The system successfully distinguished fluorene from naphthalene, fluoranthene and anthracene.

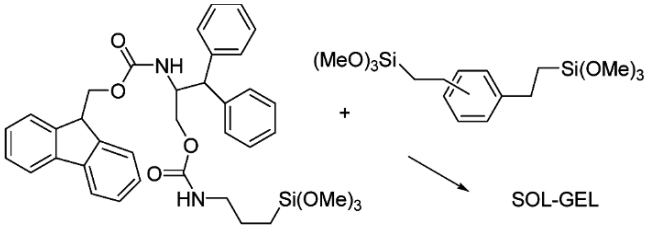

Fig. 7.25 Synthesis of fluorene-functionalized sol-gel [147]

In a second 2008 study [145] by Shi and co-workers (Tsinghua University, Beijing), a fluorescent pyrene- Si_8O_{12}(*i*-propyl)$_7$ vapor sensor was synthezied in an esterification reaction between 1-pyrenebutyric acid (PBA) and a hydroxyl-functionalized Si_8O_{12} reagent (Fig. 7.26). Pyrene has a 380 nm emission in the UV region and a visible excimer emission at 450 to 500 nm, and is another example of an environmentally sensitive fluorophore having an emission wavelength dependent upon its immediate chemical environment. It can give either an on-off fluorescence sensor response (fluorescing or quenched), or a wavelength shift sensor response. The excimer emission results from π-stacking of the planar pyrene aromatic rings and is visible to the naked eye, making it suitable for sensing applications. Crystalline pyrene has strong excimer emission owing to its highly ordered structure, but spin-coated pyrene films show weak excimer emission because of their more random structure. Crystalline structures are disadvantageous in vapor sensing applications because it is difficult for the vapor to diffuse into the film and elicit a sensor response, especially in the case of low vapor pressure vapors such as nitroaromatics (explosives) and phosphonates (nerve agents and pesticides). In

order to overcome this problem, Si_8O_{12} was used to carry the pyrene fluorophores (Fig. 7.26). This resulted in a spin-coated thin film with a highly ordered structure for strong excimer emission, but also with some degree of porosity for good vapor diffusion. A strong blue pyrene excimer emission at 475 nm was observed that was rapidly quenched in the presence of trinitrotoluene (TNT), 2,4-dinitrotoluene (2,4-DNT) and nitrobenzene vapors, with a response time of one minute, faster than that of a film of pure pyrene. In a physical blend of PBA and the pyrene-Si_8O_{12} compound, pyrene monomer emission dominated excimer emission, showing a disordered distribution of pyrene in the thin film. Response time increased as film thickness increased from 4.5 nm to 21 nm, as measured by ellipsometry. The 4.5 nm film was estimated to consist of four layers of pyrene-Si_8O_{12} molecules, and had a response time of 10 seconds. Interestingly, pyrene was evaluated in the Michigan Molecular Institute study [144] in which Si_8O_{12} was functionalized with a range of fluorophores (Fig. 7.24), but was excluded from the final sensor array precisely because of its pair of emission bands, making it unsuitable for a system where it was necessary that each array component generate a single output at a single emission wavelength.

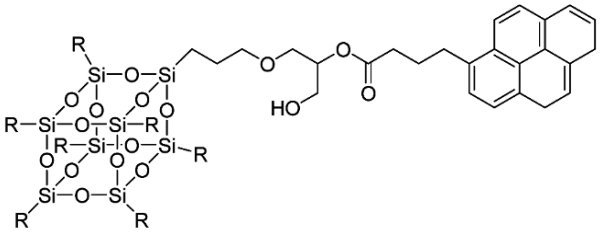

Fig. 7.26 On-off fluorescence sensor based on pyrene-functionalized Si_8O_{12} [145]

In a third 2008 study [146] by Chujo and co-workers (Kyoto University, Japan), Si_8O_{12} cores carrying multiple functional groups were used as ratiometric multimodal chemical sensors for monitoring solvent polarity via fluorescence spectroscopy and ^{19}F NMR spectroscopy. A multimodal imaging agent is a single probe that is able to generate two or more different kinds of information. The combination of fluorescence and ^{19}F magnetic resonance imaging (MRI) information is particularly useful for in-vivo small animal studies, and requires a probe that carries a fluorophore and a fluorinated contrast agent. Probes that respond to a stimulus by generating one signal of increased intensity, and a second corresponding signal of decreased intensity are termed ratiometric probes. Si_8O_{12} was selected as a scaffold for a ratiometric fluorescence/^{19}F MRI multimodal chemosensor because it is multifunctional, and has good biocompatibility and low toxicity (see Chapter 9). An Si_8O_{12} core carrying five trifluoroacetyl groups (for ^{19}F - MRI), two phosphoryl groups for enzyme interaction (e.g., with alkaline phosphatase, AP) and one CCVJ fluorophore (for fluorescence) was synthesized in several steps from octa-ammonium POS, and the desired molecular ions were observed by MALDI-TOF MS after each synthetic step. (Fig. 7.27, top). CCVJ (9-(2-carboxy-2-cyanovinyl) julolidine) is a molecular rotor fluorophore that increases its emission intensity in a

high viscosity environment, and decreases its emission intensity in a low viscosity environment, where internal molecular rotations occur more easily and suppress emission [149]. In polar conditions, the Si_8O_{12} probes formed a cluster resulting in high fluorescence intensity (500 nm in methanol, inhibited molecular rotation) but a low intensity ^{19}F NMR signal (little tumbling). In non-polar conditions, the probes were widely dispersed, resulting in suppressed fluorescence (unhindered molecular rotation) and enhanced ^{19}F NMR signals (tumbling possible). The probe was used to monitor solvent polarity changes occurring during enzymatic reactions.

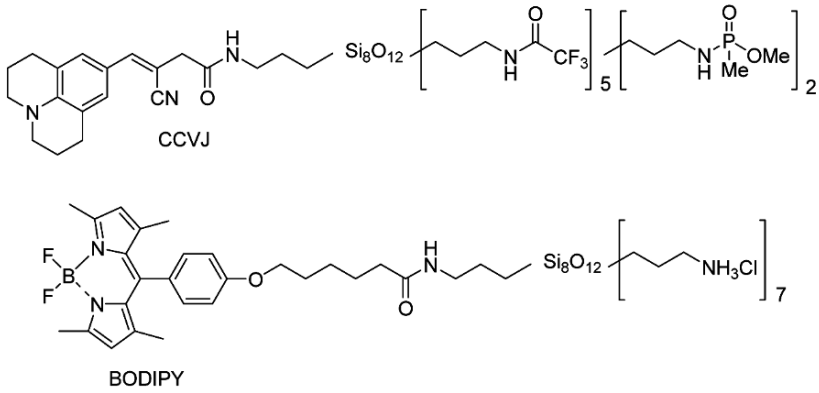

Fig. 7.27 Si_8O_{12} carrying a molecular rotor fluorophore (CCVJ), trifluoroacetyl groups and phosphoryl groups (top) [146], and Si_8O_{12} carrying a BODIPY fluorophore and ammonium groups (bottom) [150]

In another earlier example [150] of a fluorophore-carrying Si_8O_{12} core in a life sciences study (Rotello and co-workers, University of Massachusetts Amherst, 2005), Si_8O_{12} was functionalized with ammonium groups (~90%) and a BODIPY fluorophore (4,4-difluoro-4-bora-3a,4a-diaza-s-indacene, ~10%), see Fig. 7.27, bottom. It was evaluated as a drug carrier and drug delivery agent (see also Section 9.4.1, Chapter 9). Si_8O_{12} is biocompatible, stable, highly water-soluble with suitable functionalization, and has high cellular uptake and low toxicity (see Chapter 9). Water solubility means that the drug can be taken orally, and the small size and high charge density of octa-ammonium-Si_8O_{12} means that the unit may easily be transferred through vascular pores. The monodisperse nature of Si_8O_{12} compounds also eliminates the problems associated with polydisperse linear polymers and the complex syntheses associated with dendrimers. Octa-ammonium-Si_8O_{12} was neutralized with triethylamine and then reacted with the succinimidyl ester of BODIPY in order to attach the fluorophore. An amine terminated BODIPY compound (i.e., with no Si_8O_{12} content) was used as a control. Cos-1 cell cultures were exposed to Si_8O_{12}-BODIPY and control BODIPY. Live fluorescence confocal microscopy showed cell uptake of Si_8O_{12}-BODIPY in the cytosol (rather than the nucleus), but no uptake of the control. Hence it was shown that an Si_8O_{12} carrier has the potential to deliver drugs either with low water solubility or with poor tissue uptake. The BODIPY family of fluorophores [151] are widely used long-wavelength fluorescent labels that are comparatively non-polar and a have a high fluorescence

intensity and a wide multiphoton excitation cross section.

In a 2007 study by Wu and co-workers, Fudan University, Shanghai [152] another catioinc Si_8O_{12} species, (octa-aminophenyl hydrochloride salt) was used as a probe for DNA via resonance light scattering (RLS), see also Section 9.4.3, Chapter 9. In this application, cationic Si_8O_{12} had the advantage of water solubility and stability across a wide pH range. Electrostatic interaction and complexation between cationic POS and DNA polyanion in aqueous solution enhanced the RLS signal, and the enhancement was proportional to nucleic acid concentration. Foreign species such as metal ions and amino acids did not affect signal enhancement. Complexation was shown by various band shifts in the FTIR spectrum, and cationic Si_8O_{12} was prepared from octaphenyl Si_8O_{12} by nitration with nitric acid followed by reduction to the amine over palladium-carbon.

7.5.2 Polyhedral Oligomeric Silsesquioxane Sensors for Gas and Vapor Detection

Si_8O_{12}-based materials have been used to improve the performance of optical waveguides, optical fibers and surface acoustic wave sensors for the detection of gases and vapors, and the use of luminescent compounds for oxygen sensing [86] has already been alluded to in Section 7.2.4.

Optical transducers are attractive for the sensing of flammables such as jet fuel and hydrogen because the electronics are at a remote location, reducing the risk of electrical sparking. An ideal coating for such a transducer must be robust, and must have high surface area and allow fast diffusion of vapors for rapid sensor response. In a 2008 study by Sirbuly, Ratto and co-workers (Lawrence Livermore National Laboratory, California), single crystalline tin dioxide (SnO_2) nanowire subwavelength optical waveguides decorated with octapropylammonium- Si_8O_{12}-stabilized palladium nanoparticles were used to detect hydrogen [153]. Palladium has an ultra-high affinity for hydrogen gas, and its optical properties change when it adsorbs hydrogen, making it a suitable coating for a fiber optic hydrogen sensor. Si_8O_{12}-stabilized nanoparticles were found to have a number of advantages over conventional palladium nanocrystal coatings including higher affinity for the tin dioxide surface, a better match between the palladium species absorbance spectrum and the tin dioxide waveguide fluorescence spectrum, shorter path lengths (50 micron vs. 2 mm for other optical fiber gas detectors) that could achieve reasonable sensitivity (0.5%), and higher porosity resulting in response times as fast as 1-2 seconds for hydrogen in solution. The Si_8O_{12}-Pd nanoparticles were attached to the waveguide by injecting a POS-Pd colloid in methanol into a sensing microchannel. This was subsequently dried with air, and then hydrogen-argon mixtures were introduced via the same microchannel. This system also has the potential to be extended into an array or electronic nose by coating a number of waveguides with a variety of chemo-responsive nanoparticles. The Si_8O_{12}-Pd nanoparticles could be

washed off the waveguide using aqua regia, while conventional palladium coatings cannot be removed from the wave guide without damaging it and preventing its re-use.

In a related application, a 2007 Ocean Optics, Inc. patent [154] described a system in which an optical sensing molecule (capable of a change in absorbance or emission in response to an analyte) is encapsulated in a transparent silsesquioxane matrix, coated onto an optical fiber and used to detect oxygen in a jet fuel tank environment. One benefit is that the matrix is resistant to hydrocarbons (particularly jet fuels) but still permeable to oxygen. A mixture of fluorescent organoruthenium molecular oxygen sensor and 3,3,3-trifluoropropyl triethoxysilane and methyltrimethoxysilane sol-gel monomer was coated onto the tip of the fiber, which was designed to monitor dissolved oxygen in fuels, and headspace oxygen in fuel tanks. Tris(4,7-diphenyl-1,10-phenanthroline)ruthenium(II) perchlorate absorbs at 460 nm (blue) and emits at 620 nm (orange-red), and the fluorescence is quenched as a function of the concentration of oxygen (a triplet species capable of dynamic fluorescence quenching). Similar compounds are used as temperature sensors, but in these cases the luminophores must be sealed in order to prevent exposure to oxygen in the environment.

Surface acoustic wave (SAW) sensors are piezoelectric quartz systems where the frequency of the surface acoustic wave is a function of mass [155]. Hence if the sensors are coated with a material that can interact reversibly with a given vapor, a mass change and a response to that vapor may be recorded. SAW sensors are normally used in cross-reactive arrays [156], where each SAW in the array carries a different coating, and each SAW in the array gives a different mass change and frequency value in response to a given vapor (see Fig. 7.23), thus generating a 'fingerprint' of frequencies for that vapor. The collection of coatings must cover the full range of solubility interactions (dispersion, dipole-dipole and hydrogen-bonding), and needs to include non-polar, polarizable, dipolar, hydrogen-bond basic and hydrogen-bond acidic polymers. Almost all polymers exhibiting these types of interactions are commercially available, with the key exception of hydrogen-bond acidic polymers carrying phenol or fluorinated alcohol functionality, which are of particular importance in the detection of hydrogen-bond basic entities such as nerve agents (Fig. 7.28) and nitroaromatic explosives in security and defense applications [157,158]. Given the hazards of chemical warfare agents, hydrogen-bond acidic SAW polymers are normally tested against nerve agent simulants such as dimethyl methylphosphonate (DMMP, Fig. 7.28) [157-160]. In addition to carrying the desired hydrogen-bond acidic sensor groups and having good initial sensitivity to species such as DMMP and nitroaromatics, hydrogen-bond acidic SAW sensor polymers must be robust enough to withstand multiple vapor challenges and maintain their sensitivity over time. However, it is non-trivial to achieve a combination of good sensor properties and robust coating properties in a single polymeric material, although some attempt has been made to address this issue by cross-linking polysiloxane SAW coatings [161].

An alternative approach was taken by Hartmann-Thompson and co-workers

at Michigan Molecular Institute in 2007, where a series of Si_8O_{12} nanofiller compounds functionalized with hydrogen-bond acidic sensor groups was prepared, characterized by IR, ^{1}H, ^{13}C and ^{29}Si NMR and MALDI-TOF MS, and formulated into polycarbosilane coatings for 500 MHz SAW sensor platforms [162,163]. Sensor responses to the explosives simulant dinitrotoluene (DNT) and to the nerve agent simulant DMMP were studied, and the performances of the Si_8O_{12} formulations were compared to those of conventional hydrogen-bond acidic linear SAW sensor polymers carrying the same sensor groups (Fig. 7.28). The Si_8O_{12} formulations gave good initial responses to the simulants, maintained 40 to 65% of their original response over a period of six months (Fig. 7.29) and maintained their sensitivity down to a simulant vapor concentration of 1 ppb v. The surface compositions of the SAW sensor coatings were characterized by sum frequency generation (SFG) spectroscopy. SFG is a comparatively novel technique for obtaining surface-specific vibrational spectra, and can be used to study chemical groups at interfaces to a depth of 10 nm or less. Unlike XPS, it does not require high vacuum conditions, and is thus of particular interest in life sciences studies. SFG spectra are generated by a non-linear optical phenomenon that occurs when two pulsed laser beams (one of fixed visible wavelength and one of variable IR wavelength) hit a point on an interface at the same time [164]. Highly ordered isobutyl surfaces dominated in SXFA Si_8O_{12} (Fig. 7.28) while highly ordered polycarbosilane surfaces (with contributions from silicon-methyl and silicon-phenyl groups) dominated in the FPOL Si_8O_{12} (Fig. 7.28). Another technique that has been used to look at the surface of Si_8O_{12}-polymer composites is time-of-flight secondary ion mass spectrometry (ToF-SIMS), which has been used to study the surfaces of octabenzyl- Si_8O_{12}-polycarbonate systems [165].

In another example of a hydrogen-bond acidic Si_8O_{12} species [166], Esker and co-workers at Virginia Polytechnic Institute (USA, 2005) described Langmuir-Blodgett (LB) films of open-cage trisilanolphenyl polyhedral oligomeric silsesquioxane that were found to bind strongly with the nerve agent simulant DMMP, probably owing to its acidic character when compared to the open-cage trisilanolisobutyl analogue, and also to conventional untreated silica (SiOH) surfaces. DMMP did not adsorb to silica, but heating to 150 °C was required to desorb DMMP from the trisilanolphenyl polyhedral oligomeric silsesquioxane surface. The ability of a material to interact selectively, rapidly and reversibly with a given vapor can also be important in the preconcentrator component of a sensor device (as well as in the transducer component of the device that actually performs the 'sensing'). In cases where a vapor has a very low concentration or a very low vapor pressure, it is necessary to pre-concentrate it before it reaches the transducer. This enables the transducer to encounter a high enough concentration of analyte to register a response. Insufficiently high concentrations of analyte are a problem across a range of sensing techniques including SAW sensors and ion mobility spectroscopy (IMS), especially for low vapor pressure species such as nitroaromatics (i.e., explosives). Molecularly imprinted nanoporous organosilicas have been used as preconcentrators in systems for the detection of TNT in an electrochemical cell by square-wave

voltammetry [167]. Benzene and diethylbenzene-bridged organic-inorganic species were used, templating was achieved using decylaminetrinitrobenzene during the bistrialkoxyorganosilane sol-gel reaction, and pore size was controlled through use of surfactants.

The idea of dispersing a sensing silsesquioxane agent in a non-sensing matrix [162,163] is unusual in the sensor field, and it is far more common for a silsesquioxane to be used as a non-sensing matrix to carry some other sensor species. In one case sodium iodide or potassium iodide was used as the ozone sensitive material in a continuous polymethylsilsesquioxane matrix [168]. In another example, a silicone ladder (silsesquioxane) polymer was mixed with a quaternary ammonium salt, cast onto the gate of a field-effect transistor and polymerized, and the ion-sensitive field-effect transistor showed a linear response to nitrate ions [169]. In a third example bromocresol green was adsorbed onto a polymethylsilsesquioxane surface and its colorimteric indicator responses to ammonia and to sulfur dioxide in air were studied [170]. In a final example [171], a polysilsesquioxane matrix was used to carry nanostructured silicon powder luminophores. These materials were used to make pressure sensitive paints for use in wind tunnel testing. Pressure sensitive paints are generally based upon oxygen permeable polymers carrying photoluminescent fillers (e.g., ruthenium(II) complexes or various metal porphyrins) whose photoluminescence is quenched by oxygen, and quenching is a function of pressure, enabling pressure mapping of surfaces.

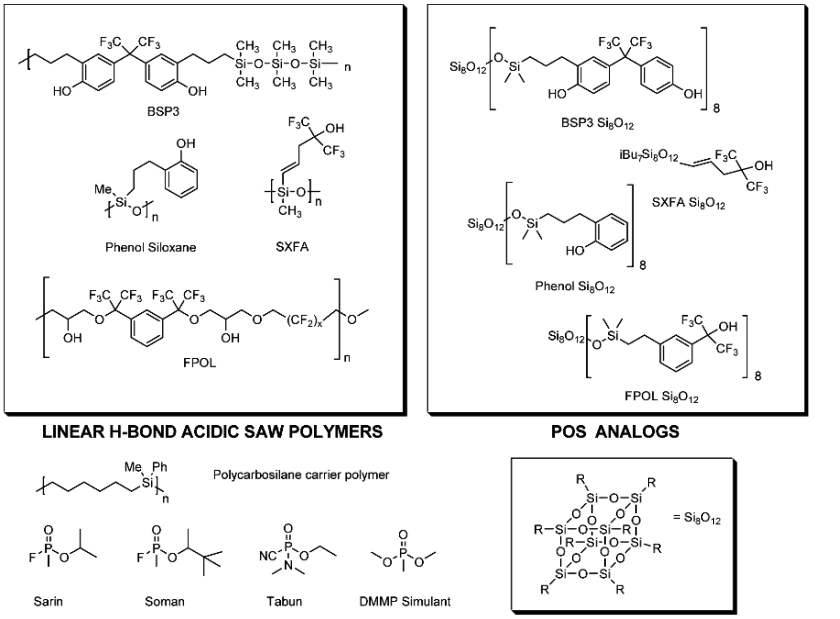

Fig. 7.28 Conventional linear hydrogen bond acidic polymers, hydrogen-bond acidic Si_8O_{12} analogues, the polycarbosilane polymer used to carry the Si_8O_{12} sensors, and hydrogen bond-basic nerve agents and DMMP simulant [162]

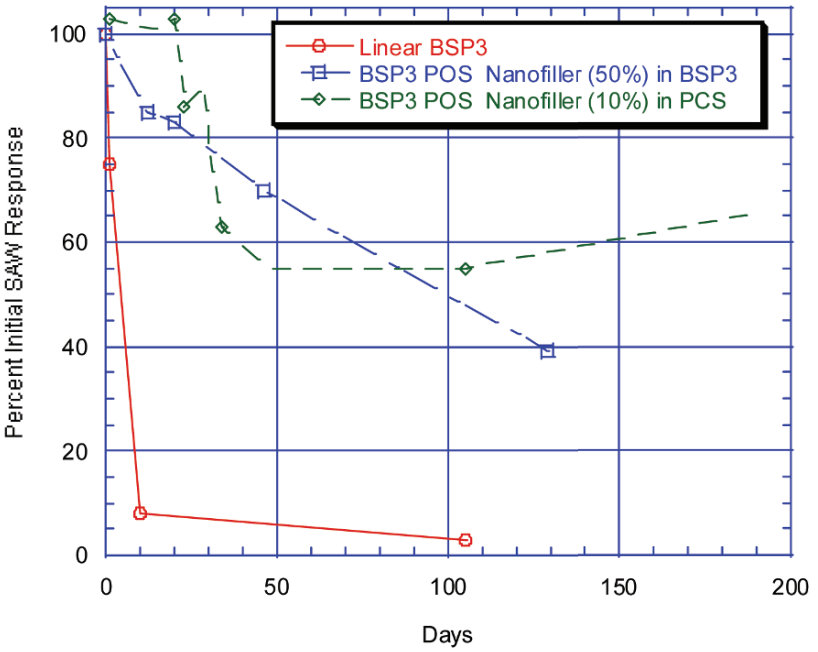

Fig. 7.29 Changes in SAW DMMP responses with time for systems containing BSP3-type sensor groups [162]

7.5.3 Polyhedral Oligomeric Silsesquioxanes in Conducting Composite and Electrochemical Sensors

One variety of electronic nose [172] may be fabricated by assembling many different polymers, each carrying carbon black, into an array of conducting carbon-polymer composites [173,174]. Each component of the array has a different gas-polymer partition coefficient for a given vapor, and gives a different degree of swelling and a different change in resistivity in response to that vapor (since resistivity increases as the conducting carbon structures move apart upon swelling). Thus the vapor generates a 'fingerprint' comprised of a unique set of *n* resistance changes for an *n* component array (Fig. 7.23). These polymer composite arrays have the advantage of operating at room temperature, in contrast to metal oxide systems that require high temperatures [175]. In several studies by Castaldo, Massera and co-workers (ENEA Centro Di Ricerche Di Portici, Naples, Italy, 2007-2008), a polymer carrying pendant Si_8O_{12} groups, poly[(propylmethacryl-heptaisobutyl- Si_8O_{12})-*co*-(*n*-butylmethacrylate)] (Fig. 7.30, left), plus 20 wt % additional filler (carbon, silicon, zinc, copper and carbon alloys of the three latter components) was evaluated in an array of this type [176-178]. The alkyl components of this copolymer impart

weak dipolar character, and the methacryl groups impart hydrogen bond-basic character [179].

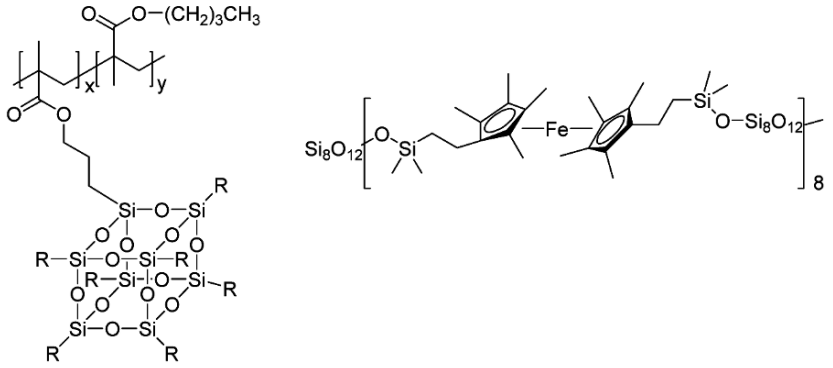

Fig. 7.30 Si_8O_{12} copolymer used as matrix in conducting composite sensor (left) [178], and as a component of three-dimensional Si_8O_{12}-ferrocenyl network used as a mediator on a glucose detection electrode (right) [180]

Instead of an array of different polymer-carbon black composites (where the polymer was varied and the filler did not change), this array was created by combining the single pendant Si_8O_{12} polymer (Fig. 7.30, left) with a range of fillers, where the filler was varied and the polymer did not change. Since noise varies with polymer in a conventional electronic nose, the authors speculated that using the same polymer throughout the array should enable the question of noise to be treated as a simple systematic error. A relative humidity sensor with a rapid response and complete reversibility was fabricated. However, the response could not be explained by the conventional polymer matrix-carbon swelling model. The sensor had an unexpectedly high sensitivity, and its conductivity varied by several orders of magnitude over the 0 to 100% relative humidity (RH) range. When the composite was tested with water and with hexane, the material did not swell, and conductivity increased (rather than decreased as would be expected in a polymer-carbon composite that was swelling in the presence of an analyte). Furthermore, a control film of pendant Si_8O_{12} polymer without additional filler behaved in the same way. The fillers were prepared using a planetary ball-milling technique and had particle sizes of 500 nm or less, and Raman spectroscopy was used to show that the two-component systems were true alloys, and that no chemical reaction had taken place between carbon and either silicon, zinc or copper. Composite films with a thickness of ~500 nm were prepared by spin-coating from particle suspensions in THF- Si_8O_{12} copolymer solutions. Gold interdigitated contacts were deposited on the films by electron-gun evaporation. Poly[(propylmethacryl-heptaisobutyl-Si_8O_{12})-*co*-(n-butylmethacrylate)] with 15 wt % Si_8O_{12} and with 25 wt % Si_8O_{12} contents were compared in the absence of additional filler, and their ac electrical frequency response properties were investigated over a range of temperatures in order to understand the sensing mechanism [178]. Glass transition temperature was measured in-situ in films and devices using this ac electrical technique rather

than the usual techniques for measuring T_g (e.g., DSC), and the T_g values were found to increase with increasing ac field frequency. The authors suggest a porosity model in which water molecules create a hydrogen bond network that allows charge transfer between the Si_8O_{12} cages, although this does not fully explain the earlier observation of increased conductivity in the presence of hexane, albeit a smaller increase than that observed for water [176]. The 15 wt % Si_8O_{12} system performed better than the 25 wt % Si_8O_{12} system, and the authors attributed this to differences in Si_8O_{12} cage mobility and differences in water content in the pore structure [177]. Capacitance-temperature measurements (for permittivity) and conductivity-temperature measurements suggest that water is unable to crystallize at 273 K within the confinement of the pores, and that a super-cooled water phase is present below 230 K. The 15% copolymer was studied with and without additional filler at 20 wt %, and the responses to water, hexane and ammonia were studied [177]. The filled systems showed a 35% improvement in sensitivity relative to the unfilled system, and the filled systems all behaved similarly, further confirming that the fillers themselves did not directly contribute to conductivity, but did influence the pore structure, thus contributing to the conductivity and sensing mechanism.

In another array-based 'electronic nose' system, micromachined capacitors were used to detect changes in the dielectric constants of an array of chemoselective polymers in the presence of various analytes [181] (in contrast to the changes in resistivity in composites discussed above [176-178]), and the changes in frequency in the SAW sensors discussed in Section 7.5.2). Aminopropyl-polysilsesquioxane was a vital component in an array designed for the selective detection of hypergolic fuels, e.g., the nitrogen tetroxide oxidizer and various hydrazine compounds, associated with ballistic missiles.

Most of the earlier discussion has covered the detection of species in the gas or vapor phase, but some work has also been done on the detection of species in the liquid phase. In this area, electrodes carrying various smart coatings are used widely. In another example of silsesquioxane composites with conducting fillers, trimethoxysilanes with additional amino functionality were used to make silsesquioxanes with graphite present during the sol-gel process, where the amino groups acted as basic catalysts [182]. The resulting electrically conducting silsesquioxane-graphite composites were used as electrochemical sensors for the potentiometric detection of various anions in aqueous solution via amino acid-base chemistry at the electrode surface. In a second example, Losada, Armada and co-workers at Universidad Politécnica de Madrid (Spain, 2004) used Si_8O_{12}-ferrocenyl and Si_8O_{12}-permethylferrocenyl polymers (Fig. 7.30, right) as mediators in amperometric electrodes for the detection of glucose [180]. Such electrodes carry glucose oxidase enzyme, and generate information either by monitoring hydrogen peroxide generation (a mediator-less system) or by monitoring the oxidation state of a mediator affected by the enzyme reaction (a mediated system). Electron accepting materials such as ferrocene make excellent mediators, and hence much work on immobilizing ferrocene on electrode surfaces has been carried out (e.g., by addition of ferrocene to polymers, or by binding of ferrocene to carbon

or platinum). Electron-accepting polycationic polymers are also good mediators, adsorb well to graphite, and readily bind enzymes. Methylated ferrocenes are known to have different redox properties and different enzyme interactions to non-methylated ferrocenes, and were found to be better mediators (requiring lower working potentials) for glucose detection. Analogous three-dimensional materials based on cyclotetrasiloxanes instead of Si_8O_{12} were also studied. The networks were synthesized in hydrosilylation reactions between octahydrido Si_8O_{12} and divinyl-ferrocene species. A platinum electrode carried both the Si_8O_{12}-ferrocene material (applied by solution casting) and the glucose oxidase (applied by electrostatic immobilization), and the performance of the electrodes was studied by cyclic voltammetry.

7.6 Polyhedral Oligomeric Silsesquioxanes in Fuel Cell Applications

Fuel cells are electrochemical cells that convert hydrogen, methanol or related fuels into electrical energy, and are a widely researched area of the alternative energy field. The two most important categories of fuel cells are solid oxide (SOFC) and polymer electrolyte membrane (PEMFC, Fig. 7.31). The former tend to be used in stationary power and co-generation applications, while the latter tend to be used in automotive and portable electronic power applications [183]. The high operating temperatures of SOFCs (>600 °C) rule out the use of polymers, but many polymer material challenges may be found in the PEMFC area. Fuel cell proton exchange membranes (PEMs) need to have high proton conductivity across a wide temperature and humidity range, low fuel permeability (to prevent fuel crossover), good mechanical strength and dimensional stability, good resistance to oxidative and acidic conditions (i.e., peroxides at the cathode, and protons respectively), good catalyst compatibility, and the ability to operate above 80 °C (to increase catalyst efficiency and to minimize the size of automotive radiators). The current industry standard material for hydrogen or methanol fuel cell PEM is Dupont's Nafion® sulfonated fluoropolymer (Fig. 7.32). Nafion® has a hydrophilic phase and a hydrophobic phase, and proton conduction occurs in the hydrophilic channels. Sulfonated aromatic polymers of various compositions and architectures have also been extensively studied as proton exchange membranes [184]. There have been many attempts to improve fuel cell performance by adding microscale or nanoscale particles to these PEM polymers, or by forming particle-like domains in the membranes in-situ. Examples include zirconium phosphate [185-187], calcium phosphate [188], titanium dioxide nanoparticles [189], silica [190-197] and nanosilica [198-200]. Hydrophilic particles are used to improve membrane water retention, leading to improved conductivity in low humidity conditions, but water-soluble hydrophilic particles can be at risk of being leached out of the membrane.

Particles also improve the physical properties of the membrane and reduce methanol permeability, but often decrease the conductivity because they interfere with the paths and mechanisms of proton conduction. One way to circumvent this trade-off is to use particles functionalized with proton conducting groups, e.g., silica carrying sulfonic acid groups [201-209] or zeolites carrying sulfonic acid groups [210]. Such groups also improve compatibility between the reinforcing filler and the sulfonated matrix that carries the filler. The use of sulfonated Si_8O_{12} (S-Si_8O_{12}) fillers and related silsesquioxane materials will be reviewed in this section.

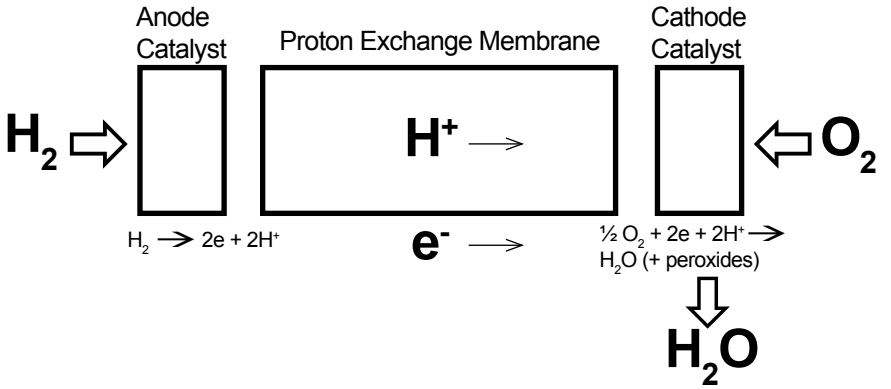

Fig. 7.31 Processes occurring within a polymer electrolyte membrane hydrogen fuel cell

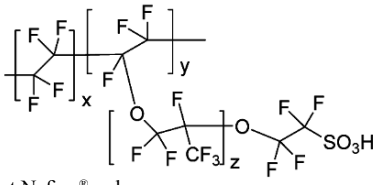

Fig. 7.32 Structure of Dupont Nafion® polymer

A 1992 French patent described a silsesquioxane electrolyte for ion exchange resin, battery or fuel cell applications [211,212] where benzyltriethoxysilane ($PhCH_2Si(OEt)_3$) was used to prepare a silsesquioxane that was subsequently sulfonated to give a material with a conductivity in the range 2 x 10^{-3} S cm^{-1} to 7 x 10^{-3} S cm^{-1} at room temperature. As the membrane was heated, conductivity decreased as water content decreased. The membrane was evaluated as an electrolyte in a Zn/MnO_2 battery system, and also in a hydrogen fuel cell system. The silsesquioxane was prepared using triflic acid in water at room temperature, and an M_n of 3600 was determined by SEC. The primary composition of matter claim covered polyorganosiloxane of the form $O_{3/2}Si$-R in which R was a sulfonated benzyl group (-CH_2PhSO_3H) imparting conductivity, or in which R was some other organic group deployed to tailor the mechanical properties of the membrane, and in which at least 10% of the R groups were sulfonated benzyls. The preferred sulfonating agent was chlorosulfonic acid ($ClSO_3H$), and the sulfonation was carried out in

carbon tetrachloride solution for 30 minutes at room temperature. The sulfonated product precipitated out and was characterized by IR, where a band at 1730 cm^{-1} was assigned to $SO_3H.H_2O$. In the two decades since this patent was published, the use of silsesquioxanes in fuel cells has expanded dramatically.

The sulfonation of octaphenyl- Si_8O_{12} to make S- Si_8O_{12} S-POS (Fig. 7.33) has two non-trivial aspects, and it is suggestive that sulfonated phenyl groups bonded directly to silicon (in which R = $PhSO_3H$, and the phenyl group is not separated from silicon by a methylene spacer) were not claimed in the 1992 patent [211,212]. The first is that a phenyl group directly bonded to silicon (SiPh) is less activated to electrophilic aromatic substitution than a benzyl group bonded to silicon ($SiCH_2Ph$). However, methylene units such as those found in the benzyl group (CH_2Ph) are undesirable in fuel cell membranes where chemical stability in both acid and oxidizing conditions is required. The second is that *ipso* electrophilic attack at silicon (PhSi) competes with the desired electrophilic attack at hydrogen (PhH) positions [213], and in a phenyl-Si_8O_{12} system this would result in cleavage of the phenyl groups from the Si_8O_{12} cage. Hence S- Si_8O_{12} materials require full characterization by IR, ^1H NMR, ^{13}C NMR, ^{29}Si NMR and ion exchange capacity (IEC). IR will show that sulfonic acid groups are present, with four bands corresponding to SO_3 (symmetric and asymmetric) and SO_2 (symmetric and asymmetric) [214,215], and IEC will determine the number of sulfonic acid groups per unit mass (mmol g^{-1}). ^1H NMR will give information on the ratio of *meta*-substituted to unsubstituted phenyl rings, but neither IEC nor ^1H NMR will reveal whether the phenyl groups are attached to the Si_8O_{12} cage [215,216]. Hence ^{29}Si NMR is essential to determine which phenyl groups are still attached to Si_8O_{12} (O_3SiPh, -60 to -70 ppm), and which Si_8O_{12} silicon atoms have lost their phenyl groups in an *ipso* attack and been converted to O_3SiOH groups (-120 ppm). A 2006 study [217] mentions the use of sulfonated Si_8O_{12} and alkyltrimethylammonium bromide surfactant to make lamellar organic-inorganic nanocomposites, but the octaphenyl-Si_8O_{12}/ chlorosulfonic acid reaction conditions (Fig. 7.33) are not described, and no characterization data are given for the S- Si_8O_{12} product.

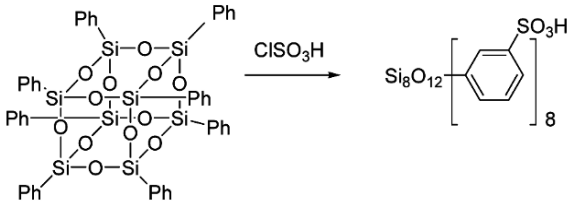

Fig. 7.33 Sulfonation of octaphenyl- Si_8O_{12} to obtain S- Si_8O_{12} (S-POS) [216]

In a 2008 Michigan Molecular Institute study, an almost fully-sulfonated Si_8O_{12} was prepared by reaction of octaphenyl-Si_8O_{12} with neat chlorosulfonic acid at room temperature (Fig. 7.33) and fully characterized [216,218]. This material had an IEC value of 3.5 mmol g^{-1} SO_3H, corresponding to mono-sulfonation of 74% of the phenyl rings, and ^{29}Si NMR showed that an aryl-substituted POS structure had been

retained [219]. S-Si_8O_{12} was formulated into single layer [216] and multilayer [214] sulfonated polyphenylsulfone (S-PPSU) membranes (Fig. 7.34) by Chemsultants, Inc. (Mentor, Ohio, USA). S-PPSU was prepared by sulfonating Solvay Radel R5000® to a level of 1.5 mmol g^{-1} SO_3H. Multilayer membranes were fabricated with the aim of improving water retention and reducing brittleness. S-Si_8O_{12}/S-PPSU membranes cast from a mixed NMP/DMAc/DMSO solvent system had 100 nm Si_8O_{12} domains, and optimum conductivity was achieved with an S-Si_8O_{12} mass loading of 20 wt %. Loadings of S-Si_8O_{12} below 20 wt % resulted in lower overall IEC values for the membranes, and loadings of S-Si_8O_{12}above 20 wt % resulted in particle aggregation that impeded proton conductivity. Casting from NMP resulted in larger Si_8O_{12} domains. In low humidity conditions (25% RH) the three-layer membrane shown in Fig. 7.34 had superior proton conductivity to a Nafion® membrane, a pure S-PPSU membrane and a single layer 20% S-Si_8O_{12}/80% S-PPSU membrane (Fig. 7.35). Across all humidity conditions, both single-layer and multilayer S-Si_8O_{12}/S-PPSU membranes showed superior dimensional stability and less swelling when compared with Nafion®. No evidence of loss of additive was observed in water leaching experiments upon the single-layer S-Si_8O_{12}/S-PPSU membranes, and in the multilayer membranes, the water soluble S-Si_8O_{12} resided in a central layer protected from water leaching by the two pure S-PPSU outer layers (Fig. 7.34).

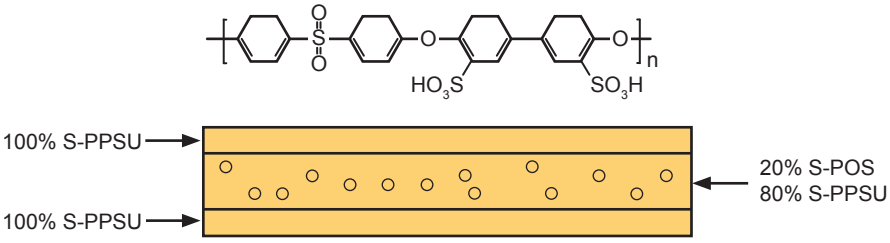

Fig. 7.34 Structures of sulfonated polyphenylsulfone (S-PPSU) repeat unit and of three-layer fuel cell membrane [214]

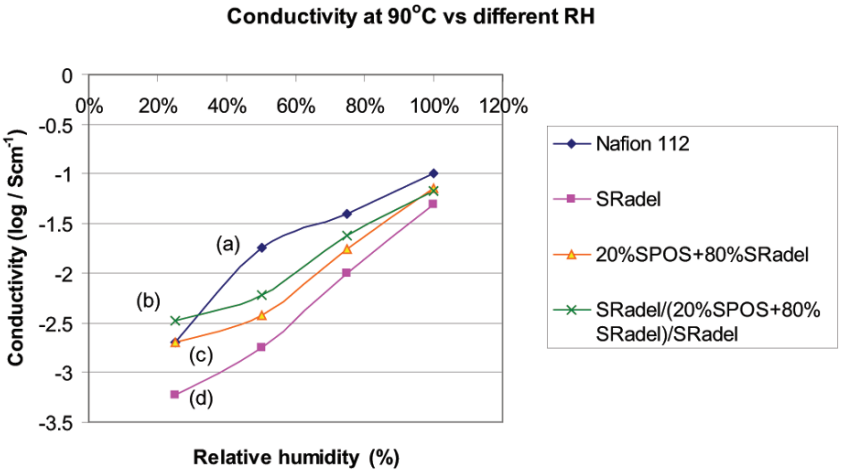

Fig. 7.35 Conductivity for different membranes. The conductivity data were collected at 90 °C at various % RH (a) Nafion® 112 (b) three-layered membrane (c) single-layered membrane with 20% S-POS and 80% S-PPSU (d) S-PPSU [214]

In this study [216], two other variants of octaphenyl-Si_8O_{12} carrying proton-conducting groups were also synthesized and evaluated in S-PPSU membranes. The first variant was an octaphenyl-Si_8O_{12} carrying both sulfonic acid groups and R_{18} alkyl groups, where the R groups were introduced in a Friedel Crafts alkylation of octaphenyl-Si_8O_{12}, and the product was subsequently sulfonated with sulfuric acid. Owing to the activating effect of the alkyl groups, mild sulfonation conditions could be used (in contrast to the more forcing chlorosulfonic acid sulfonation conditions necessary for octaphenyl-Si_8O_{12}). The second variant was an octaphenyl-Si_8O_{12} carrying phosphonic acid groups, where octaphenyl-POS was brominated and reacted with $(PhO)_2POCl$ in the presence of butyl lithium. The phosphonic ester was then hydrolyzed to the half ester.

In a later University of South Australia study [215], a partially sulfonated S-Si_8O_{12} with lower water solubility was prepared in order to reduce the likelihood of the additive being leached out of the membrane by water. A material with an IEC value in the range 2 to 2.5 mmol g^{-1}, corresponding to sulfonation of ~40% of the phenyl rings, was prepared by reaction of octaphenyl-Si_8O_{12} with chorosulfonic acid in chloroform at 0 °C for 4 hours. This S-Si_8O_{12} material was incorporated into a Nafion® 117 membrane, and also into a three-component membrane with Nafion® 117 and the ionic liquid 1-butyl-3-methylimidazolium bis(trifluoromethylsulfonyl) imide (BMI-BTSI). BMI-BTSI was introduced to act as a charge carrier in low humidity conditions, and S-Si_8O_{12} was used as a reinforcing filler to offset the plasticizing effect of BMI-BTSI upon the physical properties of the Nafion® 117 membrane. S-Si_8O_{12} was introduced at low levels (~1%) by immersing a swollen Nafion® 117 membrane into an alkaline aqueous solution of S-Si_8O_{12}, and BMI-BTSI

was introduced by immersion of the membrane in a methanol solution of BMI-BTSI. S-Si_8O_{12} aggregates of 20 to 200 nm in size were observed by TEM throughout the membrane. At 100% RH and 80 °C the S-Si_8O_{12} / Nafion® membrane had a conductivity slightly higher than that of Nafion® (0.11 S cm^{-1} versus 0.09 S cm^{-1}), but a lower water uptake than Nafion®. In anhydrous conditions the conductivity of the S-Si_8O_{12} / Nafion® membranes increased as temperature increased, and was much higher than the Nafion® membrane. This was attributed to the ability of S-Si_8O_{12} to facilitate proton hopping between ionic Nafion® clusters. The addition of the ionic liquid to the S-Si_8O_{12} / Nafion® membrane increased conductivity under anhydrous and low humidity conditions.

In contrast to the closed-cage S-Si_8O_{12} species and to the composite membranes discussed above [214-218], a 2007 US-Korean collaboration [220] between Case Western Reserve University and Hanyang University describes a cross-linked membrane incorporating open-cage species (Fig. 7.36). An open-cage compound carrying three glycidyl epoxy groups was reacted with 4-hydroxybenzenesulfonic acid, and the resulting product (Fig. 7.36) was blended with polyvinylalcohol (PVA). As well as proton-conducting sulfonic acid groups, the compound also carried hydroxyl groups for PVA compatibility. The blend was cross-linked using ethylenediaminetetraacetic dianhydride (EDTAD). Membranes with various open cage to PVA ratios were prepared by mixing the two components with EDTAD in DMSO for 30 minutes at room temperature and then casting from DMSO solution. Unreacted (i.e., non-crosslinked) PVA and open cage compound were removed by immersion in DMSO. Proton conductivity increased with increasing sulfonated cage content, and was comparable with Nafion® at 20 wt % loading, and superior to Nafion® at 50 wt % loading. The membranes also had desirably low methanol permeability (an order of magnitude less than Nafion®) that decreased with increasing cage content. Related polysilsesquioxane composite membranes [221] based on (3-glycidoxypropyl)trimethoxysilane and oxidized (3-mercaptopropyl) trimethoxysilane have also been reported to have good conductivity (~0.1 S cm^{-1} at 70 °C in fully hydrated conditions).

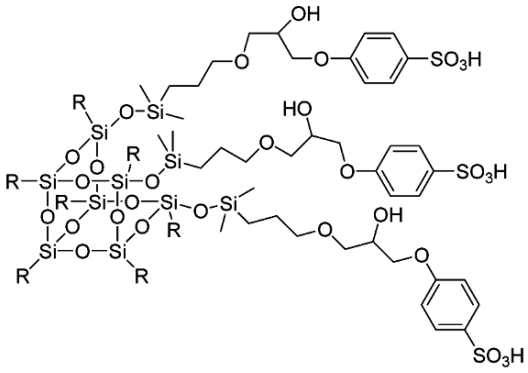

Fig. 7.36 Open-cage polyhedral oligomeric silsesquioxane functionalized with sulfonic acid and hydroxyl groups [220]

Instead of using perfluoro polymers carrying sulfonic acid groups (e.g., Nafion®) or sulfonated aromatic polymers [184], and attempting to manipulate their morphologies and create proton-conducting channels, e.g., block copolymers [223-225], or by fabricating composite membranes (such as the Si_8O_{12} composite membranes discussed earlier in this section), an entirely different approach [222,226] to fuel cell membrane design has been taken by Pintauro and co-workers at Vanderbilt and Case Western Reserve Universities in the US. In this approach proton-conducting channels were created by fabricating a three-dimensional network of interconnected polyelectrolyte nanofibers in an inert non-conducting matrix, where the nanofibers were made in an electrospinning process. Performance could be optimized by varying the composition of the nanofiber, the nanofiber diameter, the nanofiber volume fraction and the composition of the inert matrix. Performance was found to improve when the fully sulfonated variant of S-Si_8O_{12} (Fig. 7.33) [214,216,218] was added to the nanofibers [226]. The inert matrix, being entirely free of hydrophilic functionality (e.g., SO_3H) had no tendency to swell, and had excellent mechanical properties. In the initial 2008 study [222], a polyphenylene ethersulfone (PES) with 58% repeat units sulfonated was used as the nanofiber. A nanofiber mat was electrospun from DMAc solution, and then compressed to increase the density of nanofibers. Intersecting fibers were then interconnected to form proton-conducting paths by exposing the mat to DMF vapor. The mats were observed by SEM at various stages of fabrication and it was shown that the diameter of the nanofibers remained constant. The nanofiber mat was then impregnated with a UV-curable urethane adhesive to form the inert matrix. When in-plane conductivity *versus* nanofiber volume fraction was measured, no percolation threshold was observed, demonstrating the interconnectedness of the structure even at low nanofiber volume fractions. Conductivity increased linearly with nanofiber volume fraction as expected, and a 0.8 volume fraction nanofiber membrane had a conductivity of ~0.12 S cm^{-1} at 25 °C, versus 0.09 S cm^{-1} for Nafion® 117 under the same conditions. In a later study [226], conductivity was shown to increase with increasing IEC (SO_3H content) of the PES nanofiber material, and hence S-Si_8O_{12} (with its high density of SO_3H functionality) was introduced into the nanofiber in order to further increase its IEC. Nanofibers with 40 wt % S-Si_8O_{12} content were slightly thicker than those made from pure PES (400 nm versus 300 nm) and some precipitation of S-Si_8O_{12} outside the fiber was apparent. At 30 °C and 80% RH the 40 wt % S-Si_8O_{12} nanofiber membrane had a conductivity of 0.094 S cm^{-1} while the Nafion® 212 control membrane had a conductivity of 0.037 S cm^{-1}. The S-Si_8O_{12} nanofiber membrane retained its mechanical integrity at high relative humidity (>80%), while conventional composite membranes cast from PES/S-Si_8O_{12} mixtures lost their mechanical strength.

The introduction of polar nitrile groups [227] into sulfonated aromatic polymer PEMs is known to increase their affinity for inorganic fillers and to decrease their water uptake and swelling [228]. In a 2009 National University of Singapore study [227], polyacrylonitrile (PAN) chains were grafted to the corners of a mixture of T_8, T_{10} and T_{12} methacryl-substituted cages via atom transfer radical polymerization

(ATRP) (Fig. 7.37). The Si_8O_{12}-ATRP initiator was synthesized by reaction of the methacryl groups with bromine, and then polymerization with acrylonitrile was carried out using 2,2'-bipyridyl and copper(I) bromide. SEC showed that chain length was largely independent of reaction time (6 hours versus 20 hours) but M_n increased from 11,300 to 33,700 as the acrylonitrile-CuBr molar ratio increased from 200 to 600. No further mass increase was observed above the 600 ratio, but a decrease in the rate of polymerization was observed. This was rationalized in terms of steric hindrance occurring after comparatively short chains had grown from the vertices of the Si_8O_{12} cages [229]. The resulting starburst Si_8O_{12} product was added to Nafion® to fabricate composite membranes with low methanol permeability for direct methanol fuel cells (DMFC). Membranes carrying 5, 15 and 25 wt % Si_8O_{12} were cast from solutions of Nafion® 117 and Si_8O_{12} compound in DMAc. FTIR for hydrogen bonding between nitrile (CN) and sulfonic acid groups, intrinsic viscosity measurements and DSC studies all showed that the Si_8O_{12} additive had an affinity for the hydrophilic sulfonic acid regions of Nafion®, and was repelled from the hydrophobic perfluoro regions owing to the polar nitrile groups in PAN. This caused a severe disruption to the normal two-phase Nafion® morphology and its proton conducting channels. At 5 wt % loading, the Si_8O_{12} additive improved the power output of a DMFC by 122% at 80 °C. The 5% membrane left enough proton-conducting channels unperturbed for efficient conduction, but enough hydrophilic regions were perturbed by nitrile groups (repelling water and methanol) to give low methanol permeability. Performance also improved with the length of the PAN chains, although the nature of the Si_8O_{12}-initiated ATRP process limits the length of the chains, and keeps the overall size of the starburst structure below 20 nm in diameter.

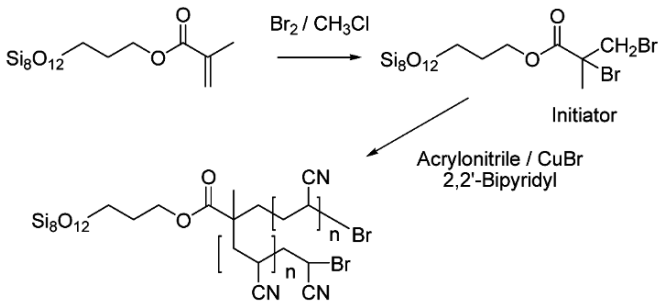

Fig. 7.37 Preparation of starburst polyacrylonitrile (PAN)-grafted Si_8O_{12} via atom transfer radical polymerization (ATRP) [227]

In an earlier study [230] carried out by the same group at the National University of Singapore, a hydrophobic octavinyl-Si_8O_{12} was added to Nafion® 117 at 5, 15 and 25 wt % loadings and used as a membrane in direct methanol fuel cells in order to reduce methanol crossover. The vinyl groups were polymerized in-situ in the membrane in the presence of UV light and a 2,2-dimethoxy-2-phenylacetophenone (DMPA) initiator, and nanosilica domains were generated and observed by SEM.

When DMAc-recast Nafion® membranes were compared with recast Nafion®-Si_8O_{12} membranes, the Nafion® membrane had a random matrix while the Nafion®-Si_8O_{12} membrane had a non-random matrix. The Nafion®-Si_8O_{12} membranes displayed lower methanol permeation, higher power density, lower activation energy to proton conduction and lower thermal stability than the pristine Nafion® membrane. A 2008 Chinese study by Zhao and Huang [231] describes the addition of Si_8O_{12} to a sulfonated polyphthalazinone ether ketone membrane that was solvent cast from a mixture of the two components. A conductivity comparable to that of Nafion® 117 was reported.

A number of studies of polysilsesquioxane fuel cell membranes [221,232-235], hybrid Nafion®-polysilsesquioxane membranes [236-238] and hybrid sulfonated polyetheretherketone (S-PEEK)-polysilsesquioxane [239,240] have also been carried out, especially in methanol fuel cells where reduction of methanol permeability is vital. In these hybrid membranes, polysilsesquioxanes are either formed in-situ [236,240] or else introduced as additives [237-239]. The structure, proton conductivity and chemical, thermal and mechanical stability can be optimized by controlling the sol-gel reaction conditions, e.g., pH, solvent, silicon to water ratio, catalyst and drying. Polysilsesquioxanes with either pendant propylsulfonic acid functionality or pendant ethylphosphonic acid functionality were prepared in sol-gel hydrolysis and condensation reactions using 3-(trihydroxysilyl)-1-propanesulfonic acid and trihydroxysilylethane phosphonic acid, respectively, and clear and colorless membranes were prepared by further reaction with various di-functional cross-linking agents [234]. The propylsulfonic acid membrane had a through-plane conductivity of 0.04 S cm^{-1} at 80 °C temperature and 100% RH, while the ethyl phosphonic acid membrane had lower conductivity (0.01 S cm^{-1} at 80° C and 100% RH) but higher thermal stability. Sulfonated polysilsesquioxane membranes prepared in nitric acid oxidations of disulfide-bridged polysilsesquioxane membranes had conductivities of 0.0062 S cm^{-1} under full humidification [232,233].

In another study, a Nafion® 117 membrane, pre-treated to generate the Nafion® sodium salt, was immersed in a TEOS-alkoxysilane mixture, and the sol-gel reaction proceeded inside the swollen Nafion® to give a hybrid Nafion®-ORMOSIL (organically modified silica) membrane [236]. The alkoxysilanes included vinyltriethoxysilane, diethoxydimethylsilane and diethoxydiphenylsilane. In another example of hybrid Nafion®-polysilsesquioxane membranes, a Nafion®/polyphenylmethylsilsesquioxane(PPSQ) / calcium hydroxyphosphate membrane and a Nafion®/PPSQ membrane were fabricated by dispersive mixing and sonication in DMF followed by solvent casting [237,238]. The membranes were then evaluated for application in direct dimethylether (DME) fuel cells above 100 °C. SEM showed that the PPSQ powder was 10 to 200 micron in size, but the domains in Nafion® were smaller than 1 micron in diameter and good dispersion was achieved. DME is a high energy density fuel with comparable performance to methanol, but in order to overcome slow oxidation kinetics at the electrode it is necessary to run DME fuel cells at temperatures above 100 °C. Both the crystallinity and the temperature of onset of thermal decomposition increase as the PPSQ content increases. The

composite membranes appeared to have superior conductivity at high temperatures and high RH, and better single cell performance than Nafion® 115 at 100-120 °C and 1-2 atm pressure. A hybrid fuel cell membrane based on phosphonated polysilsesquioxane and S-PEEK has been reported, and a conductivity of 0.142 S cm^{-1} was measured at 120 °C, 100% RH and 40 wt % polysilsesquioxane loading [239]. An imidazole-functionalized polysilsesquioxane-S-PEEK membrane has also been reported [240]. Polysilsesquioxanes carrying sulfonic acid groups have also been used as hollow particle additives with holes on the surface [241] and have been added to membranes to decrease swelling. The work reviewed above concerns acidic membranes for proton conduction, but polysilsesquioxanes have also been used in alkaline membranes [242].

7.7 Polyhedral Oligomeric Silsesquioxanes in Battery Applications

In battery applications, polyhedral oligosilsesquioxanes have primarily been used in the electrolyte component of secondary (i.e., rechargeable) lithium ion batteries, although an early patent [211,212] suggested a sulfonated silsesquioxane electrolyte for a Zn/MnO_2 battery application as discussed in the previous section. Of all classes of battery, lithium has the highest energy density (Wh kg^{-1}) for electrochemical reasons associated with its high charge density in cationic form and its low atomic mass. Today's ubiquitous lithium ion battery is comprised of a carbon anode, a lithium salt cathode (e.g., $LiCoO_2$) and one of two major classes of electrolyte. The first class are liquids comprised of a lithium salt, e.g., $LiPF_6$, $LiAsF_6$, or $LiCF_3SO_3$, and an aprotic liquid, e.g., ethylene carbonate (EC), propylene carbonate (PC), ethyl methyl carbonate (EMC), dioxolane (DN), or fluorinated variants [243]. These systems have good conductivity (0.001 to 0.02 S cm^{-1} at 20 °C) and good lithium transport numbers, but do not function well at higher temperatures. In addition, liquid systems must be carefully sealed to prevent leaking, and may be flammable or explosive under certain conditions. The second class comprises the polymer electrolytes used in lithium-ion-polymer batteries, often referred to as 'lithium-polymer' batteries. These are safer and can be used at higher temperatures (60 to 100 °C). They can be used as both electrolyte and separator (enabling lightweight packaging and much greater flexibility in battery shape, design and aspect ratio), but they have low ionic conductivities and lithium transport numbers. Since electrolytes must have low reactivity with lithium, polymer electrolyte systems are usually based on polyethylene oxide (PEO, also known as polyethylene glycol, PEG), poly(methyl methacrylate) (PMMA), polyurethane, polyacrylonitrile (PAN) or fluoropolymers such as poly(vinylidene fluoride) (PVDF). Polymers may be used either alone, or as gelled polymer electrolytes (GPEs) in combination with a liquid and/or plasticizer. GPEs may be either homogenous and single phase, or else consist of a solvent phase

in a porous polymer matrix. PEO alone with lithium salt has a very low conductivity (10^{-8} S cm^{-1} at 20 °C) whereas GPEs have conductivities as high as 0.009 S cm^{-1} at 20 °C [243]. Polymer-lithium salt electrolytes and GPEs have different mechanisms of lithium ion transport, and the GPE mechanism is dominated by diffusion of the liquid component [243].

Many strategies have been employed to improve conductivity without compromising the other beneficial properties of polymer electrolytes. High viscosity, high crystallinity, high glass transition temperature (T_g) and high cross-link density are all severely detrimental to ionic conductivity in linear polymer electrolytes. Hence, liquid plasticizers such as polypropylene carbonate have been added to improve conductivity, and gel electrolytes in which lithium salt/aprotic liquid electrolytes are trapped in polymer matrices have been developed [244]. However both of these approaches have some of the same drawbacks as the lithium salt/aprotic liquid electrolytes themselves. One way to obtain a system with a decreased glass transition temperature is to switch from a linear polymer architecture to a hyperbranched polymer architecture [245-252], and another approach has been to add micro- or nanooxide fillers (e.g., TiO_2, SiO_2 or Al_2O_3) in order to disrupt or suppress crystallinity, to lower T_g, and hence to improve conductivity [253,254].

Extensive studies of the effect of Si_8O_{12} filler addition upon the properties of lithium battery polymer electrolytes have been carried out by the Wunder research group at Temple University (Philadelphia, USA). In the first reports in 2002 and 2003, a study of PEO-grafted silicas for battery and pharmaceutical applications was extended to include Si_8O_{12} [255,256]. Two trimethoxy-PEO silanes (PEO-Si(OMe)$_3$, M_w 460 and 5000) were grafted onto untreated fumed silica, and several allyl-terminated PEO species were grafted onto octakis(hydridodimethylsiloxy)-Si_8O_{12} (Fig. 7.38) [255]. Allyl-terminated PEO variants with 2, 4, 8 and 12.5 repeat units were prepared in allylation reactions using allyl bromide and base. The glass transition temperatures of the starting allyl materials and the PEO-functionalized Si_8O_{12} materials (Fig. 7.38) were measured (Table 7.4). These results show that grafting to Si_8O_{12} has the potential to suppress the crystallinty of PEO, e.g., in the n = 4 case, the free PEO is completely crystalline while the Si_8O_{12}-grafted PEO is an amorphous liquid with a T_g of -85 °C. An elimination of crystallinity was also observed for PEO grafted to silica [257].

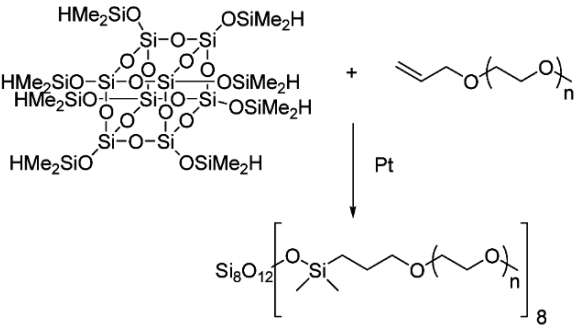

Fig. 7.38 Preparation of PEO-functionalized Si_8O_{12} [255]

Table 7.4 Glass transition temperatures (T_g) and melting points (T_m) measured by DSC for various free PEO(n = x) species and PEO(n = x) grafted onto Si_8O_{12} [255]

Material	T_g (°C)	T_m (°C)
Allyl PEO (n = 2)	-126	Completely amorphous
Allyl PEO (n = 4)	None	-28
Allyl PEO (n = 8)	None	-5
Allyl PEO (n = 12.5)	None	22
Si_8O_{12}-PEO (n = 2)	-89	None
Si_8O_{12}-PEO (n = 4)	-85	None
Si_8O_{12}-PEO (n = 8)	-80	-4
Si_8O_{12}-PEO (n = 12.5)	-69	19

Binary mixtures of lithium salts and Si_8O_{12}-PEO $(n = x)_8$ compounds of the type above (with the range of compositions extended to include n = 2, 4, 6, 8 and 12.5) were used to form viscous electrolyte solutions, and their conductivities were measured by ac impedance spectroscopy [258]. T_g increased with increasing chain length n, and the tendency of the chains to crystallize increased with increasing n. The lithium salts lithium chlorate ($LiClO_4$) and lithium bis(perfluoroethylsulfonyl) imide (LiBETI, $LiN(CF_3CF_2SO_2)_2$) were evaluated at oxygen to lithium (O/Li) ratios in the range 8/1 to 32/1. The conductivities of the Si_8O_{12}-PEO $(n = x)_8$ / lithium salt mixtures increased with decreasing T_g of the PEO component at low temperatures (close to the T_g). At high temperatures, conductivity increased with increasing PEO content, consistent with the lack of contribution of the Si_8O_{12} component to conductivity. Si_8O_{12}-PEO $(n = 4)_8$ with an O/Li ratio of 32/1 gave a conductivity of 2 x10^{-4} S cm^{-1} at 90 °C. Binary mixtures of Si_8O_{12}-PEO $(n = x)_8$ compounds and $LiClO_4$ had conductivities of 10^{-3} S cm^{-1} at 50 °C and 10^{-4} S cm^{-1} at room temperature, comparable to oligomeric PEO (M_w 300-500). The T_g values for these mixtures were between -60 and -70 °C [259]. In a later study [260], the same set of Si_8O_{12}-PEO $(n = x)_8$ compounds was formulated with a wider range of lithium salts including the original pair plus $LiN(CF_3SO_3)_2$, $LiPF_6$, $LiAsF_6$ and $LiBF_4$. The glass transition temperature increased with increasing salt concentration and PEO chain length. When comparing lithium salts at high temperatures and low viscosities, the less associative salts ($LiClO_4$, $LiN(CF_3CF_2SO_2)_2$, $LiN(CF_3SO_3)_2$, $LiPF_6$ and $LiAsF_6$) contributed more charge carriers and gave higher conductivities than the more associative salts ($LiBF_4$ and $LiCF_3SO_3$). When comparing lithium salts at low temperatures and high viscosities, the low T_g systems gave higher conductivity than the high T_g systems. Lithium salts either lower the T_g through the plasticizing effects of large organic anions (e.g., $LiN(CF_3CF_2SO_2)_2$) or affect the T_g by complexation with PEO, where the less associative salts have a greater tendency to complex with PEO and raise the T_g. The highest conductivity obtained in this system was 1.1 x 10^{-4} S cm^{-1} for Si_8O_{12}-PEO $(n = 4)_8$ and $LiN(CF_3CF_2SO_2)_2$ with an oxygen to lithium (O/Li) ratio of 16/1.

This work on viscous liquid electrolytes formed a basis for the design of solid polymer electrolytes that were prepared by blending Si_8O_{12}-PEO $(n = 4)_8$ with high molecular weight PEO (M_w 600,000) and $LiClO_4$ at various ratios [261]. The O/Li = 8/1 and 12/1 compositions had a tendency to microphase-separate into a high T_g amorphous phase (dominated by PEO) and a low T_g amorphous phase dominated by Si_8O_{12}-PEO $(n = 4)_8$. The O/Li = 16/1 compositions had the same two amorphous phases plus a third crystalline phase comprised entirely of PEO. As expected the conductivities were dictated by the nature of the continuous phase, where a continuous low T_g amorphous phase gave the highest values and a continuous crystalline phase gave the lowest values. The highest conductivity obtained was 8 x 10^{-6} S cm^{-1} at room temperature versus 2 x 10^{-6} S cm^{-1} for PEO itself at the same O/Li = 12/1 ratio.

Beyond closed-cage Si_8O_{12} itself, several other attempts have been made to use sol-gel derived materials to improve electrolyte conductivity. In one example, PEO chains of approximately 40 repeat units were grafted to a sol-gel derived siliceous framework via urea linkages, and a conductivity value of 6 x 10^{-6} S cm^{-1} at room temperature was recorded [262]. In a second, highly successful study, conductivity was increased by two orders of magnitude, and values in the region of 10^{-4} S cm^{-1} were obtained [263]. This was achieved by performing in situ sol-gel chemistry in PEO using 3-glycidopropyltrimethoxysilane (GLYMO) to produce a solid single-ion conducting (SIC) composite electrolyte with a three-dimensional network structure, where the glycidyl groups were selected to enhance compatibility with the PEO. Silicate particles with a diameter of 15 nm were prepared by reacting the three sol-gel reagents (GLYMO, tetramethoxysilane (TMOS) and the sodium salt of trihydroxysilylpropylmethylphosphonate) to give a system with immobile phosphonate anions and mobile sodium cations. Owing to the SIC nature of the system, near-unity cation transferance values were obtained, in contrast to conventional PEO electrolytes where ion mobility is associated with aggregates of ions; hence there is less of a contribution from single ions, and transfer numbers are significantly less than one.

Other examples of silsesquioxanes in battery technology include a Samsung patent [264] reporting that a hydrogen silsesquioxane was sintered and used in an anode for a lithium battery with improved charge and discharge performance, and a German patent [265] reporting that oligomeric silicon-oxygen clusters improved the chemical and thermal stability of lithium battery separators. The separator was made from a porous non-conducting polymer support coated with a ceramic, and $Si_8O_{12}(OSiR_3)_8$ was incorporated into the polymer support. The function of a battery porous separator is to separate cathode and anode, to be permeable to electrolyte under normal operating conditions, but to close its pores and shut down the battery in the event of a thermal runaway.

7.8 Polyhedral Oligomeric Silsesquioxanes as Lubricants

In 1982, a Russian group [266] first suggested that alkyl oligosilsesquioxanes with aliphatic chain lengths up to 6 carbons in length (i.e., hexyl) might be useful as lubricants, and more recently, Si_8O_{12} compounds have been patented [267] as lubricants and as additives to lubricant materials for control of viscosity, wear and thermal performance, where Si_8O_{12} chemical and thermal stability and tailorable properties have proved to be an advantage. These Si_8O_{12} compounds, functionalized with various octyl and hexyl groups, have been described as 'molecular ball-bearings'. In the patent examples they were formulated with a polyester lubricant, MIL-L-7808, and enabled the lubricant to avoid mass loss for longer at a given temperature, and to reduce the wear of metal components in a three-ball disc test. This patent also covered the use of Si_8O_{12} compounds in place of conventional mold-release agents (i.e., mineral oils, silicones or fluorinated polysiloxanes, as also alluded to in Chapter 5). Since mechanical systems must function from low temperatures up to extremely high temperatures (e.g., 500 °C and above in jet engines), the key materials challenges are to achieve stability at high temperatures, and to achieve lubricating properties across a wide temperature range. In addition, lubricants should be non-volatile, non-corrosive and should not decompose to form solid deposits that can impede mechanical functions. Next-generation automotive engines are expected to be smaller, and to function at higher temperatures in order to maximize fuel efficiency; hence this could be beyond the abilities of existing hydrocarbon mineral oil-based lubricants. Various high temperature lubricants based upon complex formulations of silicones, carboxylic acids or polyhydroxyl esters with antioxidants have been proposed. When used as an additive, the size of the Si_8O_{12} compound (0.7 to 3.0 nm) enables it to occupy sites within the lubricant, and to alter its free volume. The additive may be physically mixed or reactively blended with the lubricant. Si_8O_{12}-based lubricants resemble conventional lubricants in that they behave in a Newtonian manner, and their viscosity decreases at higher temperatures.

A Nigerian study by Dare [268] showed that the hydraulic fluid properties of Si_8O_{12} compounds were comparable with the commercial hydraulic fluids Mobil® EAL 224H (vegetable oil-based), Super-V® (AP) (petroleum-based) and Puroil® SHO (synthetic siloxane-based). Several alkyl-functionalized Si_8O_{12} compounds were prepared in hexachloroplatinic acid-catalyzed hydrosilylation reactions of $Si_8O_{12}(H)_8$ with 7-bromo-1-heptene, 8-bromo-1-octene, allyltrichlorosilane and 2-methyl-3-butyn-2-ol, respectively. The three colorless liquids in Table 7.5 showed the greatest promise as lubricants, as did the compound $Si_8O_{12}(CH_2Ph)_8$ that had been prepared in a Friedel Crafts alkylation of octavinyl-Si_8O_{12} with benzene and aluminum chloride. Typical industrial lubricants have kinematic viscosities (kv) in the range 5 to 15 cSt at 100 °C, and pour points from -40 to +6 °C.

Table 7.5 Some properties of Si_8O_{12}-based lubricants versus commercial lubricants [268]

	kv (cSt) 40°C	kv (cSt) 100°C	Onset of solidification (°C)	Pour point (°C)
$Si_8O_{12}[(CH_2)_7Br]_8$	35	6	0	--
$Si_8O_{12}[(CH_2)_8Br]_8$	38	6	8	--
$Si_8O_{12}[(CH_2)_6Cl]_8$	40	7	-5	-38
$Si_8O_{12}(CH_2Ph)_8$	48	11	-20	-25
Mobil® EAL	35	8	--	--
Super-V®	22	15	--	--
Puroil® SHO	42	7	--	--

In addition, methylsilsesquioxane particles (0.3 micron) prepared by emulsion polymerization were proposed as anti-wear lubricants for magnetic memory devices [269]. The use of Si_8O_{12} materials as lubricants during the processing of polypropylene [270-272] or nylon 6 [273] has also been studied in depth (see also Section 5.5.2, Chapter 5).

7.9 References

1. Donald A, Windle A, Hanna S (2005) Liquid Crystalline Polymers, Cambridge University Press, 2nd Ed. Cambridge, UK.

2. Pan Q, Fan X, Chen X, Zhou Q (2006) Huaxue Jinzhan 18(5):616-621.

3. Teyssie D, Boileau S (2000) Liquid Crystalline Silicon-containing Polymers. In Jones RG, Ando W, Chojnowski J (eds) The Science and Technology of their Synthesis and Applications, Kluwer, Dordrecht, Netherlands, Ch 22, pp 593-613.

4. Gray GW (1987) Thermotropic Liquid Crystals, John Wiley and Sons, Chapter 6.

5. Mehl GH, Goodby JW (1997) Mol Cryst Liq Cryst 303:15-21.

6. Mehl GH, Thornton AJ, Goodby JW (1999) Mol Cryst Liq Cryst 332:2965-2971.

7. Xie P, Guo JS, Dai DR, Jin SZ, Liu DS, Li Z, Zhang RB (1996) Polym Adv Technol 7:98.

8. Xie P, Wan Y, Zhou B, Hou J, Dai D, Li Z, Liu D, Zhang R (1996)

Macromol Chem Phys 197:745.

9. Kreuzer FH, Maurer R, Spes P (1991) Macromol Symp 50:215-228.

10. Saez IM, Styring P (1996) Adv Mater 8(12):1001-1005.

11. Mehl GH, Saez IM (1999) Appl Organomet Chem 13(4):261-272.

12. Serrano JL (1996) Metallomesogens, VCH, Weinheim.

13. McArdle CB (1989), Side Chain Liquid Crystals, Blackie, Glasgow, UK.

14. Lewthwaite AR, Gray GW, Toyne K (1992) J Mater Chem 2:119.

15. Sellinger A, Laine RM, Chu V, Viney C (1994) J Polym Sci Part A Polym Chem 32:3069-3089.

16. Aquilera C, Bartulin J, Hisgen B, Ringsdorf H (1983) Makromol Chem 184:253.

17. Sellinger A, Laine RW (1994) Polym Prepr (Am Chem Soc Div Polym Chem) 35(2):665-666.

18. Saez IM, Styring P (1997) Mol Cryst Liq Cryst 299:163-168.

19. Mehl GH, Goodby JW (1996) Angew Chem Int Ed 35:2641.

20. Mehl GH, Goodby JW (1996) Chem Ber 129:521.

21. Ibn Elhaj M, Skoulios A, Gouillon D, Newton J, Hodge P, Coles HJ (1995) Liq Cryst 19:373.

22. Saez IM, Goodby JW (1999) Liq Cryst 26(7):1101-1105.

23. Ahsan MS, Sasaki S, Kawakami Y (2007) React Funct Polym 67(11): 1200-1210.

24. Elsasser R, Mehl GH, Goodby JW, Photinos DJ (2000) Chem Commun 10:851-852.

25. Karahaliou PK, Kouwer PHJ, Meyer T, Mehl GH, Photinos DJ (2007) Soft Matter 3(7):857-865.

26. Laine RM, Zhang C, Sellinger A, Viculis L (1998) Appl Organomet Chem 12:715.

27. Zhang CX, Bunning TJ, Laine RM (2001) Chem. Mater 13:3653-3662.

28. Kim K-M, Chujo Y (2001) Polym Bull 46(1):15-21.

29. Saez IM, Goodby JW (2001) J Mater Chem 11(11):2845-2851.

30. Saez IM, Goodby JW, Richardson RM (2001) Chem- Eur J 7:2758-2764.

31. Pan Q, Chen X, Fan X, Shen Z, Zhou Q (2008) J Mater Chem 18(29):3481-3488.

32. Link DR, Natale G, Shao R, Maclennan JE, Clark NA, Korblova E, Walba DM (1997) Science 278:1924.

33. Cui L, Collet JP, Zhu L (2007) Polym Mater Sci Eng Prep 97:408-409.

34. Cui L, Collet JP, Xu G, Zhu L (2006) Chem Mater 18(15):3503-351.

35. Miao J, Lei (2010) J Phys Chem B 114(5):1879-1887.

36. Pan Q, Gao L, Chen X, Fan X, Zhou Q (2007) Macromolecules 40(14):4887-4894.

37. Mather PT, Chaffee KP, Haddad TS, Lichtenhahn JD (1996) Polym Prepr Am Chem Soc Div Polym Chem 37(1):765-766.

38. Somlai AP, Iyer S, Schiraldi DA (2004) Polym Prepr (Am Chem Soc Div Polym Chem) 45(1):650-651.

39. Sethumadhaven M, Kennedy SD, Barton CL (2004) World Pat. 2004114732 A1.

40. Kim KM, Chujo Y (2001) J Polym Sci 39(22):4035-4043.

41. Jeng S-C, Hwang S-J, Yang C-Y (2009) Opt Lett 34(4):455-457.

42. Jeng S-C, Kuo C-W, Wang H-L, Liao C-C (2007) Appl Phys Lett 91(6):061112/1-061112/3.

43. Teng WY, Jeng SC, Kuo CW, Lin YR, Liao CC, Chin WK (2008) Opt Lett 33:1663.

44. Hwang S-J, Jeng S-C, Yang C-Y, Kuo C-W, Liao C-C (2009) J Phys D: Appl Phys 42(2):025102/1-025102/6.

45. Chen W-Z, Tsai Y-T, Lin T-H, (2009)Appl Phys Lett 94(20):201114/1-201114/3.

46. Kim E-H, Myoung S-W, Lee W-R, Jung Y-G (2009) J Korean Chem

Soc 54(3):1180-1186.

47. Pope M, Kallmann H, Magnante PJ (1962) J Chem Phys 38:2042.

48. Burroughes JH, Bradley DDC, Brown AR, Marks RN, Mackey K, Friend RH, Burns PL, Holmes AB (1990) Nature (London) 347:539.

49. Friend RH, Gymer RW, Holmes AB, Burroughes JH, Marks RN, Taliani C, Bradley DDC, Dos Santos DA, Bredas JL, Logdlund M, Salaneck WR (1999) Nature (London) 394:121.

50. Lee J, Ch H-J, Cho NS, Hwang D-H, Shim H-K (2006) Synth Met 156(7-8):590-596.

51. Chan KL, Sonar P, Sellinger A (2010) J Mater Chem 19(48):9103-9120.

52. Ranger M, Rondeau D, Leclerc M (1997) Macromolecules 30:7686-7691.

53. Lin W-J, Chen W-C, Wu W-C, Niu Y-H, Jen AKY (2004) Macromolecules 37(7):2335-2341.

54. Chou C-H, Hsu S-L, Yeh S-W, Wang H-S, Wei K-H (2005) Macromolecules 38(22):9117-9123.

55. Cho C-H, Hsu S-L, Dinakaran K, Chiu M-Y, Wei K-H (2005) Macromolecules 38(3):745-751.

56. Xiao S, Nguyen M, Gong X, Cao Y, Wu H, Moses D, Heeger AJ (2003) Adv Funct Mater 13(1):25-29.

57. Xiao S, Nguyen MT (2003) US Pat. US 20030204038.

58. Shin S-B, Gong S-C, Jang J-K, Gong M-S, Chang Y-C, Sun Y-B, Chang H-J (2008) J Appl Polym Sci 110(6):3678-3682.

59. Fenenko L, Adachi C, Nakanishi Y, Smertenko P, Svechnikov S (2007) Mol Cryst Liq Cryst 467:303-309.

60. Lee J, Cho H-J, Jung B-J, Cho NS, Shim H-K (2004) Macromolecules 37(23):8523-8529.

61. Lee J, Cho H-J, Nam S, Hwang D-H, Kang J-M, Lim E, Lee J-I, Shim H-K (2006) J Polym Sci Part A Polym Chem 44(9):2943-2954.

62. Takagi K, Kunii S, Yuki Y (2005) J Polym Sci Part A Polym Chem 43(10):2119-2127.

63. Pu K-Y, Zhang B, Ma Z, Wang P, Qi X-Y, Chen R-F, Wang L-H, Fan Q-L, Huang W (2006) Polymer 47(6):1970-1978.

64. Xiao Y, Lu X, Tan L-W, Ong KS, He C (2009) J Polym Sci Part A Polym Chem 47(21):5661-5670.

65. Nguyen TP, Lee CW, Hassen S, Le HC (2009) Solid State Sciences 11(10):1810-1814.

66. Sellinger A, Laine RM (2002) World Pat. WO2002005971.

67. Cammack JK, Jabbour GE, Li S, Froehlich J (2005) US Pat. 0123760 A1.

68. Lee CW, Josse Y, Hsu CH, Nguyen TP (2008) Eur Phys J Appl Phys 42(3):213-218.

69. Renaud C, Josse Y, Lee C-W, Nguyen T-P (2008) J Mate Sci Mater Electron 19(1):S87-S91.

70. He C, Xiao Y, Huang J, Lin T, Mya KY, Zhang X (2004) J Am Chem Soc 126:7792-7793.

71. Brick CM, Tamaki R, Kim S-G, Asuncion MZ, Roll M, Nemoto T, Ouchi Y, Chujo Y, Laine RM (2005) Macromolecules 38(11):4655-4660

72. Brick CM, Ouchi Y, Chujo Y, Laine RM (2005) 38(11):4661-4665.

73. Xiao Y, Liu L, He C, Chin WS, Lin T, Mya KY, Huang J, Lu X (2006) J Mater Chem 16:829-836.

74. Eom J-H, Mi D, Park M-J, Cho H-J, Lee J, Lee J-I, Chu HY, Shim H-K, Hwang D-H, (2009) J Nanosci Nanotech 9(12):7029-7033.

75. Imae I, Kawakami Y (2005) J Mater Chem 15:4581-4583.

76. Sellinger A, Tamaki R, Laine RM (2005) Chem Commun 29:3700-3702.

77. Cho H-J, Hwang D-H, Lee J-I, Jung Y-K, Park J-H, Lee J, Lee S-K, Shim H-K (2006) Chem Mater 18(16):3780-3787.

78. Froelich D, Young R, Nakamura Y, Ohmori S, Li S, Mochizuki A, Lauters M, Jabbour GE (2007) Chem Mater 19:4991.

79. Lo MY, Zhen CG, Lauters M, Gabbour GE (2007) J Am Chem Soc 129:5808.

80. Yang X, Froehlich JD, Chae, HS, Li S, Mochizuki A, Jabbour GE (2009)

Adv Funct Mater 19(16):2623-2629.

81. Park J-L, Lee T-W, Kakimoto MA, Pu LS (2007) US Pat. US0045619 A1.

82. Singh M, Chae HS, Froehlich JD, Kondou T, Li S, Mochizuki A, Jabbour GE (2009) Soft Matter 5:3002-3005.

83. Chen K-B, Chang YP, Yang SH, Hsu C-S (2006) Thin Solid Films 514(1-2):103-109.

84. Xu Y, Peng J, Jiang J, Xu W, Yang W, Cao Y (2005) Appl Phys Lett 87(19):193502/1-193502/3.

85. Liang B, Jiang C, Chen Z, Zhang X, Shi H, Cao Y (2006) J Mater Chem 16(13):1281-1286.

86. Dukart CR, Ranzau SL, Pappenfus TM (2010) 239th ACS National Meeting, San Francisco, CA, USA, 21-25 March 2010, CHED-740.

87. Bozano L, Tuttle SE, Carter SA, Brock P (1998) J Appl Phys Lett 73:3911-3913.

88. Carter SA, Scott JC, Brock P (1997) J Appl Phys Lett 71(9):1145-1147.

89. Blom PWM, Schoo HFM, Matters M (1998) J Appl Phys Lett 75:3914.

90. Gong X, Soci C, Yang C, Heeger AJ, Xiao S (2006) J Phys D Appl Phys 39(10):2048-2052.

91. Lee R-H, Lai H-H (2007) Eur Polym J 43(3):715-724.

92. Cui Y, Chen L, Qian G, Wang M (2008) J Non-Crystall Solids, 543(12-13):1211-1215.

93. Xi H, Li Z, Liang Z (2001) Chinese J Polym Sci, 19(4):421-427.

94. Xie G, Sun D (2007) PMSE Prep 97:730-732.

95. Jeng RJ, Chen YM, Jain AK, Kumar J, Tripathy SK (1992) Chem Mater 4(5):972-975.

96. Oviatt HW, Shea KJ, Kalluri S, Shi Y, Steier WH, Dalton LR (1995) Chem Mater 7(3):493-498.

97. Han S, Li Z, Ji S, Dai D, Zhang R, Zhu C, Wang C (2000) J Sol-Gel Sci Tech, 18(2):137-144.

98. Choi KM, Shea KJ (1998) Plastics Engineering, Photonic Polymer Systems, Marcel Dekker, Inc., New York, pp. 437-480.

99. Luther-Davies B, Samoc M, Woodruff M (1996) Chem Mater 8(11): 2586-2594.

100. Su H-W, Chen W-C, Lee W-C, King J-S (2007) Macromol Mater Eng 292(5):666-673.

101. Xie P, Guo JS, Dai DR, Jin SZ, Liu DS, Li Z, Zhang RB (1996) Polym Adv Technol 7:98-103.

102. Prasad PN, Williams DJ (1991) Introduction to Nonlinear Optical Effects in Molecules and Polymers, John Wiley and Sons, Inc.

103. Sutherland RL (1996), Handbook of Nonlinear Optics, Marcel Dekker Inc., New York.

104. Sarkar A, Mirza S, Rahman S, Rayfield G (2011) Carbon Nanotubes For Optical Power Limiting Applications, In Wang ZM, Neogi A (Eds) Nanoscale Photonics and Electronics, Springer.

105. Su X, Guang S, Xu H, Liu X, Li S, Wang X, Deng Y, Wang P (2009) Macromol 42:8969-8976.

106. Su X, Guang S, Li C, Xu H, Liu X, Wang X, Song Y (2010) Macromolecules 43(6):2840-2845.

107. Ceyhan T, Yuksek M, Yaglioglu HG, Salih B, Erbil MK, Elmali A, Bekaroglu O (2008) Dalton Trans 2407-2413.

108. Costela A, Garcia-Moreno I, Cerdan L, Martin V, Garcia O, Sastre R (2009) Adv Mater 21:4163-4166.

109. Garcia O, Sastre R, Garcia-Moreno I, Martin V, Costela A (2008) J Phys Chem 112:710.

110. Argitis A, Niakoula D, Douvas AM, Gogolides E, Raptis I (2009) Int J Nanotech 6(1-2):71-87.

111. Xia Y, Rogers JA, Paul KE, Whitesides GM (1999) Chem Rev 99(7): 1823-1848.

112. Hirai T, Leolukman M, Liu CC, Han E, Kim YJ, Ishida Y, Hayakawa T, Kakimoto M, Nealey PF, Gopalan P (2009) Adv Mater 21(43):4334-4338.

113. Dai J, Chang SW, Hamad A, Yang D, Felix N, Ober CK (2006) Chem Mater 18:3404-3411.

114. Kanagasabapathy, S., Barclay, G.G., Cameron, J.F., Pohlers, G., Huby, F., Wiley, K. Abstracts of Papers, 227th ACS National Meeting, Anaheim, CA, USA, March 28-April 1, 2004, POLY-550.

115. Korchkov VP, Martynova TN (1985) Zhur Prikladnoi Khimii 58(9):2089-2096.

116. Gonsalves KE, Wang J, Wu H (2000) J Vac Sci Technol B Microelectron Nanometer Struct Process Meas Phenom 18(1):325-327.

117. Wu H, Hu Y, Gonzales KE, Yakaman MJ (2001) J Vac Sci Technol B 19:851.

118. Azam AM, Gonzales KE, Golovkina V, Cerrina F (2003) Microelectron Eng 65:454.

119. Wu H, Gonazles KE (2001) Adv Mater 13:670.

120. Bellas V, Tegou E, Raptis I, Gogolides E, Argitis P, Iatrou H, Hadjichristidis N, Sarantopoulou E, Cefalas AC (2002) J Vac Sci Technol B 20:2902.

121. Gonzales KE, Merhari L, Wu H, Hu Y (2001) Adv Mater 13:703.

122. Sarantopoulou E, Kollia Z, Kocevar K, Musevic I, Kobe S, Drazic G, Gogolides E, Argitis P, Cefalas AC (2003) Mater Sci Eng C23(6-8): 995-999.

123. Ali MA, Gonsalves KE, Batina N, Golovkina V, Cerrina F (2003) Proc SPIE Int Soc Opt Eng 5039:1173-1180.

124. Tegou E, Bellas V, Gogolides E, Argitis P, Dean KR, Eon D, Cartry G, Cardinaud C (2003) Proc SPIE Int Soc Opt Eng 5039:453-461.

125. Gogolides E, Argitis P, Bellas V, Tegou E (2003) World Patent WO2003102695.

126. Koh K, Sugiyama S, Morinaga T, Ohno K, Tsujii Y, Fukada T, Yamahiro M, Ijima T, Oikawa H, Watanabe K, Miyashita T (2005) Macromolecules 38:1264.

127. Eon D, Cartry G, Fernandez V, Cardinaud C, Tegou E, Bellas V, Argitis P, Gogolides E (2004) J Vac Sci Technol B Microelectron Nanometer Struct Process Meas Phenom 22(5):2526-2532.

128. Eon D, Raballand V, Cartry G, Cardinaud C, Vourdas N, Argitis P, Gogolides E (2006) J Vac Sci Technol B Microelectron Nanometer Struct Process Meas Phenom 24(6):2678-2688.

129. Douvas AM, Van Roey F, Goethals M, Papadokostaki KG, Yannakopoulou K, Niakoula D, Gogolides E, Argitis P (2006) Chem Mater 18:4040-4048.

130. Tegou E, Bellas V, Gogolides E, Argitis P, Eon D, Cartry G, Cardinaud C (2004) Chem Mater 16:2567-2577.

131. Zheng L, Waddon AJ, Farris RJ, Coughlin BE (2002) Macromolecules 35:2375.

132. Kim J-B, Ganesan R, Choi J-H, Yun H-J, Kwon Y-G, Kim K-S, Oh TH (2006) J Mater Chem 16:3448-3451.

133. Park JY, Kim MG, Kim J-B (2008) Macromol Rapid Commun 29(18):1532-1537.

134. Allen RD, Sooriyakumaran R, Sundberg LK (2006) US Pat 0189779 A1.

135. Hao J, Lin MW, Palmieri F, Nishimura Y, Chao H-L, Stweart MD, Collins A, Jen K, Wilson CG (2007) Proc SPIE Int Soc Opt Eng 6517: 651729-1-651729-9.

136. Palmieri F, Stewart MD, Wetzel J, Hao J, Nishimura Y, Jen K, Flannery C, Li B, Chao H-L, Young S, Kim WC, Ho PS, Wilson CG (2006) Proc SPIE Int Soc Opt Eng 6151:61510J/1-61510J/9.

137. Palmieri F, Stewart M, Jen K, Wilson CG, Schmid G (2007) Solid State Technol 50(9):42-45.

138. Sellinger A, Laine RM (1996) Chem Mater 8:1592-1593.

139. Hartmann-Thompson C, Hu J, Xu N (2007) unpublished results, Michigan Molecular Institute.

140. Xu Y, Zhu X, Yang S (2009) ACS Nano 3(10):3251-3259.

141. Moon JH, Seo JS, Xu Y, Yang S (2009) J Mater Chem 19:4687-4691.

142. Jang JH, Ullal CK, Gorishny T, Tsukruk VV, Thomas EL (2006) Nano Lett 6:740-743.

143. Jeganathan SG, Bramer D, Kote R, Maladkar GJ (2008) US 0029739.

144. Hartmann-Thompson C, Keeley D, Pollock K, Keinath SE, Dvornic PR, Dantus M, Gunaratne T, Lecaptain D (2008) Chem Mater 20(8): 2829-2838.

145. Bai H, Li, C, Shi G (2008) Chem Phys Chem 9(13):1908-1913.

146. Tanaka K, Inafuku K, Chujo Y (2008) Bioorg Med Chem 16(23):10029-10033.

147. Carlson CA, Lloyd JA, Dean SL, Walker NR, Edmiston PL (2006) Anal Chem 78(11):3537-3542.

148. Haupt K, Mosbach K (2000) Chem Rev 100:2495-2504.

149. Haidekker MA, Ling T, Anglo M, Stevens HY, Frangos JA, Theodorakis EA (2001) Chem Biol 8:123.

150. McCusker C, Carroll JB, Rotello VM (2005) Chem. Commun:996-998.

151. Haugland RP (2005) The Handbook. A Guide To Fluorescent Probes and Labelling Technologies, 10th edn. Invitrogen Corp, Eugene, Oregon.

152. Zou Q-C, Yan Q-J, Song G-W, Zhang S-L, Wu L-M (2007) Biosens Bioelectron 22(7):1461-1465.

153. Sirbuly DJ, Letant SE, Ratto TV (2008) Adv Mater 20(24):4724-4727.

154. Shahriari MR (2007) US Pat. 0122311 A1.

155. Ballantine DS, Rose SL, Grate JW, Wohljen H (1986) Anal Chem 58:3058.

156. Albert KJ, Lewis NS, Schauer CL, Sotzing GA, Sitzel SE, Vaid TP Walt DR (2000) Chem Rev 100:2595-2626.

157. Grate JW (2000) Chem Rev 100:2627-2648.

158. Grate JW (2008) Chem Rev 108:726-745.

159. Hartmann-Thompson C, Hu J, Dvornic PR, Kaganove SN, Keinath SE, Keeley D (2004) Chem Mater 16(24):5357-5364.

160. Hartmann-Thompson C, Keeley DL, Voit B, Eichhorn KJ, Mikhaylova M (2008) J Appl Polym Sci 107(3):1401-1406.

161. Barie N, Rapp M, Ache HJ (1998) Sens Actuators B 46:97-103.

162. Hartmann-Thompson C, Keeley D, Dvornic PR, Keinath SE, McCrea K (2007) J Appl Polym Sci 104(5): 3171-3182.

163. Hartmann-Thompson C (2009) US Pat. 0263287 A1.

164. Lambert AG, Davies PB, Neivandt DJ (2005) Appl Spectrosc 40:103-145.

165. Smentkowski VS, Duong HM, Tamaki R, Keenan MR, Ohlhausen JAT, Kotula PG (2006) Appl Surf Sci 253(2):1015-1022.

166. Esker AR, Dawson KJ, Huffer SM, Karabiyik,U, Deng J, Viers BD, Ferguson-McPherson MK, Morris JR, Mao M, Ducker WA, Satija SK (2005) Polym Prepr (Am Chem Soc Div Polym Chem) 46(1):76-77.

167. Trammell SA, Zeinali M, Melde BJ, Charles PT, Velez FL, Dinderman MA, Kusterbeck A, Markowitz MA (2008) Anal Chem 80(12):4627-4633.

168. Siemens AG (2004) US Pat. 0025568 A1.

169. Tsujimura Y, Yamane M, Wakida S-I (2001) Anal Sci 17(4):485-489.

170. Merzlyuk RM, Yashina NI, Shevchenko YN (1997) Zhurnal Prikladnoi Khimii (Sankt-Peterburg) 70(4):631-635.

171. Castaldo A, Massera E, Quercia L, Di Francia G (2006) Sens Actuators B 118:328-332.

172. Gardner JW, Bartlett PN (1999) Electronic Noses: Principles and Applications. Oxford University Press, New York.

173. Lonegran MC, Severin EJ, Doleman BJ, Beaber SA, Grubbs RH, Lewis NS (1996) Chem Mater 8:2298-2312.

174. Hartmann-Thompson C (2009) Carbon-Polymer Composite Sensors in Electronic Noses. In: Lechkov M, Prandzheva S (eds) Encyclopedia of Polymer Composites: Properties, Performance and Applications, Nova Science Publishers, New York.

175. Gardner JW, Shurmer HV, Corcoran P (1991) Sens Actuators B 4:117.

176. Castaldo A, Massera E, Quercia L, DiFranca G (2007) Macromol Symposia 247:350-356.

177. Massera E, Castaldo A, Quercia L, DiFranca G (2008) Sens Actuators

B129(1):487-490.

178. Castaldo A, Quercia . DiFrancia G, Cassinese A, D'Angelo P (2008) J Appl Phys 103(5):054511/1-054511/6.

179. Ryan MA, Shevade AV, Zhou H, Homer ML (2004) Polymer Carbon Black Composite Sensors in Electronic Noses for Air Quality Monitoring, NASA Bulletin,714-719.

180. Losada J, Garcia Armada MP, Cuadrado I, Alonso B, Gonzalez B, Casado CM, Zhang J (2004) J Organometal Chem 689(17):2799-2807.

181. Hobson ST, Cemavolic S, Patel SV, Warburton M, Mlsna TE (2006) ECS Trans 2(25):11-18.

182. Colilla M, Darder M, Aranda P, Ruiz-Hitzky EJ (2005) Mater Chem 15(35-36):3844-3851.

183. O'Hayre R, Cha S-W, Colella W, Prinz FB (2006) Fuel Cell Fundamentals, John Wiley and Sons, New York.

184. Hickner MA, Ghassami H, Kim YS, Einsla BB, McGrath JE (2004) Chem Rev104:4587-4612.

185. Costamagna P, Yang C, Bocarsly AB, Srinivasan S (2002) Electrochim Acta 47:1023.

186. Alberti G, Casciola M (2003) Annu Rev Mater Res 33:129-154.

187. Silva V, Weisshaar S, Reissner R, Ruffmann B, Vetter S, Mendes A, Madeira L, Nunes S (2005) J Power Sources 145:485-494.

188. Park YS, Yamazaki Y (2005) Solid State Ionics 176:1079-1089.

189. Prashantha K, Park SG (2005) J Appl Polym Sci 98:1875-1878.

190. Miyake N, Wainright JS, Savinell RP (2001) J Electrochem Soc 148:A905.

191. Shao Z-G, Joghee P, Hsing IM (2004) J Membrane Sci 229:43-51.

192. Lin CW, Thangmuthu R, Chang PH (2005) J Membrane Sci 254(1-2):197-205.

193. Antonucci PL, Ario AS, Creti P, Ramunni E, Antonucci V (1997) Solid State Ionics 125:431.

194. Adjemian KT, Lee SJ, Srinivasan S, Benziger J, Bocarsly AB (2002) J

Electrochem Soc 149:A256.

195. Ren S, Sun G, Li C, Liang Z, Wu Z, Jin W, Qin X, Yang X (2006) J Membrane Sci 282(1-2):450-455.

196. Hong L, Liu Z-L, Zhang X, Guo B (2008) US Pat. 0233451 A1.

197. Tay SW, Zhang X-H, Liu Z-L, Hong L, Chan SH (2008) J Membrane Sci 321:139-145.

198. Su YH, Liu YL, Sun YM, Lai JY, Guiver MD, Gao Y (2006) J Power Sources 155:111-117.

199. Chang HY, Lin CW (2003) J Membrane Sci 218:295-306.

200. Wilson BC, Jones CW (2004) Macromolecules 37:9709-9714.

201. Kim D, Scibioh A, Kwak S, Oh I-H, Ha H-Y (2004) Electrochem Commun 6:1069-1074.

202. Acosta JL,Gonzalez, L, Ojeda MC, del Rio C (2003) J Appl Polym Sci 90:2715-2720.

203. Wang H, Holmberg BA, Huang L, Wang Z, Mitra A, Norbeck JM, Yan Y (2002) J Mater Chem 12:834-837.

204. Kim DS, Park HB, Lee YM, Park YH, Rhim JW (2004) J Appl Polym Sci 93:209-218.

205. Gomes D, Buder I, Nunes SP (2006) Desalination 1999:274-276.

206. Ladewig BP, Knott RB, Hill AJ, Riches JD, White JW, Martin DJ, Diniz DA, Costa JC, Lu GQ (2007) Chem Mater 19(9):2372-2381.

207. Lin YF, Yen CY, Ma CCM, Liao SH, Lee CH, Hsiao YH, Lin HP (2007) J Power Sources 171(2):388-395.

208. Su YY, Liu YL, Sun YM, Lai JY, Wang DM, Gao Y, Liu B, Guiver MD (2007) J Membrane Sci 296(1+2):21-28.

209. Su YY, Wei TH, Hsu CH, Liu YL, Sun YM, Lai JY (2006) Desalination 200(1-3):656-657.

210. Holmberg BA, Wang H, Norbeck JM, Yan Y (2004) Polym Prepr (Am Chem Soc Div Polym Chem) 45(1):24-25.

211. Poinsignon C, Denoyelle A, Sanchez JY (1992) French Pat. FR 2670212 A1.

212. Poinsignon C, Denoyelle A, Sanchez JY, Armand M (1995) EP0560899 B1.

213. Carlier E, Revillon A, Guyot A, Baumgartner P (1993) React Polym 21(1-2):15-25.

214. Decker B, Hartmann-Thompson C, Carver PI, Keinath SE, Santurri PR (2010) Chem Mater 22(3):942-948.

215. Subianto S, Mistry MK, Choudhury NR, Dutta NK, Knott R (2009) Appl Mater Interfaces 1(16):1173-1182.

216. Hartmann-Thompson C, Merrington A, Carver PI, Keeley DL, Rousseau JL, Hucul D, Bruza KJ, Thomas LS, Keinath SE, Nowak RM, Katona DM, Santurri PR (2008) J Appl Polym Sci 110:958-974.

217. Liu L, Song L, Zhang G, Guo H, Hu Y, Fan W (2006) Mater Lett 60(15): 1823-1827.

218. Nowak R, Hartmann-Thompson C, Bruza K, Thomas L, Meier D (2008) World Pat. WO 2008127645 A1.

219. Unpublished results, Hartmann-Thompson C, Keeley D, Michigan Molecular Institute, 2009.

220. Chang Y-W, Wang E, Shin G, Han J-E, Mather PT (2007) Polym Adv Technol 18:535-543.

221. Park YI, Moon J, Kim HK (2005) Electrochem Solid-State Lett 8: A191-A194.

222. Choi J, Lee KM, Wycisk R, Pintauro PN, Mather PT (2008) Macromolecules 41:4569-4572.

223. Lee HS, Roy A, Badami AS, McGrath JE (2006) Polym Mater Sci Eng 51:210-211.

224. Wang H, Badami AS, Roy A, McGrath JE (2006) Polym Mater Sci Eng 51:202-203.

225. Serpico JM, Ehrenberg SG, Fontanella JJ, Jiao X, Perahia D, McGrady KA, Sanders EH, Kellogg GE, Wnek GE (2002) Macromolecules 3: 5916-5921.

226. Choi J, Lee KM, Wycisk R, Pintauro PN, Mather PT (2008) Electro Chem Soc Trans 16(2):1433-1442.

227. Zhang X, Tay SW, Liu Z, Hong L (2009) J Membrane Sci 329:228-

235.

228. Gao Y, Robertson GP, Guiver MD, Wang G, Jian X, Mikhailenko SD, Li X, Kaliaguine S (2006) J Membr Sci 278:26-34.

229. Costa ROR, Vasconcelos WL, Tamaki R, Laine RM (2001) Macromolecules 34:5398-5407.

230. Zhang X-H, Tay SW, Hong L, Liu Z-L (2008) J Membrane Sci 320:310-318.

231. Zhao L, Huang Y (2008) Huaxue Yu Nianhe 30(1):9-12, 33.

232. Khiterer M, Loy DA, Cornelius CJ,Fujimoto CH, Small JH, McIntire TM, Shea KJ (2006) Chem Mater 18(16):3665-3673.

233. Khiterer M, Loy DA, Small JH, Shea KJ (2004) Polym Prepr 45(1): 686-687.

234. Kalaw GJD, Yang Z, Musselman IH, Yang D-J, Balkus KJ, Ferraris JP (2008) Sep Sci Technol 43:3981-4008.

235. Honma I, Nakajima H,Nishikawa O, Sugimoto T, Nomura S (2003) J Electrochem Soc 150(5):A616-A619.

236. Kim YJ, Choi WC, Woo SI, Hong WH (2004) J Membrane Sci 238(1-2):213-222.

237. Nam S-E, Song S-A, Kim S-G, Park S-M, Kang Y, Lee JW, Lee KH (2006) Desalination 200(1-3):584-585.

238. Nam S-E, Lee K-H, Kang Y, Park S-M, Lee JW (2007) Sep Sci Technol 42(13):2927-2945.

239. Pezzin SH, Stock N, Shishatskiy S, Nunes SP (2008) J Membrane Sci 325(2):559-569.

240. Karthikeyan CS, Nunes SP, Schulte K (2006) Macromol Chem Phys 207(3):336-341.

241. Fujinami T, Mase T, Takami M (2009) US Pat. 0117439 A1.

242. Wu Y, Wu C, Xu T, Lin X, Fu Y (2009) J Membrane Sci 338(1-2):51-60.

243. van Schalkwijk WA, Scrosati B (2002) Advances in Lithium Ion Batteries, Kluwer Academic/Plenum Publishers, New York.

244. Linden D, Reddy TB (eds) (2002) Handbook of Batteries, McGraw-

Hill, New York.

245. Hawker CJ, Chu F, Pomery PJ, Hill DJT (1996) Macromolecules 29:3831-3838.

246. Tiglaar DM, Meador MAB, Bennett WR (2007) Macromolecules 40(12):4159-4164.

247. Tiglaar DM, Meador MAB, Kinder JD, Bennett WR (2006) Macromolecules 39(1):120-127.

248. Itoh T, Horii S, Hashimoto S, Uno T, Kubo M (2004) Ionics 10:450-457.

249. Tsujiko A (2007) World Pat. 024003.

250. Bai Y, Pan CH, Wu F, Wu C, Ye L, Feng ZG (2007) Gaodeng Xuexiao Huaxue Xuebao 28(9):1796-1800.

251. Pan CH, Bai Y, Wu F, Ye L, Wu C, Feng ZG (2007) Gongneng Cailiao 38(2):210-213.

252. Shi Q, Zhou X (2004) Gaofenzi Xuebao 1:114-120.

253. Liccocia S, Traversa E (2004) Nano-Micro Interface: 289-301.

254. Quartarone E, Mustarelli P, Magistris A (1998) Solid State Ionics 110:1.

255. Maitra P, Ding J, Wunder SL (2003) Polym Mater Sci Eng 88:568-569.

256. Maitra P, Wunder SL (2002) Chem Mater 14:4494-4497.

257. Maitra P, Ding J, Huang H, Wunder S (2003) Langmuir 19:8894-9004.

258. Zhang H, Kulkani S, Wunder SL (2004) Polym Mater Sci Eng 91:509-510.

259. Maitra P, Wunder SL (2003) Electrochem Solid-State Lett 7(4):A88-A92.

260. Zhang H, Kulkani S, Wunder SL (2006) J Electrochem Soc 153(2):A239-A248.

261. Zhang H, Kulkani S, Wunder SL (2007) J Phys Chem B 111(14):3583-3590.

262. Nunes SC, Bermudez VZ, Ostrovskii D, Silva MM, Barros S, Smith MJ, Carlos LD, Rocha J, Morales E (2005) J Electrochem Soc 152(2):A429-A438.

263. Bronstein LM, Karlinsey, RL, Stein B, Yi Z, Carini J, Zwanziger JW (2006) Chem Mater 18(3):708-715.

264. Kim H-S, Mah, S-K (2008) US Pat. 80166634 A1.

265. Hennige V, Hying C, Hoerpel G, Jost C, Kuehnle A (2004) German Pat. DE 10304734 A1.

266. Ismailov BA, Zhdanov AA, Zhurnal Obschchei Khimii, 1982, 52(3): 642-6.

267. Blanski RL, Phillips S, Rodgers SL, Lichtenhahn JD, Schwab JJ (2007) US Patent 7217683 B1.

268. Dare EO (2006) Turkish J Chem, 30:585-593.

269. Noda I, Isikawa M, Yamawaki M, Sasaki Y (1997) Inorg Chim Acta 263(1-2):149-152.

270. Misra R, Rollins K, Morgan S (2008) Polym Prepr 49(1):517-518.

271. Misra R, Fu BX, Morgan SE (2007) J Polym Sci Part B Polym Phys 45:2441-2445.

272. Misra R, Morgan SE (2006) Polym Prepr 47(1):410-411.

273. Misra R, Fu BX, Plagge A, Morgan SE (2009) J Polym Sci Part B Polym Phys 47(11):1088-1102.